Full scale validation of CFD model of self-propelled ship

Master Thesis

$$(EIv'')''=q-\rho A\ddot{v}$$

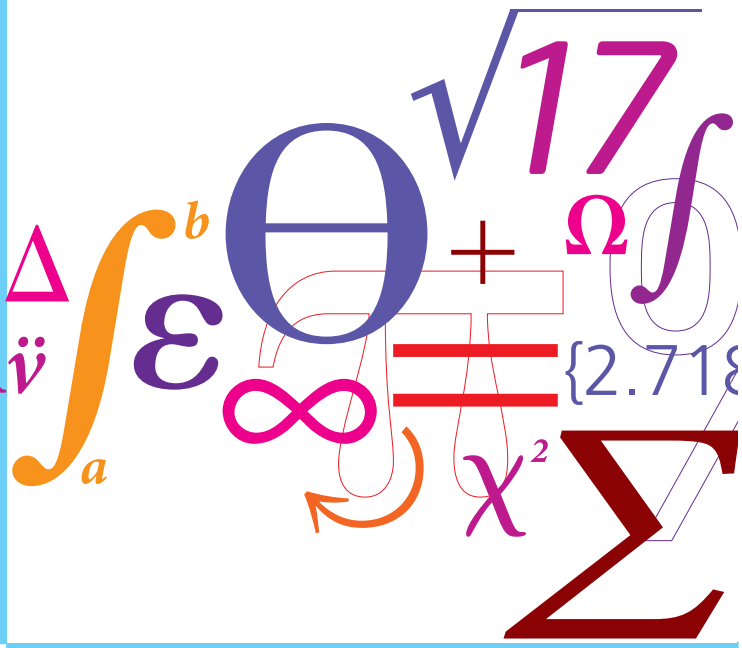

Henrik Mikkelsen
Mads Lund Steffensen
June 2016

DTU Mechanical Engineering
Department of Mechanical Engineering

Technical University of Denmark
Department of Mechanical Engineering
Nils Koppels Allé, building 404,
2800 Kongens Lyngby, Denmark
Phone +45 4525 1960
info@mek.dtu.dk
www.mek.dtu.dk

Abstract

An important part of designing a ship is to estimate the performance of the ship and the necessary propulsive power at the design stage.

Traditionally, the performance of a ship design is estimated by conducting towing tank tests on a downscaled version of the ship (model scale). The results from these towing tank tests are then extrapolated to the scale of the actual ship (full scale). An alternative to testing in a towing tank is to simulate the flow around the ship using Computational Fluid Dynamics (CFD). CFD simulations can be performed in full scale, which eliminates the need for extrapolation. A disadvantage of using CFD is the modelling errors which occur because the flow physics are simplified (e.g. turbulence in the boundary layer).

This thesis is a study of the accuracy of full scale CFD simulations in predicting the performance of a ship design. The authors have been granted unique access to data from a series of sister ships. The data includes ship geometry, towing tank tests, sea trial data and in-service performance data. With access to this data, the CFD model can be validated as it is developed.

The final CFD setup simulates the self-propelled ship in full scale. The results of these full scale self-propulsion results show an average overestimation of delivered power of 2% compared to the sea trial results. The predicted delivered power using the towing tank approach shows an average overestimation of delivered power of 6% compared to the sea trial results. In this case, the CFD approach resulted in an estimation of delivered power which was closer to the sea trial results. However, due to uncertainties, more comparison studies between full scale CFD and extrapolated towing tank tests are required. More comparison studies could provide more knowledge about CFD simulations of self-propelled ships and how CFD can be used instead of towing tank tests to predict a ships performance at design stage in the future.

Preface

This thesis is submitted as partial fulfilment of the requirement for the degree of MSc in Mechanical Engineering at the Technical University of Denmark (DTU), Lyngby, Denmark.

The work has been performed over the time period January 2016 to June 2016. The project was carried out at the Section of Fluid Mechanics, Coastal and Maritime Engineering (FVM) at the Department of Mechanical Engineering (MEK) in cooperation with DNV GL. The authors have been stationed at the headquarters of DNV GL in Oslo in the project period. The thesis has been supervised by Jens Honoré Walther (MEK) and Poul Andersen (MEK).

Mads Lund Steffensen and Henrik Mikkelsen

Oslo, Norway.
May, 2016.

Acknowledgements

Of the many people who helped us during this project, we would first like to thank our two supervisors, Jens Honoré Walther and Poul Andersen for their guidance and support as well as for some good discussions throughout the project. We would like to thank Olav Rognebakke for inviting us to Oslo and his colleagues Jaeouk Sun, Cosmin Ciortan, Tormod Gjestland for sharing state-of-the-art knowledge of numerical modelling and the maritime world.

Secondly, we would like to express our sincere gratitude to the Japanese shipyard for inviting us to Japan and providing unique and rarely shared data.

Thirdly, we would like to thank Stig Staghøj Knudsen from OSK-ShipTech A/S for allowing us to use confidential setup files for numerical simulations.

Furthermore, we would like to thank the shipowner for inviting us to the sea trial of their ship, providing transportation to Japan and providing in-service performance data.

We are grateful to the software company CD-Adapco for providing their high-end software code STAR-CCM+ for unlimited use for this project.

Finally, we would to thank Dansk Maritime Fond, Reinholdt W Jorch og Hustru Fond, William Demant og Hustru Ida E. Fond and the Department of Mechanical Engineering at DTU for the financial support that made the project possible.

Contents

Nomenclature

Latin letters

A_{VS}	Projected frontal area above water of the ship	[m^2]
B	Beam of ship	[m]
C	Resistance coefficient	[-]
$c_{0.7}$	Chord length at $r/R = 0.7$	[m]
C_A	Correlation coefficient	[-]
C_{AAS}	Air resistance coefficient	[-]
C_B	Block coefficient	[-]
C_{DA}	Air drag coefficient	[-]
C_D	Propeller drag coefficient	[-]
C_{cyl}	Engine cylinder coefficient	[m^3]
C_{eng}	Engine coefficient	[-]
C_F	Frictional resistance coefficient	[-]
$C_{F,Hu}$	Frictional resistance coefficient from the Hughes line	[-]
$C_{F,Sh}$	Frictional resistance coefficient from the Schoenherr line	[-]
C_R	Residuary resistance coefficient	[-]
C_T	Total resistance coefficient	[-]
$C_{T,smooth}$	Total resistance coefficient, smooth hull, without bilge keel	[-]
C_V	Viscous resistance coefficient	[-]
C_W	Wave resistance coefficient	[-]
C_μ	Eddy viscosity coefficient	[-]
D	Propeller diameter	[m]
DW_{Design}	Design dead weight	[m]
F_D	Skin friction correction force or Towing force	[N]
FI	Fuel injection index	[-]
Fn	Froude number	[-]
g	Gravitational acceleration	[$\frac{m}{s^2}$]
Hs	Significant wave height	[m]
J	Propeller speed of advance coefficient (Advance ratio)	[-]
J_T	Advance ratio based on thrust identity method	[-]
k	Form factor	[-]
k	Turbulence kinetic energy	[$\frac{m^2}{s^2}$]
k_p	Blade roughness	[m]
K_Q	Propeller torque coefficient	[-]
k_s	Nikuradse's equivalent sand roughness	[m]

K_T	Propeller thrust coefficient	[-]
l^*	Non-dimensional cell size	[−]
L	Characteristic length	[m]
L_{BWL}	Distance of the bow to 95% of the maximum beam	[m]
L_{OA}	Overall length of ship	[m]
L_{PP}	Length between perpendiculars	[m]
L_{WL}	Waterline length of ship	[m]
n	Rate of rotation of propeller	[s^{-1}]
p	Pressure	[Pa]
p_{me}	Mean effective pressure	[Pa]
P	Engine power	[W]
P_D	Delivered power	[W]
P/D	Pitch ratio	[-]
P_W	Power correction due to waves	[W]
Q	Propeller torque	[Nm]
r	Radius or radial distance	[m]
r_T	Total resistance coefficient	[-]
R	Resistance	[N]
R_{AWL}	Added resistance due to waves	[N]
R_F	Frictional resistance	[N]
R_P	Pressure resistance	[N]
R_T	Total resistance	[N]
R_V	Viscous resistance	[N]
$R_{V,SH}$	Viscous resistance with raised surface height	[N]
R_W	Wave making resistance	[N]
Re	Reynolds number	[-]
$Re_{c0.7}$	Propeller Reynolds number at $r/R = 0.7$	[-]
Re_p	Propeller Reynolds number	[-]
S	Wetted surface area	[m^2]
S_{BK}	Wetted surface area of bilge keel	[m^2]
S_{ij}	Mean strain rate tensor	[s^{-1}]
S_S	Wetted surface of the hull and rudder	[m^2]
t	Time	[s]
t	Trust deduction	[-]
t^*	Non-dimensional time step	[-]
$t_{0.7}$	Maximum blade thickness length at $r/R = 0.7$	[m]
T	Propeller thrust	[N]
T_{AP}	Draft at aft perpendicular	[m]
T_{Design}	Design draft	[m]
T_{FP}	Draft at fore perpendicular	[m]
U	Velocity vector	[$\frac{m}{s}, \frac{m}{s}, \frac{m}{s}$]
u_*	Frictional velocity	[$\frac{m}{s}$]
u'	Fluctuating part of velocity	[$\frac{m}{s}$]
V	Speed	[$\frac{m}{s}$]
V_{Design}	Design speed	[$\frac{m}{s}$]
V_θ	Tangential rotational velocity	[$\frac{m}{s}$]
w_T	Wake fraction coefficient from trust identity method	[-]
y	Distance to wall	[m]
y^+	Non-dimensional wall distance	[-]
x	Spatial direction	[m]
Z	Number of blades	[-]

Greek letters

δ_{ij}	Kroneckers delta	[-]
ΔC_F	Roughness allowance coefficient	[-]
Δl	Cell size	[m]
ΔR_F	Roughness resistance	[N]
ΔR_{SH}	Added surface height resistance	[N]
Δt	Time step	[s]
$\Delta\theta$	Angle of rotation per time step	$[\frac{^\circ}{s}]$
ϵ	Turbulence dissipation rate	$[\frac{m^2}{s^3}]$
η_b	Propeller efficiency behind ship	[-]
η_o	Propeller efficiency in open water	[-]
η_R	Relative rotative efficiency	[-]
λ	Model-Ship scaling factor	[-]
μ	Dynamic viscosity	$[\frac{Ns}{m^2}]$
μ_t	Eddy viscosity	$[\frac{Ns}{m^2}]$
ν	Kinematic viscosity	$[\frac{m^2}{s}]$
ρ	Fluid density	$[\frac{kg}{m^3}]$
ρ_{air}	Air density	$[\frac{kg}{m^3}]$
τ_ω	Wall shear stress	[Pa]
ϕ	Coefficient used in the MARINTEK form factor method	[-]
ω	Engine rotational speed	$[\frac{rad}{s}]$
ω	Specific turbulence dissipation rate	$[s^{-1}]$
∇	Volume displacement	$[m^3]$

Subscripts

m	Index for model scale ship
s	Index for full scale ship
o	Index for open water or open water equivalent
i,j	Index for the three spatial directions

Abbreviations

CFD	Computational fluid dynamics
DFBI	Dynamical fluid-body interaction
DGPS	Differential GPS
DNS	Direct numerical simulation
DOF	Degrees of freedom
DTU	Technical University of Denmark
DWT	Dead weight tons
FVM	Section of Fluid Mechanics, Coastal and Maritime Engineering at DTU
GPS	Global Positioning System
IMO	International Maritime Organization
ITTC	International Towing Tank Committee
MCR	Maximum continuous rating
MEK	Department of Mechanical Engineering at DTU
MRF	Moving reference frame method
NACA	National Advisory Committee for Aeronautics
RANS	Reynolds-average Navier-Stokes
RPM	Revolutions per minute
RSB	Rotating solid body method
RZ	Refinement zone
SST	Shear stress transport
VOF	Volume-of-Fluid

CHAPTER 1

Introduction

At the design stage, it is essential to have an accurate and trustworthy estimate of the performance of the ship. An accurate estimation is important in order to ensure fulfilment of contractual requirements and minimize the costs of building and operating the ship and to design an eco-efficient ship. Eco-efficiency is getting increasingly important these days because of the increasing legislative requirements for a cleaner and greener shipping industry.

Traditionally, the performance of a ship design is estimated by conducting hydrodynamic tests on a model scale version of the ship. These tests are conducted in a towing tank, which is a large basin of water in which hydrodynamic tests can be conducted under controlled conditions (see Figure 1.1). Towing tank tests have been performed for more than 100 years, which has generated vast experience in conducting these tests and a large amount of knowledge about the hydrodynamics of ships. The organisation of standard procedures for carrying out towing tank tests is managed by an association named the International Towing Tank Conference (ITTC).

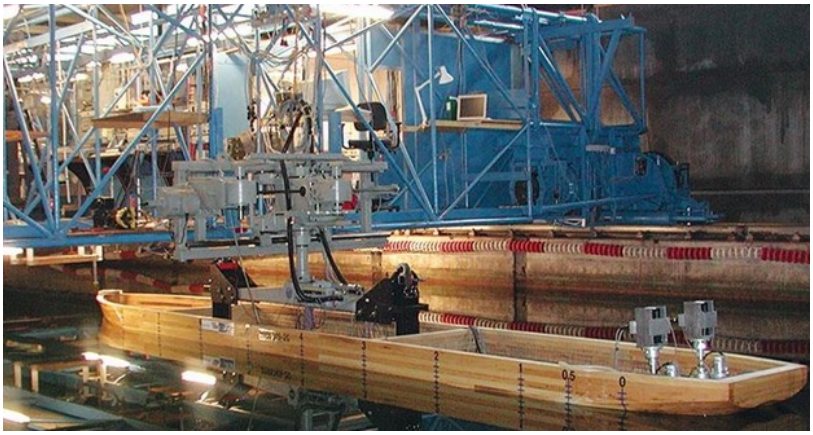

Figure 1.1: Experimental setup in towing tank. Courtesy of FORCE Technology.

One of the most significant weaknesses of predicting ship resistances by conducting towing tank tests is that the viscous effects in model scale are not the same as in full scale. In order to cope with this fact, extrapolations procedures have been developed. The procedure artificially splits the resistance components up and scales them separately. The procedures for extrapolating the towing tank measurements from model scale to full scale have been developed over the years to more accurately predict the performance of the full scale ship.

An alternative to testing in a towing tank is to use Computational Fluid Dynamics (CFD) to predict the ship resistance (see Figure 1.2). In CFD the flow is simulated by solving a large set of equations numerically using a computer. CFD has become an increasingly viable alternative with the rapid increase in available computational power in the last decades. One advantage of

CFD is that the simulations can be performed in full scale, which eliminates the challenges of extrapolation from model scale to full scale. CFD simulations also have the advantage of offering insights into the flow, which is very difficult or impossible to obtain from experiments.

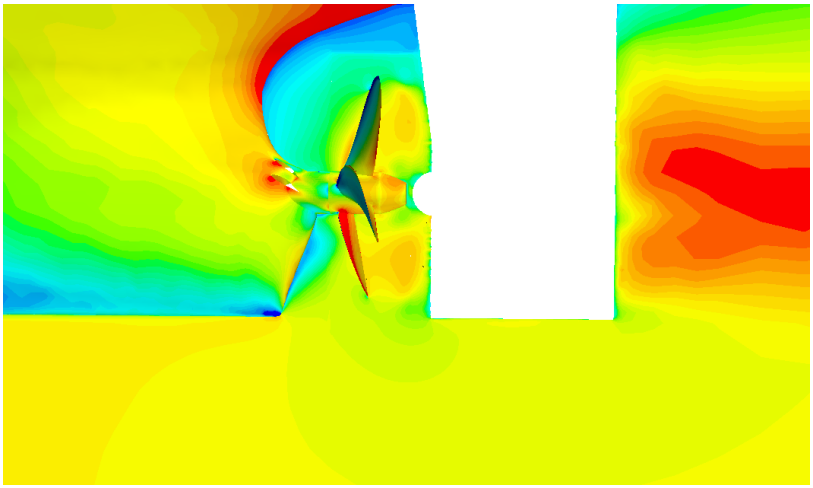

Figure 1.2: CFD self-propulsion calculation. The colors on the hull and propeller indicates the pressure. The colors around the ship indicates the velocity magnitude of the water. Blue represents low values and red represents high values.

One of the disadvantages of using CFD is the modelling errors which occur because of the simplified flow physics (e.g. turbulence in the boundary layer). Extensive studies [1, 2, 3] have shown that model scale CFD simulations can predict the resistance on the ship and the thrust and torque of the propeller within a few percentages of towing tank measurements.

This thesis includes validation of CFD simulations in predicting the performance of a ship both in model scale and full scale. In order to quantify the accuracy of the CFD simulations, some reference data is needed. Such data about the performance of a ship is almost always considered confidential information, and obtaining access to the data may be very difficult. The authors of this thesis have been provided with unique access to data from a series of sister ships. The data includes ship geometry, towing tank test data, sea trial data, and in-service performance data. Towing tank test data is used as reference for the model scale CFD simulations. Sea trial data and in-service performance data are used as reference for the full scale CFD simulations. A sea trial is the final test of a ship before it is delivered by the shipyard to the ship owner.

The key to a useful comparison is to have highly accurate sea trial data. Sea trial data generally has significant uncertainties because of the lack of control in the experimental environment. There is a focus in the industry on obtaining increasingly accurate sea trial results, as seen with introduction of the new sea trial procedure ISO 15016:2015 [4]. Besides the difficulties in conducting experiments at such a large scale, it is also important to remember that there are many stakeholders in a sea trial, each with different interests. The authors have attended a sea trial in order to gain knowledge about the sea trial procedure and the uncertainties of the data.

If full scale CFD simulations prove to be more accurate or as accurate as towing tank tests, it could potentially change the method with which the maritime industry predicts the performance of a ship before is built.

CHAPTER 2

Theory

This chapter presents in brief the theory which serves as the foundation for this thesis. Section 2.1 is devoted ship resistance and how the resistance can be split into relevant components. The following Section 2.2 presents the theory and overall ideas behind extrapolating the ship resistance from model scale to full scale. Finally Section 2.3 states the theoretical background for the CFD simulations.

2.1 Ship Resistance Components

This section introduces some of the theory about resistance on ships travelling in calm water. There are several ways of dividing the total calm water resistance R_T of a ship into components. One way is to divide the forces acting on the ship into two parts; frictionally resistance R_F, which is the forces acting tangentially to the ship surface, and pressure resistance R_P, which is the shear forces acting tangential to the ship surface. This gives rise to the following expression:

$$R_T = R_F + R_P \tag{2.1}$$

At lower speeds the frictional resistance is dominant and at higher speeds the pressure forces becomes dominant due to the increased wave making. Alternatively, the total resistance can be divided into two other parts; viscous resistance R_V (energy lost in wake), and wave resistance R_W (energy lost in wave generation). This gives an alternative expression:

$$R_T = R_V + R_W \tag{2.2}$$

When a ship travels though water, waves are generated on the water surface. The generated waves forms a wave system. A Kelvin wave is the mathematical form of the wave system made by a point source travelling along a free surface[5, Sec. 3.1.5.2]. The details on the Kelvin wave are explained by [5, Sec. 3.1.5.2, Sec. 7.3.4.3] and [6]. Figure 2.1 depicts an example of the wave system. The wave system created by the translation of the ship consists of divergent and transverse waves which is similar to a Kelvin wave.

2.2 Model-Ship Extrapolation

When designing a ship, it is important to predict the ship resistance, in order to estimate the necessary amount of propulsion power. These predictions can be done by testing a model of the ship in a towing tank. The results of these towing tank tests can then be extrapolated from model

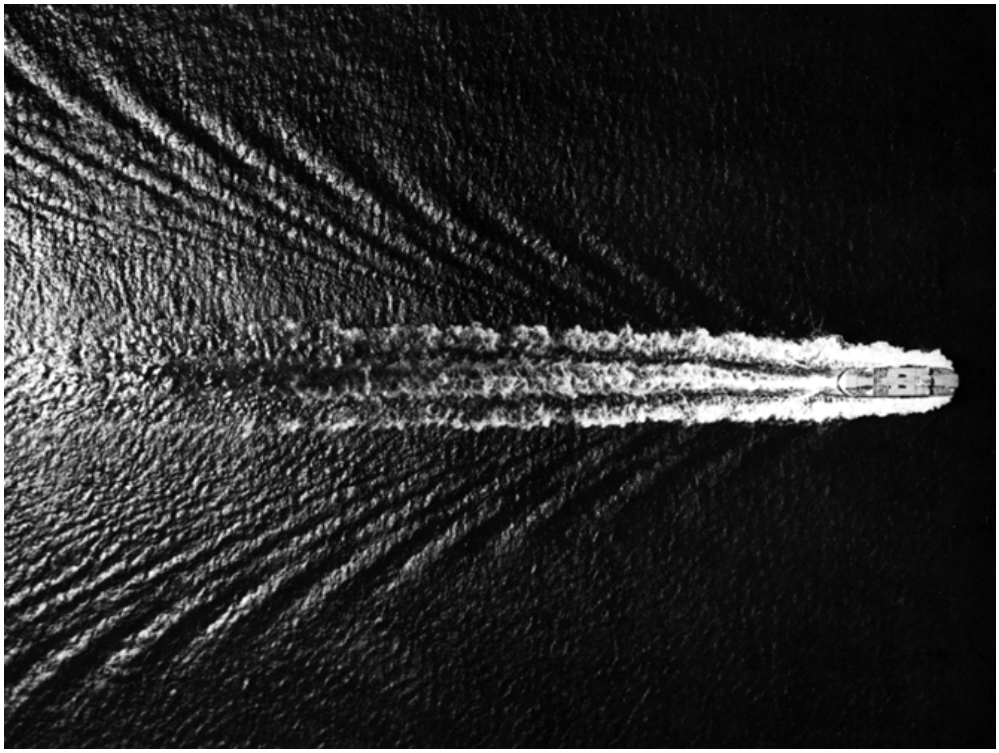

Figure 2.1: Wave system created by a travelling ship. [7, p. 117]

scale to full scale. The idea behind measuring on ships in model scale and then extrapolating the results to full scale is that the total resistance can be split into components that can be scaled individually. The methods for extrapolating resistances from model scale to full scale were first introduced by Froude in 1872 [8]. This method was then further developed by Hughes in the 1950s [9]. Hughes' method, known as the form factor method, has been adopted as the standard method for extrapolating by ITTC [10].

2.2.1 Model-Ship Scaling

The scaling factor λ between model scale and full scale is defined using a characteristic length of the full scale ship L_s and characteristic length of the model scale ship L_m as following:

$$\lambda = \frac{L_s}{L_m} \tag{2.3}$$

The method of dimensional analysis can be used to create non-dimensional quantities which are useful when scaling from model scale to full scale. The quantities are made non-dimensional using the speed V, gravitational acceleration g, kinematic viscosity of the fluid ν and waterline length of the ship L_{WL}. Two of these non-dimensional quantities are: the Froude number Fn and the Reynolds number Re:

$$Fn = \frac{V}{\sqrt{gL_{WL}}} \tag{2.4}$$

$$Re = \frac{VL_{WL}}{\nu} \tag{2.5}$$

Dimensional analysis can also be used to create a non-dimensional resistance coefficient C from a resistance R using the fluid density ρ and the wetted surface area S:

$$C = \frac{R}{\frac{1}{2}\rho S V^2} \tag{2.6}$$

The Froude number, the Reynolds number and resistance coefficients are essential non-dimensional parameters in ship hydrodynamics and are used in the form factor method.

2.2.2 Form Factor Method

The idea of the form factor method is that the total resistance can be split into viscous and wave resistances, as shown in eq. (2.2). The form factor method assumes that the viscous resistance coefficient C_V and wave resistances coefficient C_W are dependent on the Froude number and the Reynolds number respectively, as seen in the expression for the total resistance coefficient C_T:

$$C_T(Re,Fn) = C_V(Re) + C_W(Fn) \tag{2.7}$$

The viscous resistance coefficient can be substituted by a friction resistance coefficient C_F and a form factor k (hence the name form factor method) while the wave resistance coefficient is commonly referred to as the residuary resistance coefficient C_R:

$$C_V = (1+k)C_F \tag{2.8}$$

$$C_W = C_R \tag{2.9}$$

This gives an alternative expression for the total resistance coefficient:

$$C_T = (1+k)C_F + C_R \tag{2.10}$$

The total resistance coefficient can be determined from the total resistance measured in the towing tank, and the frictional resistance coefficient is calculated using an empirical formula called a friction line. The residuary resistance coefficient can then be calculated using eq. (2.10).

By testing the model ship at the same Froude number as the actual ship, the residuary resistance coefficient in model scale is equal to the residuary resistance coefficient in full scale, because the residuary resistance coefficient is assumed to be only Froude number dependent. As in model scale, the full scale frictional resistance coefficient can be found using an empirical friction line. With the full scale frictional and residuary resistance coefficient known, the full scale total resistance can be calculated using eq. (2.10).

2.2.3 Frictional Resistance Coefficient

In the form factor method described in the previous section, the frictional resistance coefficient is estimated using a flat plate friction line since it cannot be measured directly in a towing tank test. Many friction lines were proposed as candidates for a standard friction line during the initial development of the first ITTC procedure in the 1950s. Ultimately, the Hughes 2D flat plate line [11, Eq.(12.16)] was chosen to estimate the frictional resistance coefficient $C_{F,Hu}$:

$$C_{F,Hu} = \frac{0.066}{(\log_{10}(Re) - 2.03)^2} \tag{2.11}$$

The Hughes 2D flat plate line was modified by rounding off the values and by adding 11.94% in order to account for 3D effects before being adopted as the ITTC-57 correlation line [11, 12, 10]:

$$\begin{aligned} C_F &= (1 + 0.1194)\frac{0.067}{(\log_{10}(Re) - 2)^2} \\ &= \frac{0.075}{(\log_{10}(Re) - 2)^2} \end{aligned} \tag{2.12}$$

Some researchers [13] note that the ITTC-57 correlation line is a model ship correlation line, rather than a flat plate friction line because of the corrections to the original Hughes friction line described above. Some alternative friction lines proposed in the literature are: The Schoenherr line [14], the Grigson line [15] and the Katsui line [16].

The Schoenherr Line estimate of the frictional resistance coefficient $C_{F,Sh}$ is given by [14]:

$$\frac{0.242}{\sqrt{C_{F,Sh}}} = \log_{10}\left(ReC_{F,Sh}\right) \tag{2.13}$$

The alternative friction lines are compared in [13]. The existence of many different empirical friction lines could indicate that it is difficult to develop a robust and versatile friction line. In this thesis, the ITTC correlation line eq. (2.12) and the Schoenherr friction line eq. (2.13) will be used.

2.2.4 Form Factor

The form factor in the form factor method is a constant dependent on the shape of the hull. The form factor can be estimated either by performing a form factor test in a towing tank or using an empirical formula. In the towing tank test, the ship model is dragged through the water at a very low speed. At very low speeds, the viscous resistance becomes dominant and the residual resistance coefficient becomes negligible. When the residual resistance coefficient becomes negligible, the form factor can be estimated by measuring the total resistance. The ITTC recommended procedure for estimating the form factor is the Prohaska method [17, Sec. 3.6.2].

Originally the form factor was assumed to be independent of the Reynolds number. Recent studies [18, 13, 19, 20, 21] show that this assumption is not correct. The conclusion of the research has been confirmed by the ITTC Resistance Committee. In 2011 the Committee states that [12, Sec. 5.3]: *"Modern bulbous bows in "offdesign" conditions (e.g. smaller draughts than the design*

draught) make it nearly impossible to determine a reliable form factor from model tests." and *"Although the original intent is that the form factor is independent of Reynolds number this does not appear to be the case."*

This clearly indicates that the form factor is dependent on the Reynolds number, which contradicts the original assumption of the form factor. Furthermore, ITTC concludes that it is difficult to determine a form factor at off-design conditions and for ships with a bulbous bow. Today many ships have bulbous bows and/or are tested in ballast condition, which is an off-design condition at the sea trial. The sea trial is performed at ballast condition because it is practically impossible to load the ship to design draft at the sea trial.

Another method to determine the form factor is to use an empirical method. An example of an empirical method is the MARINTEK form factor method [22, p. 2]. The method uses main dimensions of the ship as block coefficient C_B, draft at aft T_{AP}, draft at fore T_{FP} and beam B to estimate the form factor:

$$k = 0.6\phi + 75\phi^3 \quad , \quad \phi = \frac{C_B}{L_{WL}}\sqrt{(T_{AP} + T_{FP})\, B} \tag{2.14}$$

The uncertainties in the estimation of the form factor is a direct contribution to the uncertainties of using towing tank tests to predict the performance of a ship design.

2.3 CFD Modelling

One of the main goals of this thesis is to model the fluid flow around a ship using CFD. This section introduces some of the background behind the used CFD method. The flow around the ship is modelled using either a single phase flow of water or a two phase flow of water and air.

The modelling of turbulence in the flow is an important aspect of CFD simulations. The most ideal approach would be to simulate the turbulence all the way down to the smallest scales in the flow, which are the Kolmogorov scales. This approach is called direct numerical simulation (DNS). Using DNS requires an enormous computational effort, and is practically impossible for most applications with the computational power available today. Another approach is to solve the Reynolds-averaged Navier-Stokes (RANS) equations using a closure model. The RANS approach is the method most commonly used in the ship building industry.

2.3.1 RANS Equations

The RANS equations are a time-averaged solution to the Navier-Stokes equations. Detailed deviations of the RANS equations are presented in a number of studies e.g. [23, Sec. 2.3]. The flow is assumed incompressible, because the water phase is a liquid which is generally assumed incompressible, and because the flow speeds are much lower than the speed of sound. For an incompressible Newtonian fluid, the RANS equations are [23, Eq. (2.24)]:

$$\rho\frac{\partial U_i}{\partial t} + \rho U_j\frac{\partial U_i}{\partial x_j} = -\frac{\partial p}{\partial x_i} + \frac{\partial}{\partial x_j}\left(2\mu S_{ji} - \rho\overline{u_j' u_i'}\right) \tag{2.15}$$

where U_i is the velocity vector, t is time, p is pressure, μ is dynamic viscosity, S_{ij} is the mean strain rate and u' is the fluctuating part of the velocity.

The RANS equations in three spatial dimensions and a mass continuity equation give four independent equations with ten unknown variables. The imbalance between equations and unknown variables makes the problem impossible to solve analytically. Normally, this is called the closure problem of turbulence. The presence of the Reynolds stresses ($\rho\overline{u_j' u_i'}$) make the turbulence problem difficult.

In order to close the problem the Reynolds stresses are modelled using a linear eddy viscosity model. The linear constitutive relationship is [23, Eq. (4.6)]:

$$-\rho\overline{u_i' u_j'} = 2\mu_t S_{ij} - \frac{2}{3}\rho k \delta_{ij} \tag{2.16}$$

where μ_t is called turbulent viscosity or eddy viscosity and k is the turbulent kinetic energy and δ_{ij} is the Kronecker's delta. The turbulent viscosity can be estimated using one of multiple methods. One of these methods is to use a two-equation model.

2.3.2 Two-Equation Model

In this thesis, the turbulent viscosity is calculated using the realisable $k-\epsilon$ turbulence model. The $k-\epsilon$ model is a two equations model using the turbulent kinetic energy k and the turbulent dissipation rate ϵ [23, Eq. (4.40)]:

$$\mu_t = \rho C_\mu \frac{k^2}{\epsilon} \tag{2.17}$$

C_μ is a combination of constants and available flow parameters. More details on the $k-\epsilon$ model can be found in [23, Sec. 4.3.2].

In the derivation of the $k-\epsilon$ model, it is assumed that the flow is fully turbulent [24]. The model is known for its accuracy within flow types as modelled in this thesis. An alternative two-equation model which is also used in the industry is the $k-\omega$ model where the second transported value is the specific dissipation ω formulated by Wilcox[25, 26]. A revised version of the $k-\omega$ model is the $k-\omega$ Shear Stress Transport (SST) [27], which combines the $k-\epsilon$ and the $k-\omega$ model.

2.3.3 Free Surface Model

The calm water surface between the water and the air is called the free surface. It is important to model the free surface around the ship, as the generated waves on the free surface contributes to the total resistance on the ship, especially for high Froude numbers.

The free surface is modelled using the volume of fluid (VOF) method [28, p. 5337-5357]. The VOF model works by calculating the fraction of water and air in each cell. In cells where with both water and air, a weighted average of the density and viscosity is used, based on the volume fraction. The position of the free surface is the interface between cells with volume fractions of air larger than 50% and cells with volume fractions of water larger than 50%.

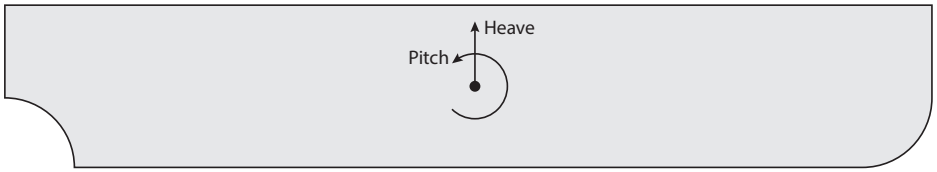

Figure 2.2: Heave and pitch motions of a ship. The black dot represents the longitudinal center of floatation. The direction of travel is left to right.

2.3.4 Fluid-Body Interaction

The interaction between the fluid and the ship is very important for the flow and the resistance on the hull. The two primary degrees of freedom (DOF) for ships in calm water are heave and pitch. The pitch and heave motions are illustrated in Figure 2.2.

The pitch and heave of the ship is dependent on the speed of the ship. At a certain speed the ship obtains a pitch and a heave through equilibrium of static and hydrodynamic forces acting on the ship. The equilibrium pitch and heave are called the dynamic pitch and heave.

The fluid-body interaction is modelling using a dynamic fluid-body interaction (DFBI) model in STAR-CCM+ [28, p. 5358-5433]. The DFBI model calculates the forces on the ship at certain intervals and translates and rotates a number of times the ship until the ship reaches an equilibrium. An adjustment i

2.3.5 Spatial Discretization

The domain is the spatial region in which the CFD simulation takes place. The domain is discretization by dividing it into small cells. The collection of all cells besides the boundary layer mesh in the domain is referred to as the volume mesh.

Geometry such as hull and propeller are inserted into the domain, in order to simulate the flow around the ship. The surfaces of these geometries are also discretized by dividing the surface into small triangular surfaces. The collection of the triangular surfaces is called the surface mesh.

It is important to model the boundary layer flow as it is used to calculate the frictional resistance on the ship. For the cases studied in this thesis, the Froude number are relatively low. The low Froude number causes the majority of the total resistance to be frictional resistance. A non-dimensional distance from a cell to the nearest wall is called the y^+ value. The y^+ value for the cells near the wall is called the wall y^+ value, and it is an indication of how well the boundary layer is discretized. The y^+value is defined as:

$$y^+ = \frac{u_* y}{\nu} \quad , \quad u_* = \sqrt{\frac{\tau_w}{\rho}} \tag{2.18}$$

where u_* is the frictional velocity, y is the distance to the nearest wall and τ_w is the wall shear stress. The boundary layer consists of three parts: the viscous sub layer ($y^+ < 5$), the buffer layer ($5 < y^+ < 30$) and the log-law layer ($30 < y^+ < 200 - 300$) [29, Chapter 2].

The boundary layer region is discretized using a boundary layer mesh. The boundary layer mesh consists of several layers of thin rectangular cells, these are also known as prism layers, on all surfaces of the ship. It is important to have a smooth transition in cell size from the boundary layer

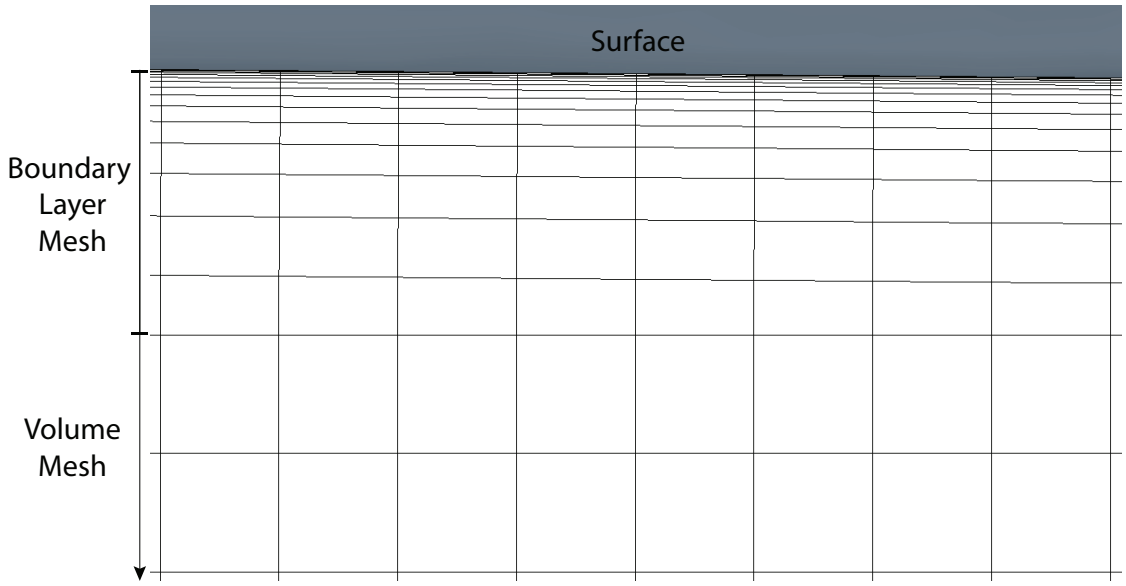

Figure 2.3: A boundary layer mesh near a surface.

cells to the volume mesh cells. Therefore, the nearer to the volume mesh the thicker he boundary layer cells are, and they increase in thickness with each layer. An example of the boundary layer mesh can be seen in Figure 2.3.

There are two approaches to model the boundary layer flow: fully resolving the boundary layer flow with sufficient cells or using a wall function to approximate the shear stress. If the wall y^+ value is sufficiently low (below 1), it means that there are sufficient cells to resolve the boundary layer flow all the way down to the viscous sublayer. This method requires more cells and therefore more computational effort. If the wall y^+ value indicates that the first cell is in the log layer (above 30), it means that there are no cells in the viscous sublayer alone. When the first cell includes part of the log layer, wall functions can be used to approximate the wall shear stress. Both methods will be used in this thesis.

When using wall functions, the CFD code STAR-CCM+ user guide advises using values larger than 30 [28, p. 3403]. The recommendation of [30] is wall y^+ value of 30 to 60 and [31, p. 35-36] recommends a wall y^+ value of 50. For all subsequent simulations which uses the method of wall functions, the aim is to use an average wall y^+ value in the range of 35 to 50.

2.3.6 Temporal Discretization

Some of the CFD simulations requires a transient solver. These include the VOF model, the DFBI model and the modelling of a rotating propeller. For all the simulations which requires a transient solver, a first order implicit unsteady solver is used. The size of the time step used for the transient solver is important. The time step size is a compromise between a small discretization error and computational resources.

CHAPTER 3

Method

This chapter describes the methods used in this thesis. The work of the thesis is based on a bulk carrier. The thesis consists of three elements: towing tank tests, sea trial tests and CFD simulations, all conducted on the bulk carrier. The towing tank tests and the CFD simulations each consists of resistance tests, open water tests and self-propulsion tests.

Firstly, the studied ship is presented in Section 3.1 followed by Section 3.2 which describes the method used for the towing tank tests and the extrapolation of the towing tank results. Secondly, the background of the sea trial is presented in Section 3.3 including the methods used to do the measurements and correct the results. Finally, Section 3.4 is devoted how the CFD simulations are set up for the resistance, open water and self-propulsion tests.

3.1 Ship

This section describes the ship studied in this thesis. The ship consists of a hull, a rudder, a propeller, a set of pre-swirl stator fins and bilge keels. The section has three subsections, each describing parts of the ship. The studied ship is a bulk carrier built by a Japanese shipyard. The main dimensions of the ship can be seen in Table 3.1.

3.1.1 Hull

The hull has been provided as a 3D geometry by the Japanese shipyard. The hull and water lines of the design and sea trial conditions is shown in Figure 3.2. The displacement of the ship in sea trial condition is 40.2 % of the displacement in the design condition. The sea trial condition is significantly lighter because the ship is completely empty, except for the ballast tanks. The coordinate system used throughout the thesis is shown in Figure 3.2. The z-direction is called the vertical direction, the y-direction is called the transverse direction and the x-direction is called the longitudinal direction.

Table 3.1: Main dimensions of the studied ship.

Length overall	L_{OA}	200 m
Beam	B	32.26 m
Design draft	T_{Design}	11.00 m
Design dead weight	DW_{Design}	62000 DWT
Design speed	V_{Design}	14.55 knots

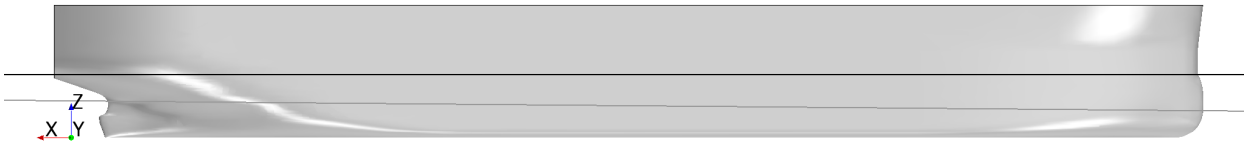

Figure 3.2: Hull geometry. The black line is the water line of the design condition, and the grey line is the water line of the sea trial condition. Seen from starboard side.

Table 3.3: Data of the actual propeller.

Diameter D	6.00 m
Boss ratio	0.1417
Pitch ratio (0.7r)	0.7284
Expanded area ratio	0.48
Number of blades	4
Direction of turning	Right handed

Table 3.4: Data of the stock propeller (No. 2141R).

Boss ratio	0.18
Pitch ratio (constant)	0.76
Expanded area ratio	0.55
Number of blades	4
Direction of turning	Right handed

3.1.2 Propeller

Two different propeller designs are associated with the ship: a stock propeller and an actual propeller. The stock propeller has a standard design and is only used for testing a model of the ship in a towing tank. The actual propeller is the propeller mounted on the actual ship. The data of the actual propeller can be seen in Table 3.3.

Due to confidentiality it has not been possible for the propeller manufacturer to provide the 3D geometry of the actual propeller. However, it has been possible for them to provide the 3D geometry of the stock propeller used in the towing tank test. Details of the stock propeller can be seen in Table 3.4, and the geometry can be seen in Figure 3.5.

The provided stock propeller geometry is not of sufficient quality to be used in CFD simulations. The leading and trailing edges of the propeller blades are flat, as opposed to rounded. The flat edges, especially the leading edge, significantly disturb the flows and cause separation. A propeller specialist from DNV GL has recreated the propeller blade based on the blade sections characteristics such as thickness, chamber, chord length etc. from the stock propeller. The recreated propeller geometry is based on the modified NACA 66 profile. An illustration of the original and recreated propeller profile can be seen in Figure 3.6. A modified hub and end cap have also been created with the same boss ratio as the original stock propeller. The modified stock propeller with hub and end cap can be seen in Figure 3.7.

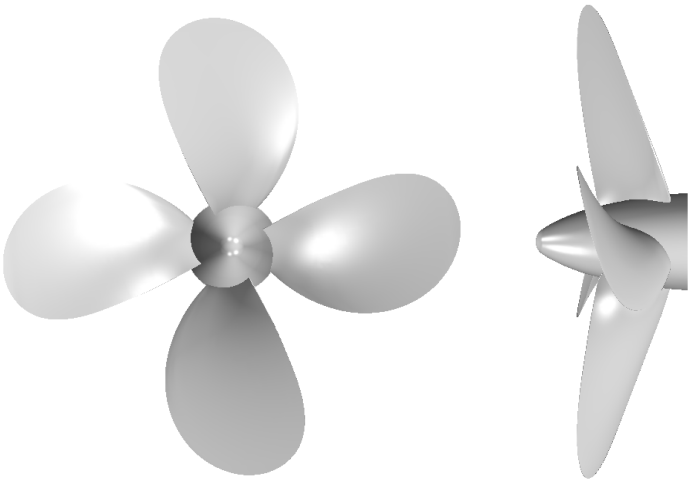

Figure 3.5: Original stock propeller geometry.

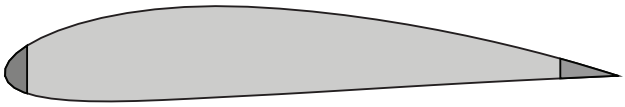

Figure 3.6: Illustration of the propeller profile. The provided stock propeller in light gray, and the recreated leading and trailing edges in dark grey. The recreated areas are exaggerated for the purpose of illustration.

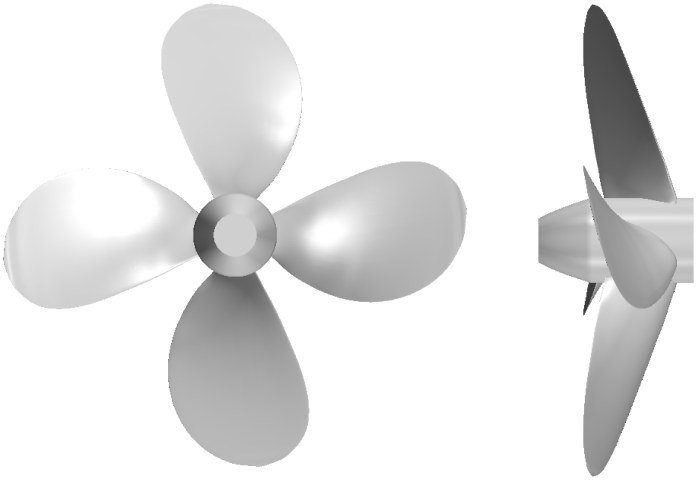

Figure 3.7: Modified stock propeller geometry.

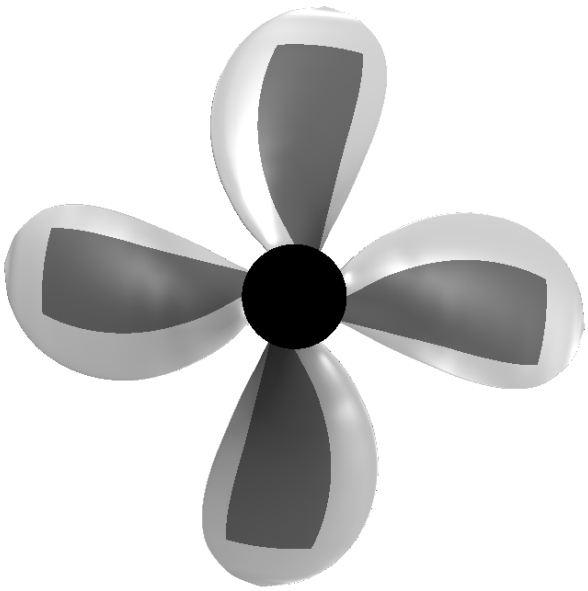

Figure 3.8: Definition of propeller parts. Light grey is the leading and trailing edges, dark grey is the suction and pressure sides, and black is the hub.

Table 3.9: Surface size settings of the surface wrapper for each of the three propeller parts.

Part of propeller	**Target surface size**	**Minimum surface size**
Leading and trailing edge	5.32×10^{-4} D	2.66×10^{-4} D
Suction and pressure side	5.32×10^{-3} D	5.32×10^{-4} D
Hub	1.06×10^{-2} D	1.06×10^{-3} D

The surface of the propeller geometry is wrapped in STAR-CCM+ in order to obtain a good surface mesh for for the CFD simulations. The propeller is divided into three parts; hub, blade surface and blade edges. The three parts can be seen in Figure 3.8. In ensure that the geometry is closed and has no sharp edges a function in STAR-CCM+ called surface wrapper is used. The settings of the surface wrapping are different for each of the three propeller parts. In order to correctly simulate the flow around the blade edges, it very important to resolve the important parts of the propeller geometry. The propeller is wrapped with the finest surface mesh around the blade edges, a coarser mesh around the blade surface, and the coarsest mesh around the hub. The surface wrapper uses a target surface size to control the intended size of the surface mesh, and a minimum surface size to prevent an excessive number of surface cells. The surface size settings can be seen in Table 3.9.

Two different versions of the propeller geometry are used; one version for the open water test and another for the self-propulsion test. The open water version can be seen in Figure 3.10, and the self-propulsion version can be seen in Figure 3.7. The difference between the two versions is the end cap. In the self-propulsion version, the end cap is cut off in order to have the correct gap between the end cap and the rudder bulb. In the open water version, the end cap is fully rounded.

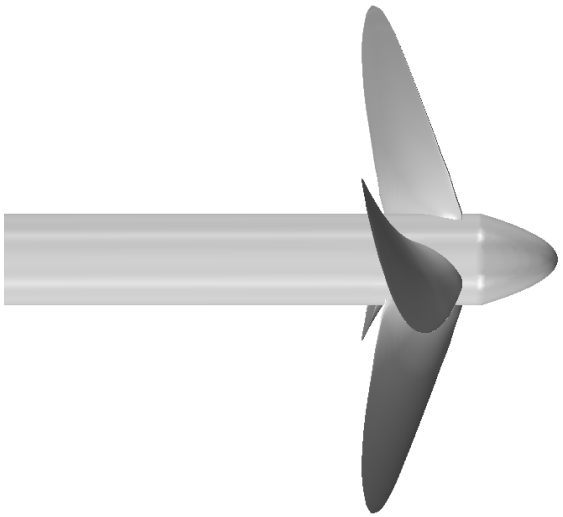

Figure 3.10: Propeller configuration of the open water test. The flow direction is right to left.

It is assumed that the cut-off of the end cap in the self-propulsion version has very little influence on the propeller performance since the end cap is downstream of the propeller blades. In the open water test, the end cap is upstream of the propeller blades and thereby has a significant influence on the flow field to the propeller. Therefore, the end cap is fully rounded in the open water version.

3.1.3 Appendages

The actual ship is mounted with a rudder, a number of upstream stator fins and bilge keels. The "to-be-built" 2D-drawings of the stator fins and rudder including rudder bulb have been provided by the Japanese shipyard. Based on these drawings, the stator fins and rudder geometry have been created in 3D, by the authors.

The stator fins are mounted upstream of the propeller. The idea behind the stator fins are to produce a so-called pre-swirl in the flow in the direction opposite of the propeller rotation direction. The stator fins increase the performance of the propeller since the propeller produces more thrust for the same power.

Bilge keels are not included in any CFD simulations since they are not mounted on the model ship in the towing tank test. They are instead accounted for in the towing tank and CFD simulations by other means.

3.2 Towing Tank Tests

The design of the ship has been tested in a Japanese towing tank prior to this project, using the ITTC procedure. The towing tank tests include a resistance test, an open water test and a self-propulsion test. The results of the towing tank test have been provided by the Japanese shipyard.

Table 3.11: List of the resistance test parameters provided by the towing tank.

Resistance Test	
Ship speed	V_m
Frictional resistance coefficient	$C_{Fm,Sh}$
Total resistance coefficient	C_{Tm}

All of the towing tank tests are conducted with rudder and pre-swirl fins mounted and in the sea trial condition.

In this section, the parameters of the towing tank tests are presented and discussed, and along with the procedure used to extrapolate the towing tank results from model scale to full scale.

3.2.1 Resistance Test

The resistance test is a test of the drag resistance of the ship at different speeds. The resistance test is conducted by dragging the test model through water while measuring the speed and the total resistance force on the model ship. In this case, the rudder and stator fins were mounted on the hull during the resistance test. The provided parameters of the resistance test can be seen in Table 3.11. The resistance test has been conducted at twelve different speeds.

The Froude number is calculated from the model scale ship speed V_m, and the waterline length of the model ship using eq. (2.4).

The frictional resistance coefficient is calculated using the Schoenherr line eq. (2.13). The Schoenherr line is not the recommended friction line in the ITTC procedure [17, Sec. 2.1], but has been used by this particular towing tank. From the results of the resistance test, the residual resistance coefficient is calculated using the form factor method [17, Sec. 3.6.1]:

$$C_R = C_{Tm} - (1 + k)C_{Fm,Sh} \tag{3.1}$$

The results of the resistance test are presented in Section 4.1.1.

3.2.2 Open Water Test

The open water test is a test of the propeller without the presence of the ship in a towing tank or cavitation tunnel where the performance of the propeller, also called the propeller characteristics, are measured. The test is usually conducted by measuring water inflow velocity V_0, thrust T_0, torque Q_0 and the rotation rate of the propeller n_0. It is conducted on the propeller alone, without the presence of the ship, which eliminates the interaction between the hull and the propeller. Results of the open water test for both the actual propeller and the stock propeller have been provided and can be seen in Table 3.12. The open water test of the actual propeller has been conducted at four different advance ratios while the open water test of the stock propeller has been conducted at eight different advance ratios.

Table 3.12: List of the open water test parameters provided by the towing tank.

Open Water Test	
Propeller Reynolds number	Re_p
Advance ratio	J_o
Thrust coefficient	K_{To}
Torque coefficient	K_{Qo}
Propeller open water efficiency	η_o

The open water test of the stock propeller has been carried out at a specific propeller Reynolds number Re_p. The rate of rotation of the propeller n_o is determined by the propeller Reynolds number using the following formula:

$$n_o = \frac{Re_p\,\nu}{D^2} = 17.59 \text{ rps} \tag{3.2}$$

The parameters of the open water test are defined in the ITTC Open Water procedure [32, Sec. 2.1]. The advance ratio of the propeller:

$$J_o = \frac{V_o}{n_o D} \tag{3.3}$$

The thrust coefficient:

$$K_{To} = \frac{T_o}{\rho n_o^2 D^4} \tag{3.4}$$

The torque coefficient:

$$K_{Qo} = \frac{Qo}{\rho n_o^2 D^5} \tag{3.5}$$

The open water propeller efficiency:

$$\eta_o = \frac{J_o K_{To}}{2\pi K_{Qo}} \tag{3.6}$$

The results of the open water test are presented in Section 4.1.2.

3.2.3 Self-Propulsion Test

The self-propulsion test is conducted similarly to the resistance test, but with the stock propeller mounted on the ship. The ship moves forward by rotating the propeller, which creates thrust. A towing force is also applied to the ship. During the self-propulsion test, the propeller thrust T, torque Q, and rotation rate along with the towing force are measured at a given speed. The

Table 3.13: List of the self-propulsion test parameters provided by the towing tank.

Self-Propulsion Test	
Ship speed	V_m
Total resistance coefficient	r_{Ts}
Thrust deduction	t
Advance ratio (thrust identity)	J_T
Wake fraction (thrust identity)	w_T
Relative rotative efficiency	η_R
Propeller open water efficiency	η_o

provided parameters of the self-propulsion test can be seen in Table 3.13. The self-propulsion test has been conducted at the same twelve speeds as the resistance test.

The resistance coefficients provided by the towing tank are normalized using two different methods. One normalization method is used for coefficients denoted with r, another for coefficients denoted with C. The two normalization methods are defined as:

$$C = \frac{R}{\frac{1}{2}\rho S V^2} \tag{3.7}$$

$$r = \frac{R}{\rho \nabla^{2/3} V^2} \tag{3.8}$$

where ∇ is the volume displacement. Coefficients normalized with one of the methods can be transformed to the other method,, as both the displacement and the wetted surface are known.

A towing force F_D is applied to the ship in the self-propulsion test. The towing force or skin correction force, as it is also called, is applied in order to compensate for the difference between the model scale and full scale frictional resistances. There are three different methods for applying the skin correction force [33, Sec. 3.4.1]: Load Varying (or Constant Speed) Method, Constant Loading Method, and Mixed Loading Method. In this case, the towing tank uses the Constant Loading Method. The skin correction force is given by [33, Sec. 2.1]:

$$F_D = \frac{1}{2}\rho_m S_m V_m^2((1+k)(C_{Fm} - C_{Fs}) - \Delta C_F) \tag{3.9}$$

where ΔC_F is the roughness allowance coefficient. This expression can be rewritten using eq. (3.7) and eq. (3.8).

$$F_D = \rho \nabla^{2/3} V^2 (r_{Tm} - r_{Ts}) \tag{3.10}$$

The model scale total resistance coefficient C_{Tm} is provided in the resistance test. This coefficient is renormalized into r_{Tm}. The full scale resistance coefficient r_{Ts} is provided in the self-propulsion test. Thereby, the skin correction force can be calculated using eq. (3.10).

The thrust of the self-propulsion test is calculated from the thrust deduction, the towing force, and the total resistance of the resistance test [33, Sec. 3.5]:

$$T_m = \frac{R_{Tm} - F_D}{(1-t)} \tag{3.11}$$

The towing tank uses the thrust identity method to derive additional parameters. The thrust identity method assumes that the thrust coefficient of the propeller behind the ship is equal to that of the open water test for a specific advance ratio [5, Sec. 8.7.4.3]. Using the thrust identity method and the parameters given by the towing tank, other parameters are calculated.

The wake fraction and the advance ratio, both derived using thrust identity, are given by the towing tank. Using these parameters, the rate of rotation of the propeller (n_m) is calculated [33, Sec. 3.5]:

$$n_m = \frac{V_m(1-w_T)}{J_T D} \tag{3.12}$$

The thrust coefficient is calculated using the thrust and the rotational rate of the propeller [33, Sec. 2.1]:

$$K_{Tm} = \frac{T_m}{\rho n_m^2 D^4} \tag{3.13}$$

The propeller open water efficiency and the relative rotative efficiency have been provided by the Japanese shipyard. The efficiency of the propeller in open water is defined in eq. (3.6), and the relative rotative efficiency is defined as [33, Sec. 3.5]:

$$\eta_R = \frac{K_{Qom}}{K_{Qm}} \tag{3.14}$$

The efficiency of the propeller behind the ship (η_b) is calculated using the propeller open water efficiency and the relative rotative efficiency:

$$\eta_b = \eta_o \eta_R \tag{3.15}$$

The propeller torque coefficient behind the ship (K_{Qm}) is calculated using:

$$K_{Qm} = \frac{J_T K_{Tm}}{2\pi\eta_b} \tag{3.16}$$

The results of the self-propulsion test are presented in Section 4.1.3.

3.2.4 Resistance Extrapolation

A variant of the form factor method has been adopted by the ITTC as the recommended procedure for extrapolating resistance tests from model scale to full scale. The current version of the extrapolation procedure is described in [10]. The form factor method assumes that the form factor is independent of the Reynolds number. The validity of this assumption is discussed in Section 2.2.4.

A resistance test is performed. The model scale total resistance coefficient and the form factor are obtained from the resistance test. The model scale frictional resistance coefficient is derived using a friction line. Based on the form factor, total and frictional coefficients, the residual resistance coefficient is calculated using the form factor method eq. (3.1).

The full scale ship speed is calculated using the Froude scaling law and the scaling factor:

$$V_s = V_m \sqrt{\lambda} \tag{3.17}$$

The full scale Reynolds number is calculated:

$$Re_s = \frac{V_s L_{WLs}}{\nu_s} \tag{3.18}$$

The total resistance coefficient in full scale without bilge keel and with smooth hull $C_{Ts,smooth}$ is given by this expression:

$$C_{Ts,smooth} = (1+k)C_{Fs} + C_R \tag{3.19}$$

The full scale total resistance coefficient, including hull roughness, air resistance, general correlation and added resistance of the bilge keel is given by [10, Sec. 2.4.1]:

$$C_{Ts} = \frac{S + S_{BK}}{S}\left((1+k)C_{Fs} + \Delta C_F + C_A\right) + C_R + C_{AAS} \tag{3.20}$$

where S_{BK} is the wetted surface of the bilge keels, C_A is the correlation coefficient, and C_{AAS} is the air resistance coefficient.

The full scale residuary resistance coefficient is assumed to be equal to the model scale residuary resistance coefficient for any specific Froude number as described in Section 2.2.

The full scale frictional coefficient is calculated using the ITTC-57 model-ship correlation line eq. (2.12).

The roughness allowance coefficient takes into account the additional roughness of the actual hull due to welding seams, fouling, anodes etc. The roughness allowance coefficient is given by [10, Sec. 2.4.1]:

$$\Delta C_F = 0.044\left(\left(\frac{k_s}{L_{WLs}}\right)^{\frac{1}{3}} - 10Re_s^{-\frac{1}{3}}\right) + 0.000125 \tag{3.21}$$

$$k_s = 150 \cdot 10^{-6} \text{ m}$$

where k_s is the Nikuradse's equivalent sand roughness. The value of k_s indicates the roughness of the hull surface. The ITTC procedure recommends a value of 150 μm if no data of the hull roughness exists.

The correlation allowance corrects for systematic errors in the extrapolation procedure. It is expressed as [10, Sec. 2.4.1]:

$$C_A = (5.68 - 0.6 \log Re_s) \cdot 10^{-3} \tag{3.22}$$

The air resistance coefficient takes into account the added air resistance of the full scale ship. It is given by [10, Sec. 2.4.1]:

$$C_{AAS} = C_{DA} \frac{\rho_A A_{VS}}{\rho_s S_s} \tag{3.23}$$

where C_{DA} is the air drag coefficient, ρ_A is the air density, A_{VS} is the projected frontal area above water, and S_s is the wetted surface of the hull and the rudder. The ITTC procedure recommends an air drag coefficient value of 0.8 as a default.

The extrapolated resistance results can be seen in Section 4.1.4.

3.2.5 Open Water Extrapolation

ITTC states that the self-propulsion extrapolation has to use the full scale open water characteristics[32]. The open water characteristics for the stock propeller have only been given in model scale and therefore have to be extrapolated to full scale. Several methods are avalible and these are discussed in [34]. The ITTC procedure for extrapolating the propeller characteristics of the open water test from model scale to full scale is described in [10]. The extrapolation is based on results from the open water test.

The local Reynolds number on the propeller blade at r/R equal to 0.7 $Re_{c0.7}$ is given by [32, Sec. 2.1]:

$$Re_{c0.7} = \frac{c_{0.7}(V_o^2 + (0.7\pi n D)^2)^{1/2}}{\nu_m} \tag{3.24}$$

where $c_{0.7}$ is the chord length at r/R equal to 0.7. The propeller drag coefficient in model scale C_{Dm} and full scale C_{Ds} are given by [10, Sec. 2.4.2]:

$$C_{Dm} = 2\left(1 + 2\frac{t_{0.7}}{c_{0.7}}\right)\left(\frac{0.044}{(Re_{c0.7})^{1/6}} - \frac{5}{(Re_{c0.7})^{2/3}}\right) \tag{3.25}$$

$$C_{Ds} = 2\left(1 + 2\frac{t_{0.7}}{c_{0.7}}\right)\left(1.89 + 1.62 \ln \frac{c_{0.7}}{k_p}\right)^{-2.5} \tag{3.26}$$

where $t_{0.7}$ is the maximum thickness of the propeller blade at r/R equal to 0.7, and k_p is the blade roughness. The ITTC procedure recommends a blade roughness value of $30 \cdot 10^{-6}$ m as

default. The default value is used in this extrapolation. The full scale thrust and torque coefficients are then calculated [10, Sec. 2.4.2]:

$$K_{Tos} = K_{Tom} + 0.3(C_{Dm} - C_{Ds})P/D\frac{cZ}{D} \tag{3.27}$$

$$K_{Qos} = K_{Qom} - 0.25(C_{Dm} - C_{Ds})\frac{cZ}{D} \tag{3.28}$$

where P/D is the pitch ratio and Z is the number of blades. The extrapolated open water results can be seen in Section 4.1.5.

3.2.6 Self-Propulsion Extrapolation

The procedure for extrapolating self-propulsion results from model scale to full scale are described in [10]. The extrapolation is based on results of the resistance test, the extrapolated resistance test and the self-propulsion test.

Firstly, the full scale wake fraction is calculated using [10, Sec. 2.4.3]:

$$w_{Ts} = (t + 0.04) + (w_{Tm} - t - 0.04)\frac{(1+K)C_{Fs} + \Delta C_F}{(1+K)C_{Fm}} \tag{3.29}$$

Then the full scale propeller load is calculated [10, Sec. 2.4.3]:

$$\frac{K_{Ts}}{J_s^2} = \frac{S_s}{2D_s^2}\frac{C_{Ts}}{(1-t)(1-w_{Ts})^2} \tag{3.30}$$

From the propeller load, the advance ratio and torque coefficient are interpolated from the full scale propeller characteristics of the actual propeller and the stock propeller. The interpolation is a linear interpolation between the two nearest data points of the propeller characteristics. The rate of rotation is given by [10, Sec. 2.4.3]:

$$n_s = \frac{(1-w_{Ts})V_s}{J_{Ts}D_s} \tag{3.31}$$

The delivered power of the ship P_{Ds} is given by [10, Sec. 2.4.3]:

$$P_{Ds} = 2\pi\rho D_s^5 n_s^3 \frac{K_{Qs}}{\eta_R} \tag{3.32}$$

$$\tag{3.33}$$

The extrapolated self-propulsion results can be seen in Section 4.1.6.

3.3 Sea Trial

A sea trial is a series of tests conducted in order to verify that the newly build ship meets the requirements of the contract, the classification society and the flag state. A sea trial consists of many tests. One of these tests is the speed trial, which is important for this thesis. The speed trial is a test of the speed at which the ship is able to sail with a certain output of the main engine. In this thesis, the results of the speed trial provide an opportunity to compare the performance of the actual full scale ship with results from the towing tank and the CFD simulations.

This section will firstly describe the sea trial method briefly. Furthermore, the measurements and corrections subsequently will be described in more detail with the measurements and corrections.

3.3.1 Speed Trial

Four sister ships of the same design have been built in total. Speed trials have been conducted for each of the four sister ships. In 2015, the International Maritime Organisation (IMO) and ITTC released ISO15016:2015 [4], an updated version of the ISO 15016:2002 standard procedure for carrying out and correcting speed trials. The speed trial of the fourth ship has been conducted mostly as described in [4]. The speed trials of the three other ships have been conducted prior to the release of that procedure, but is assumed to have been conducted using similar procedures.

The speed trial is conducted at a number of different speeds and using double runs for each speed. Double runs refer to the method of conducting one speed run, turning 180 the ship degrees and conducting a second speed run. The data gathered from a speed trial are the measured power from the main engine and the speed of the ship.

The Japanese shipyard has provided the results of these speed trials for all four ships. Furthermore, the authors were attending the sea trial of the last sister ship. This gave he authors the opportunity to experience how a speed trial is conducted, the measurements performed, and factors influencing the speed trial causing uncertainties.

The main measurements in the speed trial are speed, propeller rate of rotation, and the engine power. After the speed trial, the measurements are corrected for the environment forces to the final results.

3.3.2 Speed Measurement and Corrections

The speed of the ship during the speed trial is measured using a Differential-GPS (DGPS). There is already a DGPS installed on board, but a temporary and more precise DGPS is installed on top of the bridge during the sea trial. The temporary DGPS is connected to a laptop on the bridge of the ship. From the DGPS data, the ship speed over ground is calculated by assuming no lateral drift. The ship speed is recorded during each speed run, with a sampling frequency of about 1 Hz. From the recorded data, a mean ship speed is calculated.

The speed over ground signal is visually inspected, showing only minor fluctuation. Based on observations, it is concluded that the speed signal is reliable and that the mean is a good measurement of the actual speed over ground of the ship. To obtain the speed through water, the speed measurement has to be corrected for current.

Tidal Current Correction

The speed measured by the DGPS is the speed over ground. The measured speed is corrected for the tidal current in order to obtain the speed through water. The location of the speed trial has significant tidal current. A tidal current curve is used to calculate the speed of the tidal current in the east-west direction as a function of time. The origin of the tidal current curve is unknown to the authors. The tidal current is subtracted from the measured speed, which gives the speed though water. The tidal current curve shows that the tidal current varies by more than two knots in the time period of the speed trial. A speed correction of this magnitude is significant. To minimize the influence of the tidal current and possible discrepancies in the tidal current speed curve, the speed trial is conducted using two runs: one in the direction against the current and one with the current.

3.3.3 Power Measurement and Correction

The power of the engine is calculated from the engine rate of rotation and the amount of fuel injected (fuel index) using a formula provided by the engine manufacturer Mitsui. Both the rate of rotation and the fuel index are sampled directly from the engine control system. The RPM of the engine is measured directly on the shaft, and there is no gear box. The engine manufacturers formula for calculating the engine power is:

$$\begin{aligned} P &= C_{cyl} \cdot C_{eng} \cdot \omega \cdot p_{me} \\ C_{cyl} &= 5.339 \text{ m}^3 \\ C_{eng} &= \frac{60}{2\pi} \cdot 10 \cdot 0.7355 \cdot 10^{-3} \end{aligned} \tag{3.34}$$

Where P is the engine power, C_{cyl} is a cylinder coefficient provided by the engine manufacturer, C_{eng} is an engine constant also provided by the engine manufacturer, ω is the rate of rotation, p_{me} is the mean effective pressure, and FI is the fuel index. The mean effective pressure is calculated from the fuel index FI, which is indicating the amount of fuel injected, using a linear relation. The linear relation is also given by the engine manufacturer:

$$p_{me} = 19375FI - 105938 \tag{3.35}$$

The values of the constants in eq. (3.34) and eq. (3.35) are given by the engine manufacturer. It can be difficult to create a good model of the power output of an engine. The uncertainties of the engine formula are not easily quantified so the accuracy of the engine formula is not known, and neither can it be compared to other methods of measuring the engine power.

ISO 15016:2015 states that the power has to be measured using a torque meter mounted directly on a shaft. Such a device is also installed, but the measurements are not used in the speed trial results.

Displacement correction

The measured power is corrected for the difference between the planned and the actual displacement of the ship [4, Annex H]. The planned displacement of the ship in sea trial condition is calculated

before conducting the sea trial, and the actual displacement is measured at the beginning of the sea trial. The correction is conducted by the shipyard. The difference in displacement for the sea trial used in this thesis is very small. Therefore the correction of the power is also very small.

Wind Correction

The performance of the ship is corrected for the added wind resistance [4, Annex C]. The wind correction is based on an estimated drag coefficient, an estimated projected front area and a relative wind speed. The relative wind speed cannot be measured directly and is therefore found by subtracting the vessel velocity from the absolute wind velocity. The absolute wind velocity is measured by a wind anemometer.

The wind anemometer is placed above the bridge, just behind a rotating rectangular radar. The authors estimate that the wind anemometer is not significantly influenced by the super structure if the absolute wind direction is from the front. It is estimated by the authors that the wind measurements might be influenced by the rotating radar, especially when the wind direction is from the starboard side.

Wave Correction

The results of the speed trials are not corrected for waves. The speed trial procedure ISO15016:2015 specifies that the speed trial data should be corrected for waves [4, Sec. 7.3]. In this case, the Japanese shipyard and the ship owner agreed not to correct for waves. Omitting the wave correction gives a conservative estimate on the performance.

A simplified method for power correction due to waves is described in [4, D.1]. This method is used to correct the speed trial results for weather waves. The method requires significant wave height and direction of the waves. These two parameters were not recorded during any of the sea trials of the four sister ships. Instead, the parameters have been provided by Eirik Eisinger from DNV-GL. Eirik Eisinger is writing his master's thesis [35] at DNV-GL in Høvik in the spring of 2016. In Eisinger's thesis, ERA-Interim data [36] is used. The ERA-Interim data is based on satellite weather data and a meteorological model. The provided significant wave heights Hs and wave directions is a mean value of a 6 hour window. It was shown that significant wave height data has a relatively low uncertainty, but the wave direction has a relatively high uncertainty. The uncertainties are acceptable since the magnitude of the wave corrections are relatively small.

The added resistance due to waves R_{AWL} is estimated using following formula [4, D.12]:

$$R_{AWL} = \frac{1}{16}\rho_s g(Hs)^2 B\sqrt{\frac{B}{L_{BWL}}} \tag{3.36}$$

L_{BWL} is the distance from the ship bow to 95% of the maximum beam on the water line, as illustrated in Figure 3.14.

The power will be corrected with the power correction due to waves P_W:

$$P_W = R_{AWL}V_s$$

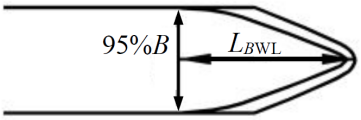

Figure 3.14: Definition of L_{BWL}, the distance from the ship bow to 95% of the maximum beam on the water line. [4, Figure D.2]

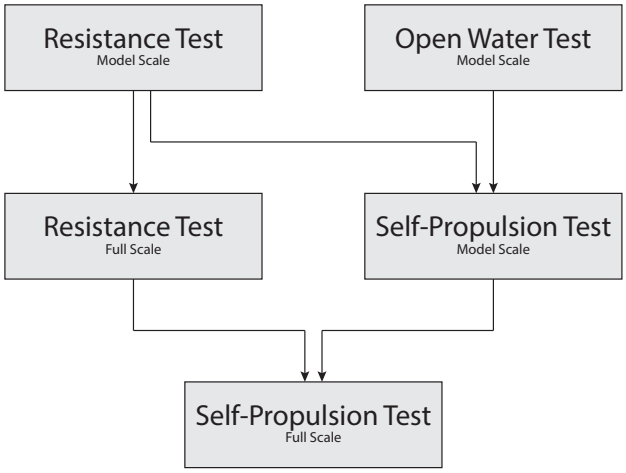

Figure 3.15: The five CFD setups. The arrows indicate the direction of the work flow.

This method has several restrictions. First of all, it is only applicable if the significant wave height satisfies the following criterion:

$$H_s \leq 2.25\sqrt{L_{PP}/100} \tag{3.37}$$

Furthermore, the pitch and heave of the ship must be small (vertical acceleration at the bow must to be less than $0.05g$). The correction is only applied if the wave direction is from ahead (from $0°$ to $\pm 45°$). The fact that waves within $45°$ degrees result in full correction and waves not within $45°$ result in no correction shows that the correction method is very coarse. Other wave correction methods are described in [4].

3.4 CFD

This section describes the CFD setups developed and used in this project. All CFD simulations in this project are performed in the commercial CFD-code STAR-CCM+ v.10.04.011 from CD-Adapco. The code is widely used in the marine industry and is well-known for its capabilities within marine applications.

In total five CFD setups are developed: model scale resistance setup, full scale resistance setup, open water setup, model scale self-propulsion setup, and full scale self-propulsion setup. The five CFD setups can be seen in Figure 3.15.

In the beginning of the project period, it was not known if the rudder and stator fins were included in the towing tank tests. Furthermore there has been some doubt about the provided drawings of the stator fins as the angles of attack of the fins are much higher than what is normally encountered by the authors and experts at DNV-GL. Therefore, the rudder and stator fins are not included in some of the CFD simulations. Later, it was confirmed from the shipyard that the rudder and stator fins were mounted in all towing tank tests and that the specifications of the stator fins were correct. Therefore, there are differences between the appendages used in some of the CFD simulations and the towing tank tests to which they are compared. These differences are mentioned when they occur.

3.4.1 Validation and Convergence Test

It is essential to trust a CFD setup before conclusions are based on the results of the setup. Several methods are used in this thesis to gain trust in the CFD setup. Both convergence studies and comparison studies are performed, where possible. This section explains the details of the methods used.

A convergence study is conducted on a CFD setup in order to determine the spatial (See Section 2.3.5) and temporal (See Section 2.3.6) discretization settings of the setup. The discretization settings are a balance between minimizing the discretization error and using the least amount of computational effort.

A convergence study is conducted by creating a series of simulations from the same CFD setup. The simulations are identical in all respects, except for either the spatial or the temporal discretization. The discretization is changed for each simulation, creating a series of simulations with a range in the discretization from coarse to fine. The solution of the simulations are expected to converge towards a certain value as the discretization becomes finer because the discretization error is minimized. From the results of the series of simulation the balance between the accepted discretization error and the computational effort is determined.

In total, three different types of convergence studies are conducted in this thesis: boundary layer mesh convergence study, volume mesh convergence study, and time step convergence study. These studies determine the discretization settings of the boundary layer mesh, the volume mesh and the time step respectively.

After the convergence study, the CFD results are compared to experimental data, if available. If the CFD results show convergence and are similar to experimental measurements, the CFD setup is considered validated. A validation does not mean that the all results from the setup can be trusted, but it is a good indication of the trustworthiness. The more cases the setup is validated for, the more the CFD setup can be trusted.

3.4.2 CFD Resistance Test

This section documents the CFD setup of the calm water resistance test, both in model scale and in full scale. First, the model scale CFD setup is created and validated by comparing results with the towing tank results. The validated model scale setup is then modified to a full scale setup. Convergence studies are conducted in both the model and full scale setup. Results of the full scale CFD setup are compared with the extrapolated resistance data from the towing tank data.

Table 3.17: Domain size of the CFD resistance setup.

Longitudinal length	5 L_{PP}
Vertical length	3 L_{PP}
Transverse length	1.5 L_{PP}

All resistance simulations are performed in the sea trial condition (see Section 3.1.1) similarly to the towing tank test.

The initial CFD setup used to estimate the calm water resistance is an automated CFD setup developed by OSK-ShipTech A/S. CFD Specialist Stig Staghøj Knudsen from OSK-ShipTech A/S has accepted the use of the setup in this thesis. The author Henrik Mikkelsen has worked extensively with the setup both in the development and validation phases during his employment at OSK-ShipTech A/S. The automated setup is a set of Java-scripts which can be played as a macro in STAR-CCM+.

Model Scale Resistance

The CFD setup presented in this section simulates the resistance test in model scale.

Physics The CFD resistance setup uses a number of different physics models to simulate the flow around the ship. The physics models used for the model scale resistance setup are briefly discussed here. For more details on the models, see Section 2.3.

The setup uses the k - ϵ two-equation model to model the turbulence of the flow. Free surface waves are modelled using volume of fluid. The hull is allowed dynamic pitch and heave motions, by use of the DFBI model, as described in Section 2.3.4. In order to model the free surface waves and the dynamic pitch and heave, a transient solver is required. The simulations are solved using a 1st order implicit unsteady solver.

Domain The domain of the simulation is the spatial region in which the simulation takes place. The shape of the domain is a rectangular box. Since the propeller is not present, it is reasonable to assume that the flow around the hull is symmetrical, with a vertical plane dividing the port and starboard sides. Due to this assumption, only the starboard side or port side of the ship needs to be simulated. This halves the number of cells in the mesh, which reduces the computing time significantly. The domain can be seen in Figure 3.16. The size of the domain as function of length between perpendiculars L_{PP} can be seen in Table 3.17, and the boundary conditions can be seen in Table 3.18.

Spatial Discretization The volume mesh consists of hexahedrons in a structured grid. The mesh is generated using the trimmer-mesh function in STAR-CCM+. Boundary layer mesh is used on the hull surface in order to make a good estimation of the shear stresses on the hull.

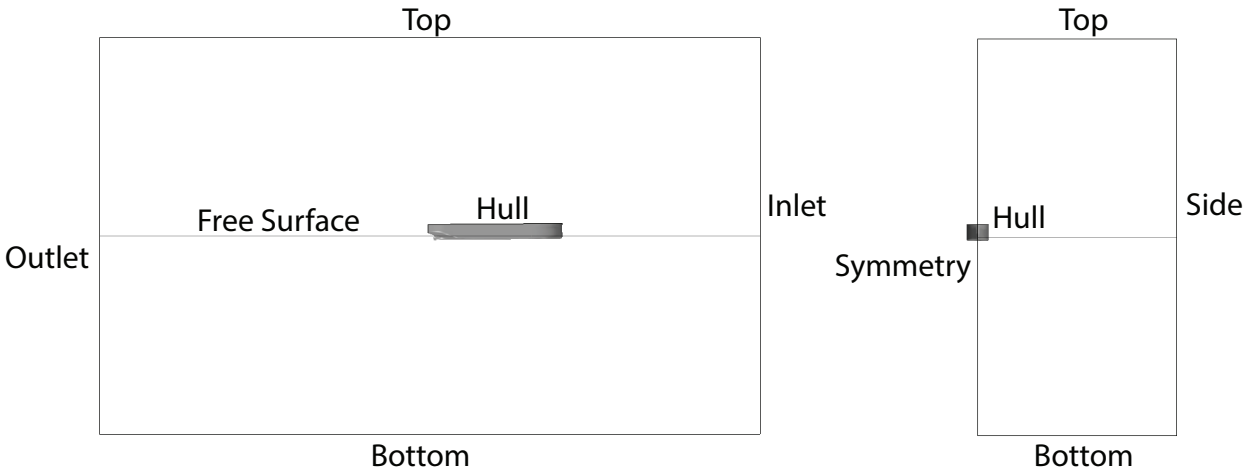

Figure 3.16: Domain of the resistance setup, with boundary names. Seen from starboard side (left) and from the front (right).

Table 3.18: Boundaries and boundary conditions of the CFD resistance setup.

Name of Boundary	**Boundary Condition**
Inlet	Velocity inlet, prescribed with V_m
Top	Velocity inlet, prescribed with V_m
Bottom	Velocity inlet, prescribed with V_m
Outlet	Pressure outlet
Symmetry	Symmetry plane
Side	Symmetry plane
Hull	No-slip wall

Table 3.19: Refinement zones of the CFD resistance setup.

Name of RZ	**Refinement Direction**
Far Free Surface RZ	Longitudinal and transverse
Middle Free Surface RZ	Longitudinal and transverse
Near Free Surface RZ	Longitudinal and transverse
Bulbous Bow RZ	All
Transom RZ	All
Vertical Free Surface RZ	Vertical

Six refinement zones (RZ) are used to refine the mesh in important regions. These six refinement zones can be seen in Table 3.19, Figures 3.20 and 3.21. The purpose of the far, middle, near and vertical free surface refinement zones is to resolve Kelvin waves. The theory behind the Kelvin waves is briefly presented in Section 2.1. The bulbous bow and transom refinement zones ensures sufficient resolution of the flow at the bow and stern. The refinement direction and cell size of the refinement zones can be seen in Table 3.19.

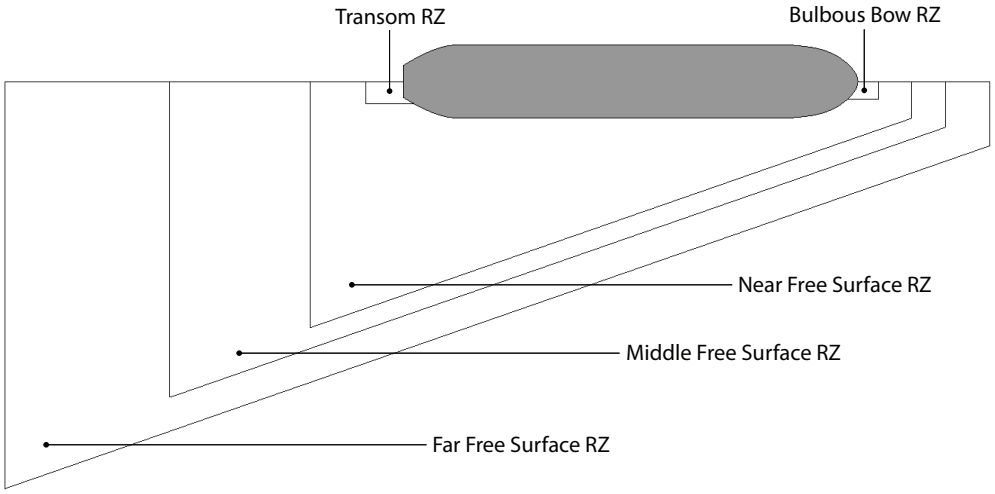

Figure 3.20: The far, middle, near, bulbous bow and transom refinement zones of the CFD resistance setup. Seen from the top.

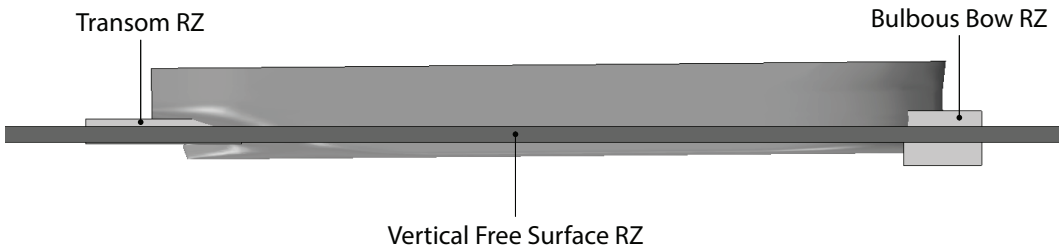

Figure 3.21: The vertical free surface, bulbous bow and transom refinement zones of the CFD resistance setup. Seen from starboard side.

Table 3.22: Appendages used in the model scale CFD resistance studies.

Study	With Rudder	With Stator Fins
Boundary Layer Mesh Convergence	No	No
Volume Mesh Convergence	No	No
Time Step Convergence	No	No
Comparison	Yes	No

Table 3.23: Appendages used in the full scale CFD resistance studies.

Study	With Rudder	With Stator Fins
Volume Mesh Convergence	No	No
Time Step Convergence	No	No
Comparison	Yes	No

Studies Four simulation studies have been conducted using the model scale resistance setup: a boundary layer mesh convergence study, a volume mesh convergence study, a time step convergence study and a comparison with the results of the towing tank resistance test. The appendages mounted on the hull is different in the four setups, and can be seen in Table 3.22.

The results of the model scale resistance studies can be seen in Section 4.3.1.

Full Scale Resistance

The full scale resistance setup is created by scaling up the model scale resistance setup with the scaling factor (2.3). Three studies have been conducted on the full scale resistance setup: volume mesh convergence study, time step convergence study and a comparison with the extrapolated resistance test from the towing tank. The appendages mounted on the hull is different in the three setups are shown in Table 3.23.

3.4.3 CFD Open Water Test

This section documents the CFD setup of the model scale open water test of the stock propeller. The stock propeller is described in Section 3.1.2. Modelling the open water test using CFD is less complex than modelling the self-propulsion test using CFD because the hull-propeller interaction is not included in the open water setup. The idea is that a separately validated resistance and open water setup can be combined to a self-propulsion setup. This self-propulsion setup can then be validated in model scale by comparing it with self-propulsion results from towing tank tests.

Physics

The setup uses the k - ϵ turbulence model. A single phase with the properties of water is used in the open water setup. For details on the physics models used in this thesis, see Section 2.3.

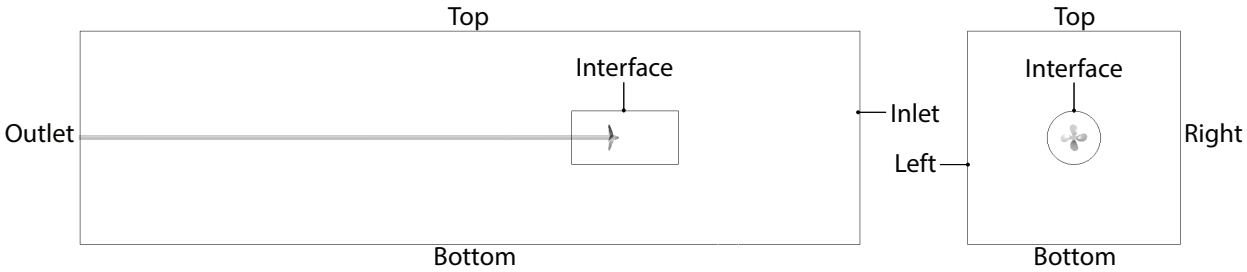

Figure 3.24: Domain of the CFD open water setup, with boundary names. Seen from the side (left) and from the front (right).

Table 3.25: Domain size of the CFD open water setup.

Stationary Domain	
Upstream length	9D
Downstream length	20D
Vertical length	8D
Transverse length	8D
Rotating Domain	
Upstream length	2.5D
Downstream length	1.5D
Diameter	2D

Table 3.26: Boundary conditions of the CFD open water setup.

Name of Boundary	**Boundary Condition**
Inlet	Velocity inlet equal to V_o
Outlet	Pressure outlet
Top	Symmetry plane
Bottom	Symmetry plane
Left	Symmetry plane
Right	Symmetry plane
Interface	Wall and internal interface
Shaft, Blades, Hub	No-slip wall

Domain

The open water setup uses two domains: A stationary domain and a rotating domain. The two domains are connected by an interface. The shape of the stationary domain is a rectangular cubeoid. The shape of the rotating domain is a cylinder which is located inside the static domain and around the propeller. A illustration of the domains can be seen in Figure 3.24. The size of the domains can be seen in Table 3.25, and the boundary conditions of the domains can be seen in Table 3.26. The size of the domains are determined, based on experience from experts at DNV-GL.

Table 3.27: Refinement zones of the CFD open water setup.

Name of RZ	Refinement Direction
Far Propeller RZ	All
Near Propeller RZ	All

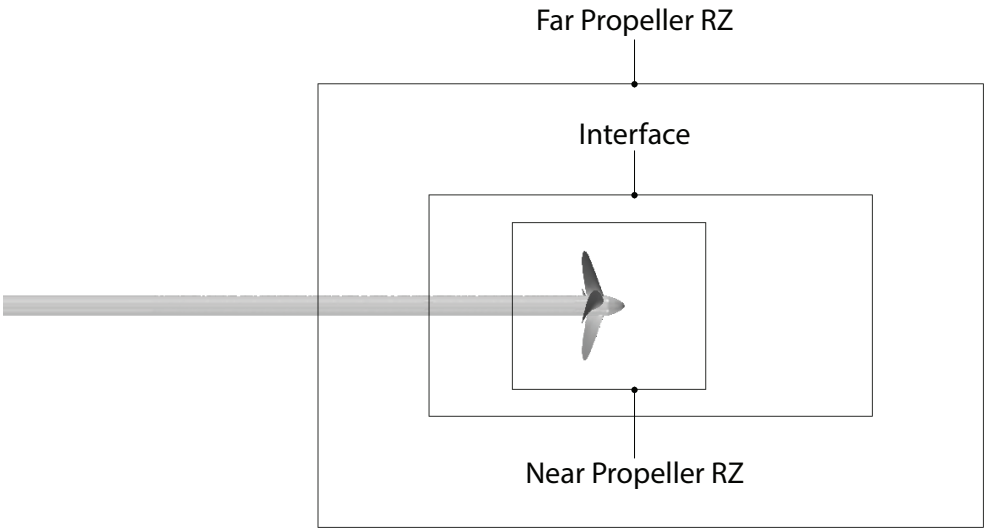

Figure 3.28: The far and near propeller refinement zones of the open water setup. Seen from the side.

Spatial Discretization

The volume mesh consists of hexahedrons in a structured grid. Boundary layer mesh is used on the shaft, blades and hub.

In order to better resolve the flow around the propeller, two refinement zones are used to refine the mesh in the volume around the propeller. The two refinement zones are illustrated in Table 3.27 and Figure 3.28. The near propeller refinement zone generates a finer mesh than the far propeller refinement zone.

Propeller Rotation

The rotation rate of the propeller in the open water setup is equal to the setup used in the open water test of the towing tank. The rotation rate of the open water test is defined in eq. (3.2).

The propeller movement can be modelled using different two methods: the moving reference frame method (MRF) or the rotating solid body method (RSB).

MRF works by adding a rotational velocity component to the flow in the rotating domain while the propeller geometry is held stationary. The added rotational velocity component V_θ can be expressed as function of the rotational rate and the radial distance from the propeller center r:

$$V_\theta = 2\pi nr$$

MRF can be simulated using a steady-state solver and it has a faster convergence compared to the rotating solid body method, which requires a transient solver.

RSB works by rotating the propeller geometry in increments at each new time step. This method requires more computational time, but is a better model of the actual propeller physics compared to the MRF method. The RSB method models the hull-propeller interaction while the MRF model does not.

The two methods can be combined for computational efficiency. The first step in the combination approach is to firstly accelerate the flow using MRF. When the simulation has converged, it is changed to the more precise and computational heavy RSB and continued until it converges again. The combination of methods saves a significant amount of computational time.

Both simulations using MRF and the combination approach have been performed. It is concluded from the results of these simulations that the increased accuracy of using the combination of methods is negligible for the open water simulations, compared to using only MRF. Therefore, it is decided only to use MRF for all open water simulations in order to save computational time.

Studies

Two simulation studies have been conducted with the open water setup: a volume mesh convergence study and a comparison with the open water test from the towing tank. The results of the open water simulations can be seen in Section 4.3.2.

3.4.4 CFD Self-Propulsion Test

The following sections present the background for the self-propulsion simulations. The first section describes the simulations in model scale and it is followed by a section describing the changes made from the model scale setup to the full scale setup.

Model Scale Self-Propulsion

This section describes the CFD setup that simulates the calm water self-propulsion test in model scale. The setup is created by combining the model scale resistance CFD setup (see Section 3.4.2) with the propeller and the open water CFD setup (see Section 3.4.3).

Physics The physics of the self-propulsion setup is similar to the physics of the resistance setup, but some changes are made. For details on the physics models used in this project see Section 2.3.

The setup uses the k - ϵ turbulence model. Based on the experience from DNV-GL, it has been decided not to model the free surface waves using the VOF model. Experience from DNV-GL shows that including the VOF model in the self-propulsion setup causes large fluctuations in the resistance, thrust and torque signals. The magnitude of these fluctuations is so large that the fluctuations make it difficult to obtain reliable signals.

Without the free surface waves, it is not possible to model the dynamic pitch and heave of the ship using the DFBI model. This is because the DFBI model works by balancing the forces acting

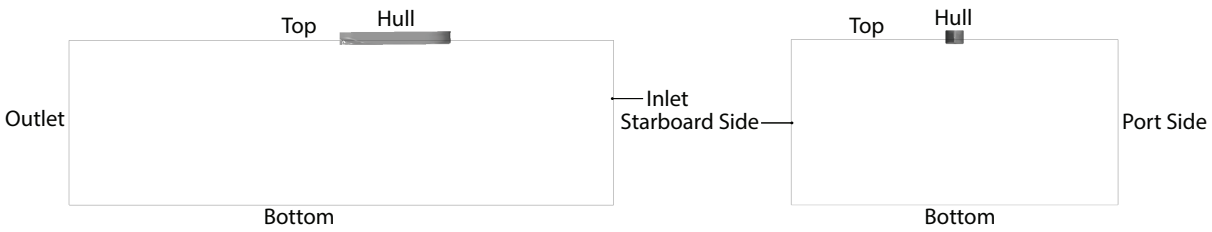

Figure 3.29: Static domain of the self-propulsion setup, with boundary names. Seen from starboard side (left) and from the front (right).

Figure 3.30: Rotating domain of the self-propulsion setup. Seen from starboard side.

on the ship. Without the free surface waves, the wave forces on the ship are not modelled, and the DFBI can not correctly balance the forces. Therefore the DFBI model is not included in the self-propulsion setup.

Instead of modelling the dynamic pitch and heave using the DFBI model, the dynamic pitch and heave of the resistance simulations are prescribed to the self-propulsion simulations before they are simulated. The influence of the propeller dynamics on the dynamic pitch and heave of the ship is neglected by using the dynamic pitch and heave of the resistance simulations instead of using the DFBI model in the self-propulsion simulations. Neglecting this influence introduces a modelling error which has not been quantified, but is assumed to be smaller than other modelling errors.

Domain As in the open water setup, the self-propulsion setup uses two domains; a large static domain, with a small rotating domain inside. The shape of the static domain is a rectangular cubeoid, and the shape of the rotating domain is a cylinder.

The static domain can be seen in Figure 3.29. The size of the domains can be seen in Table 3.31, and the boundary conditions of the domains can be seen in Table 3.32.

The static domain of the self-propulsion setup includes both the port and starboard sides of the domain. This is different from the resistance setup, where only one side is simulated while the opposite side is accounted for using a symmetry plane. The reason for simulating both sides in

Table 3.31: Domain size of the CFD self-propulsion setup.

Stationary Domain	
Longitudinal length	5 L_{PP}
Vertical length	3 L_{PP}
Transverse length	3 L_{PP}
Rotating Domain	
Upstream length	$0.11D$
Downstream length	$0.23D$
Diameter	$1.20D$

Table 3.32: Boundary conditions of the CFD self-propulsion setup.

Name of Boundary	**Boundary Condition**
Inlet	Velocity inlet, prescribed with V_m
Bottom	Velocity inlet, prescribed with V_m
Outlet	Pressure outlet
Top	Symmetry plane
Starboard Side	Symmetry plane
Port Side	Symmetry plane
Interface	Wall and internal interface
Hull, Shaft, Blades, Hub	No-slip wall

the self-propulsion setup is because propeller flow is unsymmetrical. Therefore, the self-propulsion calculations are not modelled using a symmetry plane in the center line.

Without the use of the VOF model, the self-propulsion setup only needs to model the water phase of the flow. Therefore the top of the static domain of the self-propulsion setup is at the free surface, and is prescribed with a symmetry plane boundary condition.

Removing the free surface waves from the simulations gives rise to another problem. In reality, a stern wave is created by the ship. The stern wave increases the water height above the propeller, fully submerging the propeller even at low draft conditions such as the sea trial condition. Without the free surface waves, the propeller is not fully submerged. In order to fully submerge the propeller in the self-propulsion setup, the free surface is raised approximately 3% of the draft in the sea trial condition.

Free Surface Correction The decision not to model the free surface waves and to raise the calm water surface decreases the measured resistance on the ship. In order to compensate for this change, a free surface correction is performed on the results of the self-propulsion simulations. The correction is performed in two steps. The free surface correction procedure is shown in Figure 3.33.

The first step is to correct for not modelling the free surface waves, which reduces the hull resistance by removing the wave making resistance. The wave making resistance is quantified by simulating the resistance setup both with and without the free surface waves. The difference between those two results is the wave making resistance:

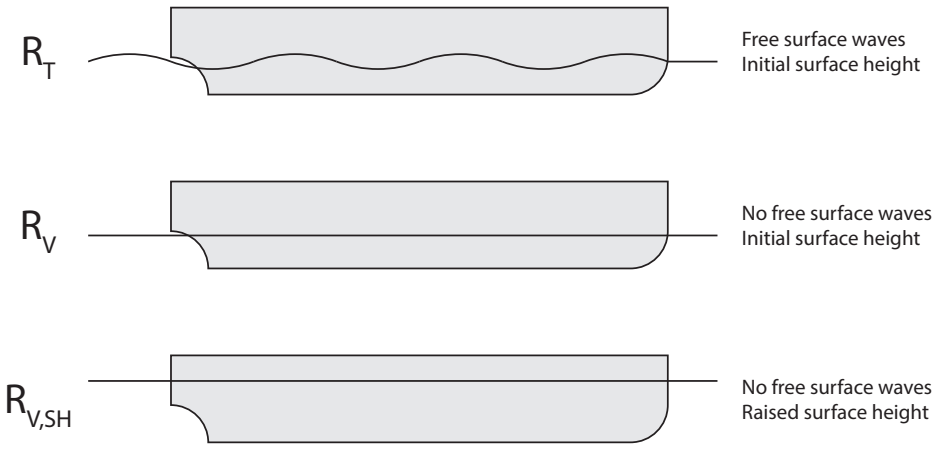

Figure 3.33: The three simulation setups of the free surface correction procedure.

$$R_{Wm} = R_{Tm} - R_{Vm} \tag{3.38}$$

where R_{Wm} is the wave making resistance and R_{Vm} is the total resistance without free surface waves, also referred to as the viscous resistance.

The second step is to correct for the raised free surface which increases the resistance on the hull, because a larger surface area is submerged. The increase in resistance is quantified by simulating the resistance CFD setup both with the initial and the raised surface heights. The difference between those two results is the added resistance due to the raised surface ΔR_{SHm} given by:

$$\Delta R_{SHm} = R_{Vm,SH} - R_{Vm} \tag{3.39}$$

The resistance of the self-propulsion simulations can then be corrected for wave making resistance and added resistance due to the raised surface height:

$$R_{Tm} = R_{Vm,SH} + R_{Wm} - \Delta R_{SHm} \tag{3.40}$$

Spatial Discretization The self-propulsion setup uses two separate meshes; one for the stationary domain and one for the rotating domain around the propeller. Using two separate meshes allows mesh options from the resistance setup to be used for the static domain and mesh options from the open water setup to be used for the rotating domain.

Four mesh refinement zones are used in the self-propulsion setup. The four refinement zones can be seen in Table 3.34 and Figure 3.35.

Propeller Rotation Two different methods or a combination of them can be used to model the rotation of the propeller. The two methods are the moving reference frame method (MRF) and the rotating solid body method (RSB). The methods are described in Section 3.4.3.

Table 3.34: Refinement zones of the CFD self-propulsion setup.

Name of RZ	Refinement Direction
Bulbous Bow RZ	All
Transom RZ	All
Far Propeller RZ	All
Near Propeller RZ	All

Figure 3.35: The four refinement zones of the self-propulsion setup. Seen from starboard side.

For the self-propulsion simulations a combination of the two methods is used. The modelling of the propeller rotation is initialized by using the MRF method, followed by the RSB method.

In the self-propulsion tests, a towing force is applied to the model ship, as described in Section 3.2.3. The CFD self-propulsion setup is carried out using the same principle. The forces on the model ship must be balanced, which leads to this expression:

$$R_{Tm} = T_m + F_D \tag{3.41}$$

The towing force has been provided by the towing tank and is defined in eq. (3.10). The corrected total resistance is calculated from eq. (3.40). The thrust is adjusted by changing the propeller rotation rate during the simulation until the forces are in balance.

In total, the self-propulsion simulation uses three stages. First, the simulation is initialized using MRF. Next, the RSB which changes the propeller rotation rate in order to balance the forces is applied. Lastly, the propeller rotation rate is frozen at the force equilibrium and the simulation is continued using RSB for one whole rotation. The three stages of the self-propulsion simulation are illustrated in Figure 3.36.

Temporal Discretization The self-propulsion setup requires a transient solver in order to simulate the rotation of the propeller. An unsteady implicit solver with a first-order scheme is used.

Figure 3.36: The three stages of the CFD self-propulsion simulations.

Table 3.37: Appendages used in the model scale CFD self-propulsion studies.

Study	With Rudder	With Stator Fins
Time Step Convergence	Yes	No
Volume Mesh Convergence	Yes	No
Comparison	Yes	Yes

The choice of time step size is based on the physics of the propeller rotation. The time step can therefore be expressed in terms of the number of degrees the propeller rotates between two time steps:

$$\Delta\theta = n \cdot \Delta t \cdot 360^\circ \tag{3.42}$$

where $\Delta\theta$ is the angle per time step and Δt is the time step size.

Studies Three simulation studies have been conducted on the model scale self-propulsion setup. The three studies are: a time step convergence study, a volume mesh convergence study and a comparison with the self-propulsion results from the towing tank. The appendages mounted in each of the three studies can be seen in Table 3.37.

The results of the model scale self-propulsion studies can be seen in Section 4.3.3.

Full Scale Self-Propulsion

The full scale self-propulsion setup is created by scaling up the model scale self-propulsion setup according to the scaling factor (2.3).

Free Surface Correction The free surface correction method is changed slightly from model scale to full scale in order to account for the roughness resistance, air resistance and bilge keel resistance which are only relevant for the full scale simulations. The method is still conducted by using the three simulations setups seen in Figure 3.33. The wave making resistance and the added resistance of the increased surface height are calculated similarly to eq. (3.38) and eq. (3.39):

$$R_{Ws} = R_{Ts} - R_{Vs} \tag{3.43}$$

$$\Delta R_{SHs} = R_{Vs,SH} - R_{Vs} \tag{3.44}$$

Table 3.38: Appendages used in the full scale CFD self-propulsion studies.

Study	With Rudder	With Stator Fins
Time Step Convergence	Yes	Yes
Volume Mesh Convergence	Yes	Yes
Comparison	Yes	Yes

The full scale resistance corresponding to eq. (3.20) is then calculated using:

$$R_{Ts} = \frac{S + S_{BK}}{S}(R_{Vs,SH} + \Delta R_F) + R_{Ws} + R_{AAS} - \Delta R_{SHs} \tag{3.45}$$

where ΔR_F is the roughness resistance of eq. (3.21), and R_{AAS} is the air resistance of eq. (3.23). The correlation allowance of eq. (3.22) is not included in eq. (3.45) because its purpose is to correct for systematic errors in the towing tank extrapolation procedure.

An alternative to using the ITTC procedure to estimate the roughness, air and bilge keel resistances is to model them in the CFD simulations. The roughness resistance can be modelled using a wall roughness model [28, p. 3405-3406]. The air resistance requires the superstructure of the ship as a 3D geometry. If the 3D geometry of the superstructure is available, the air resistance can be estimated either by including the superstructure directly in the CFD simulations, or by running a separate set of simulations with the superstructure alone. The added resistance from the bilge keels can quite easily be estimated by adding the bilge keels to the hull geometry.

Propeller Rotation The full scale self-propulsion setup uses the same method as the model scale setup for modelling the propeller rotation (see Figure 3.36). The force balance used in the full scale setup is changed slightly from eq. (3.41) because there is no towing force in full scale:

$$R_{Ts} = T_s \tag{3.46}$$

The thrust is adjusted by changing the propeller rotation rate until the thrust is equal to the resistance. The adjustments are performed by a proportional controller programmed by the authors.

Studies The studies conducted on the full scale self-propulsion setup are a time step convergence study, a volume mesh convergence study, and a comparison with the extrapolated self-propulsion simulation from the towing tank. Both the rudder and stator fins are mounted in all full scale self-propulsion simulations, as seen in Table 3.38.

The results of the full scale self-propulsion simulations can be seen in Section 4.3.3.

CHAPTER 4

Results

This chapter presents the results from towing tank tests in Section 3.4 followed by the speed trial results in Section 3.4. Finally the results from the CFD simulations are presented in Section 4.3.

4.1 Towing Tank Test

The design of the ship has been tested in a towing tank prior to the project period of this thesis. The conducted tests include resistance test, open water tests and self-propulsion tests. All of the towing tank tests are conducted with rudder and pre-swirl fins mounted and at the sea trial condition. The sea trial condition has 40.2% of the displacement of the design condition as explained Section 3.1.1. The method behind the towing tank tests and the procedure for extrapolating from model scale to full scale are presented in Sections 3.2.4 to 3.2.6. The following sections present the provided towing tank test results and the extrapolated full scale results.

4.1.1 Results of Resistance Test

A resistance test has been carried out at the towing tank, as described in Section 3.2.1. The model scale total resistance coefficient and the model scale frictional resistance coefficient have been provided by the towing tank. The frictional resistance coefficient is based on the Schoenherr frictional line in eq. (2.13). The residual resistance coefficient is calculated using eq. (3.1). The model scale total, frictional and residual resistance coefficients are presented in Figure 4.1.

From Figure 4.1 it is seen that the frictional resistance is the largest part of the total resistance in the studied Froude number range. It is also seen as expected, that the frictional resistance coefficient becomes smaller as the Froude number and the Reynolds number increases, and that the residual resistance coefficient becomes larger.

4.1.2 Results of Open Water Test

An open water test of the stock propeller has been carried out in the towing tank, as described in Section 3.2.2. Data of the stock propeller can be seen in Table 3.4. The model scale propeller characteristics of the stock propeller provided by the towing tank are presented in Figure 4.2.

As seen in Figure 4.2 the open water test is only conducted for advance ratios in the range relevant for this ship design. Therefore propeller characteristics are not provided in the the bollard pull range or in the range where the open water efficiency decreases.

4.1.3 Results of Self-Propulsion Test

A self-propulsion test has been carried out at the towing tank, using the stock propeller. The self-propulsion test is described in Section 3.2.3. Data of the stock propeller is presented in Table 3.4.

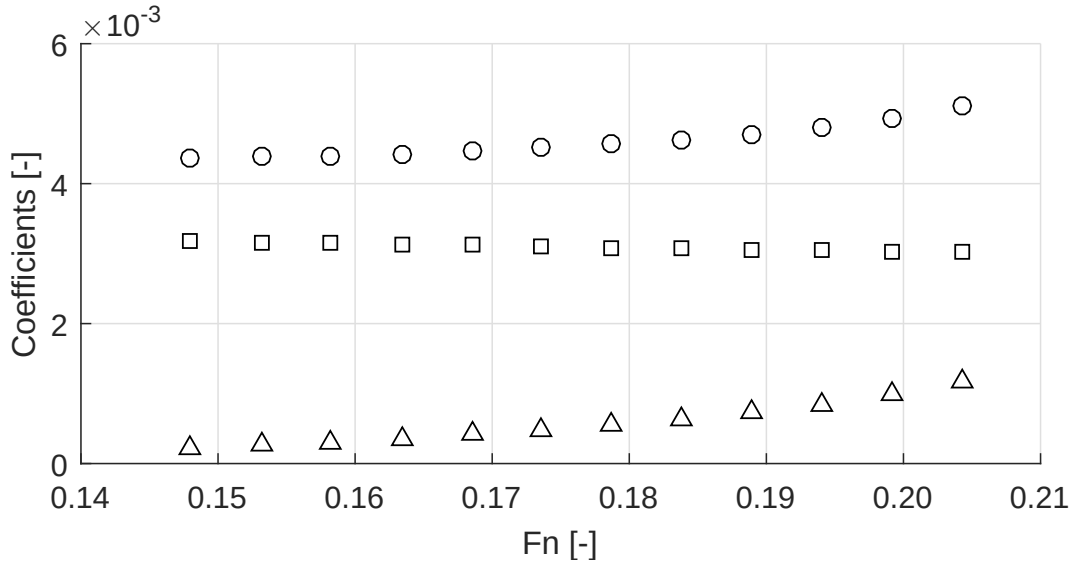

Figure 4.1: Results of the resistance test from the towing tank. Model scale total resistance coefficients C_{Tm} (circle), frictional resistance coefficients $C_{Fm,Sh}$ (square) and residual resistance coefficients C_R (triangle) as a function of Froude number Fn.

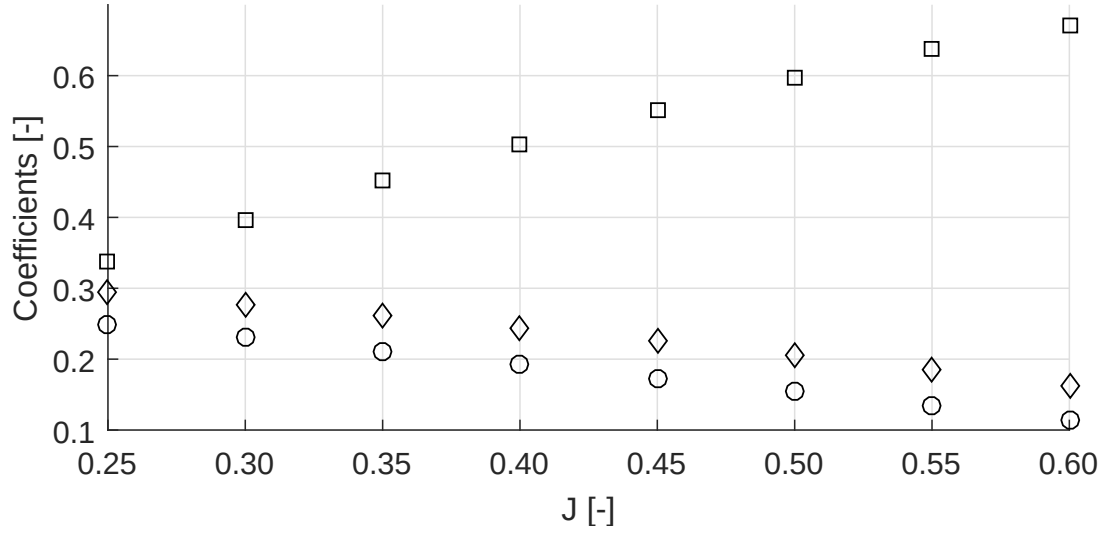

Figure 4.2: Results of the open water test from the towing tank. Propeller thrust coefficient $K_{Tom,stock}$ (circle), 10 times torque coefficient $10K_{Qom,stock}$ (diamond) and open water efficiency $\eta_{om,stock}$ (square) of the stock propeller in model scale as a function of advance ratio J.

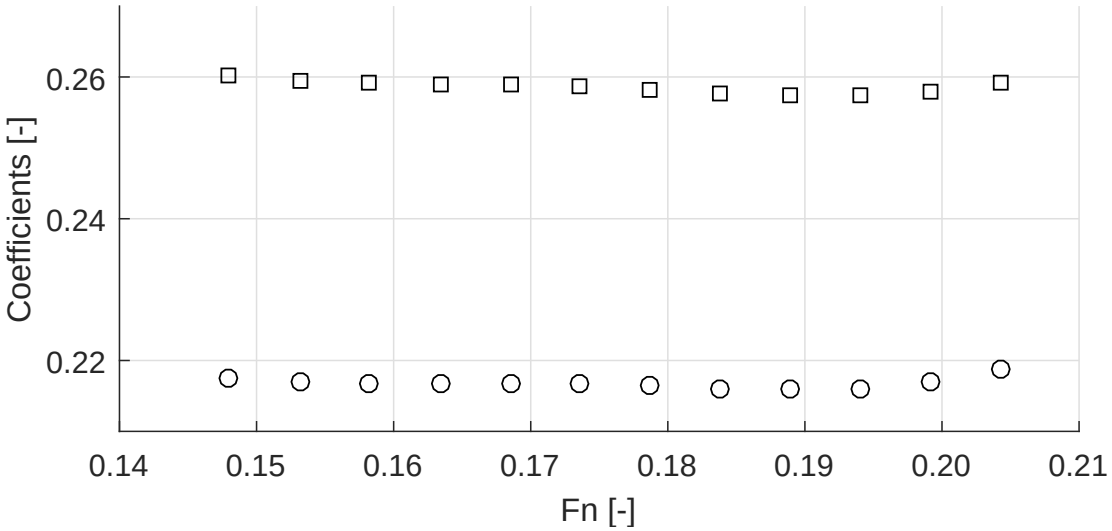

Figure 4.3: Results of the self-propulsion test from the towing tank in model scale. Propeller thrust coefficient K_{Tm} (circle) and propeller torque coefficient K_{Qm} (square) as a function of Froude number Fn.

The thrust identity method has been used to derive parts of the self-propulsion results and is explained briefly in Section 3.2.6 and [5, Sec 8.7.4.3]. The thrust coefficient eq. (3.13) and the torque coefficient eq. (3.16) is shown in Figure 4.3. It is observed that the thrust and torque coefficients have a limited dependence on the Froude number.

4.1.4 Extrapolation of Resistance Test

The results of the resistance test shown in Section 4.1.1 are extrapolated to full scale using the ITTC extrapolation method [10, Sec. 2.4.1] as explained in Section 3.2.4. The extrapolation is based on the full scale propeller characteristics of the actual propeller. The total resistance coefficient eq. (3.20), the smooth total resistance coefficient eq. (3.19), the frictional resistance coefficient eq. (2.12) and the residuary resistance coefficient eq. (3.1) are presented in Figure 4.4.

From Figures 4.1 and 4.4 it is seen that the frictional resistance is still the largest part of the total resistance in full scale, but it is a smaller part than in model scale. This means that in full scale, the frictional resistance is less of the total resistance and the wave making resistance (residuary resistance) is more of the total resistance.

4.1.5 Extrapolation of Open Water Test

The open water characteristics of the actual propeller in full scale have been given by the shipyard. Data of the actual propeller can be seen in Table 3.3. However, the open water characteristics of the stock propeller provided by the shipyard is in model scale. Data of the stock propeller can be seen in Table 3.4. In order to compare the actual propeller with the stock propeller, the open water characteristics of the stock propeller presented in Section 4.1.2 need to be extrapolated. The

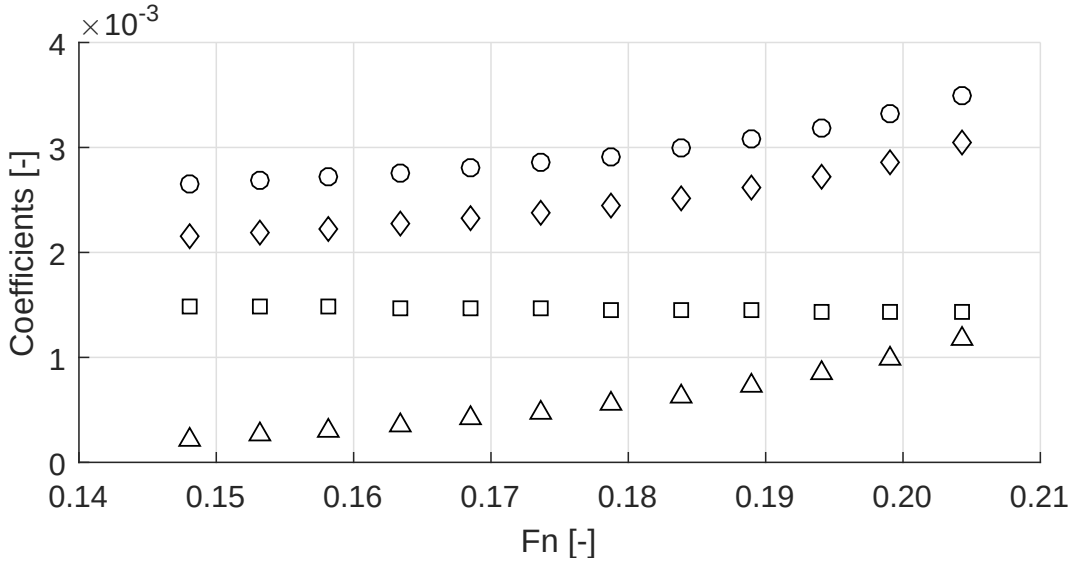

Figure 4.4: Results of the extrapolated resistance test from the towing tank. Full scale total resistance coefficient C_{Ts} (circle), total resistance coefficient with smooth hull and without bilge keels $C_{Ts,smooth}$ (diamond), frictional resistance coefficient C_{Fs} (square) and residuary resistance coefficient C_R (triangle) as a function of Froude number Fn. The extrapolation is conducted using the standard ITTC extrapolation method.

ITTC procedure for extrapolating open water characteristics is described in Section 3.2.5. The extrapolated open water characteristics of the stock propeller are compared to the provided open water characteristics of the actual propeller in Figures 4.5 and 4.6.

A difference between the performance characteristics of the actual and stock propellers can be seen in Figures 4.5 and 4.6. The actual propeller delivers about 1% to 3% more thrust and about 4% to 9% more torque than the stock propeller. This results in a lower open water efficiency of the actual propeller of 2% to 6% compared to the stock propeller, as seen in Figure 4.6. It is important to remember that the percentages are within the expected magnitude of the measurement and extrapolation uncertainties.

4.1.6 Extrapolation of Self-Propulsion Test

The results of the self-propulsion test and the open water test shown in Section 4.1.3 are extrapolated to full scale using the ITTC extrapolation method [10, Sec. 2.4.3] as explained in the Section 3.2.6.

The extrapolation is done using both the actual propeller characteristics and the extrapolated stock propeller characteristics. The delivered power of the extrapolated self-propulsion results can be seen in Figure 4.7.

The extrapolation using the stock propeller predicts a $4-5\%$ lower delivered power than the extrapolation using the actual propeller. The difference in delivered power between the stock propeller and the actual propeller is discussed in Section 5.3.

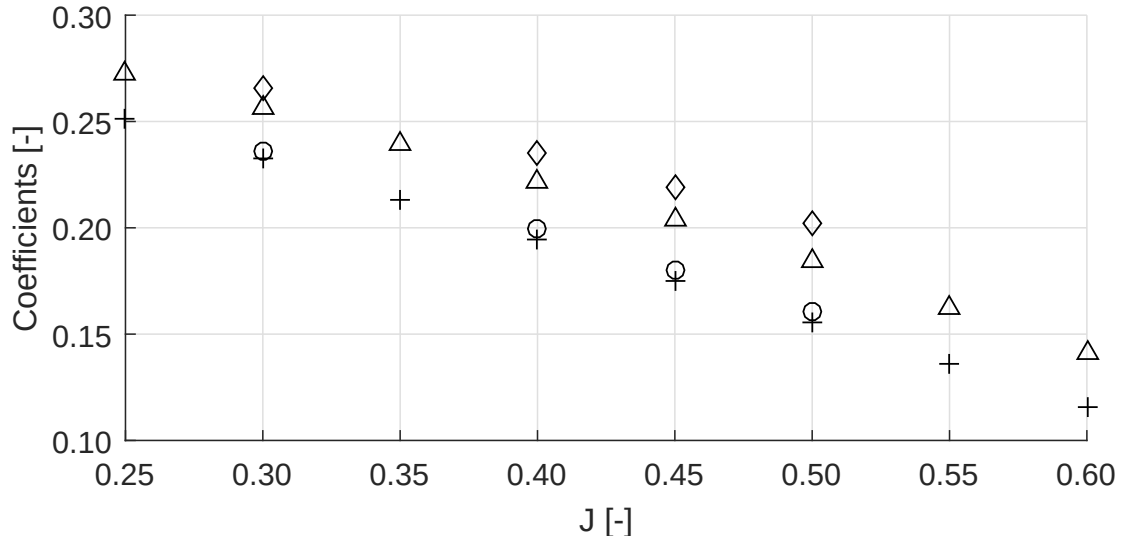

Figure 4.5: Results of the extrapolated open water test from the towing tank. Thrust coefficient $K_{Tos,stock}$ (plus sign) and 10 times the torque coefficient $10K_{Qos,stock}$ (triangle) of the stock propeller as function of advance ratio J. Thrust coefficient $K_{Tos,actual}$ (circle) and 10 times the torque coefficient $K_{10Qos,actual}$ (diamond) of the actual propeller as function of advance ratio J. The extrapolation is conducted using the standard ITTC extrapolation method.

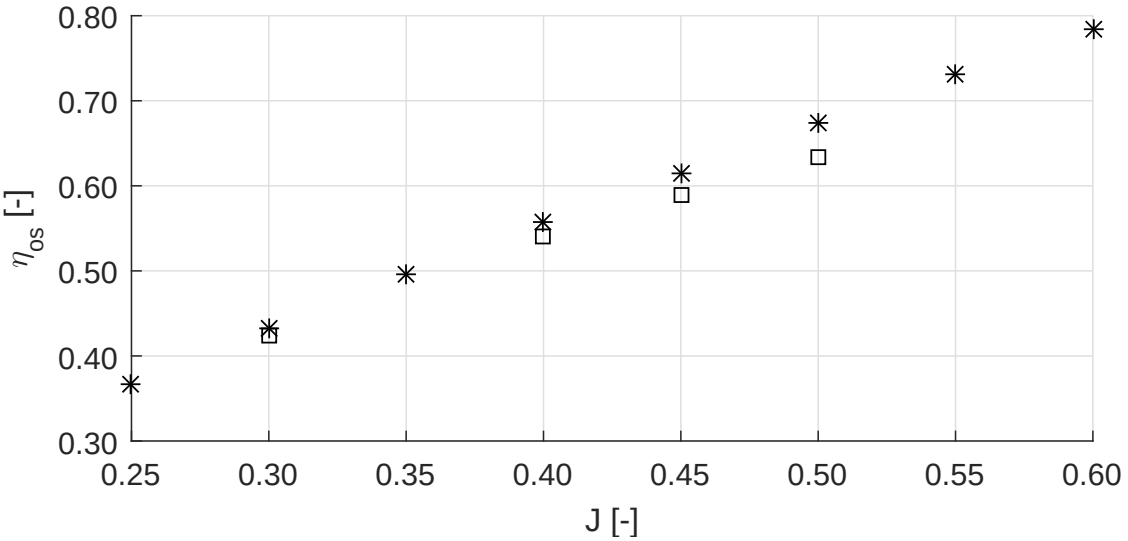

Figure 4.6: Results of the extrapolated open water test from the towing tank. Open water efficiency $\eta_{os,stock}$ of the stock propeller (asterisk) and open water efficiency $\eta_{os,actual}$ of the actual propeller (square) as a function of advance ratio J. The extrapolation is conducted using the standard ITTC extrapolation method.

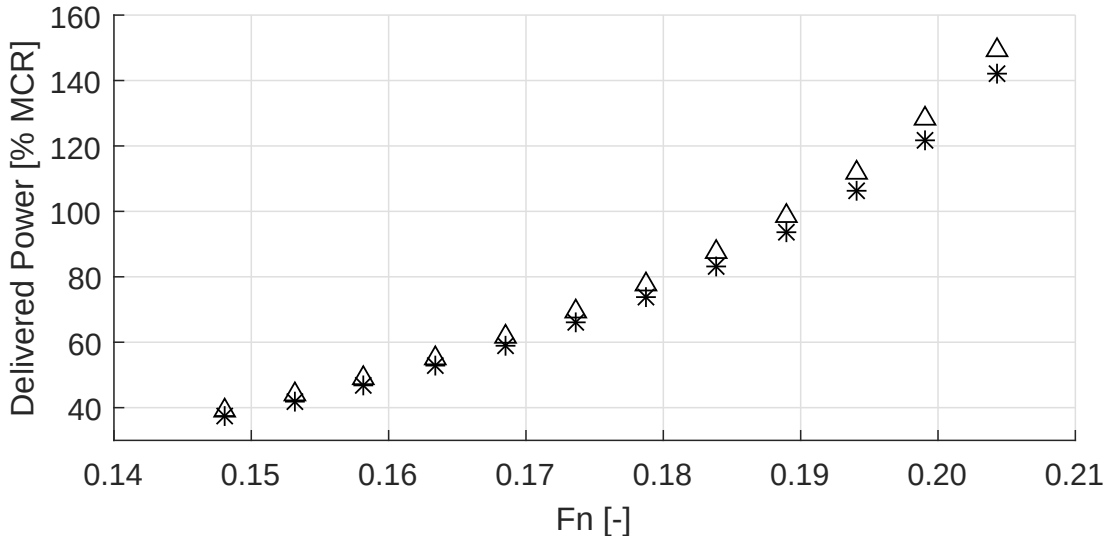

Figure 4.7: Results of the extrapolated self-propulsion test from the towing tank. Delivered power P_{Ds} in full scale using stock propeller (asterisk) and actual propeller (triangle) as a function of Froude number Fn. The extrapolation is conducted using the standard ITTC extrapolation method.

4.2 Sea Trial

This section presents the results from the speed trial. The results provided by the shipyard are the measured values corrected for wind and current. The procedures of the sea trial and corrections are described in Section 3.3.

The weather data shows that only one of the ships has to be corrected for waves using the ISO 15016:2015 standard. The relative difference between the uncorrected and the corrected power due to waves is between 1% and 3.5%. The corrected speed trial data of the four sister ships can be seen in Figure 4.8.

4.3 CFD

The following sections present the results of the CFD simulations. Details on the simulations can be found in Section 3.4. First, the results of the resistance test are presented followed by the results of the open water. Finally, the results of the self-propulsion results are presented. The used computational power for calculating one speed for the different test types can be seen in Table 4.9.

4.3.1 CFD Resistance Test

This section presents results of the model scale and full scale resistance setup. First, the model scale results are presented, and then the full scale results are presented. The model scale and full scale resistance CFD setups are described in Section 3.4.2.

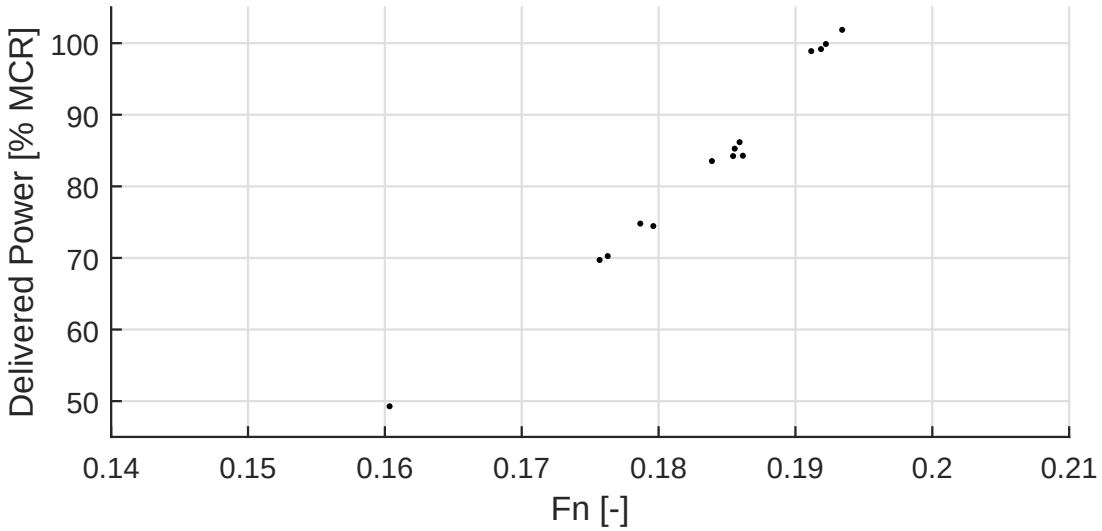

Figure 4.8: Results of the speed trial for all four sister ships. Delivered power as a function of Froude number Fn. Conducted and corrected using the ISO 15016:2015 procedure [4].

Table 4.9: Used computational power for a single simulation. All simulations are performed on 16-core nodes (Either Xeon E5-2650 or Xeon E5-2670 running at 2.60 GHz)

Simulation	**Computational Cost**
Resistance	450 CPU hours
Open water	32 CPU hours
Self-propulsion	550 CPU hours

Model Scale Resistance

Before trusting the results of the CFD resistance simulations, convergence tests and validation with model scale resistance experiments are essential as explained in Section 3.4.1. The following sections present validation and convergence studies of the boundary layer mesh, spacial discretization, temporal discretization and finally a comparison with towing tank test results.

Boundary Layer Mesh The boundary layer mesh is the part of the mesh situated closest to the hull (See Figure 2.3). The frictional resistance is dependent on the wall y^+ value of the hull, which is controlled by the thickness of the inner most boundary layer as explained in Section 2.3.5. A wall y^+ study is conducted in order to determine the boundary layer thickness to be used in the subsequent simulations.

There are multiple ways of defining a representative global y^+ value for a simulation. In this study, the global wall y^+ value is assumed to be the average wall y^+ of all cells on the wetted surface of the hull.

It has been decided to perform the y^+ study at the lowest speed tested in the towing tank, which corresponds to a Froude number equal to 0.1480. The reason for performing the study at

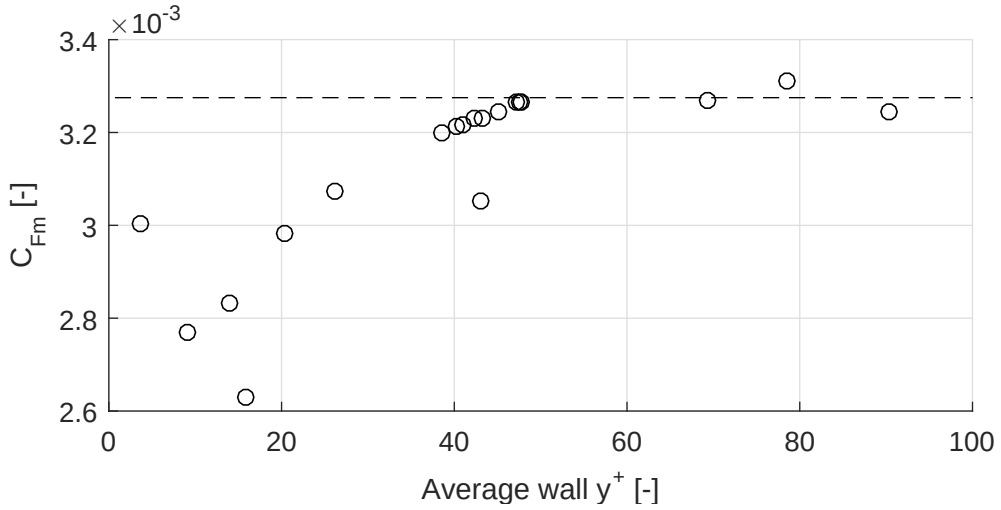

Figure 4.10: Results of the wall y^+ study in model scale, showing the frictional resistance coefficient C_{Fm} from CFD (circle) as a function of average wall y^+ value, together with the ITTC Mode-Ship Correlation Line eq. (2.12) (dash line). Simulations are performed at a Froude number Fn equal to 0.1480, using 2M cells.

Table 4.11: Boundary layer settings of the model scale CFD resistance setup, used to achieve wall y^+ values in the range of 35 to 50.

Number of boundary layers	7
Total boundary layer thickness	$8.4 \times 10^{-3} L_{pp}$
boundary layer stretching	1.4

the lowest speed is that the frictional resistance is the largest part of the total resistance at the lowest speed as described in Section 2.1.

The wall y^+ study is conducted by running a series of simulations with different values of boundary layer thickness while keeping all other mesh settings constant. The frictional resistance coefficients of the series of simulations can be seen in Figure 4.10, along with the ITTC Model-Ship Correlation Line eq. (2.12).

It is seen in Figure 4.10 that the frictional resistance coefficient converges at a wall y^+ value of approximately 35 to 50, which is expected as the inner cell is in the log layer as described in Section 2.3.5. This range of wall y^+ values is achieved by using the boundary layer settings shown in Table 4.11 for all speed.

Spatial Discretization A mesh convergence study is conducted in order to determine the mesh settings of the volume mesh and the six refinement zones. The refinement zones are described in Section 3.4.2.

The mesh convergence study is conducted by running a series of simulations with different mesh settings while all other settings of the simulations are kept constant. Three of these simulation series are conducted, each at a different Froude number. The three Froude numbers are chosen

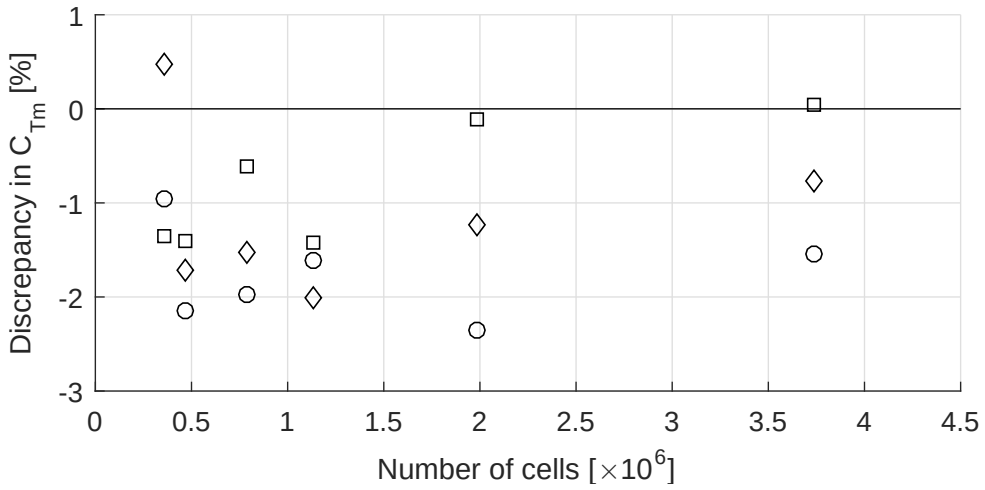

Figure 4.12: Results of the volume mesh convergence study for the model scale resistance setup. Total resistance coefficient C_{Tm} of the CFD simulations relative to the results of the towing tank resistance test at three speeds as a function of the number of cells. Froude number Fn equal to 0.1634 (circle), Froude number Fn equal to 0.1736 (diamond) and Froude number Fn equal to 0.1940 (square).

from the range of Froude numbers used in the towing tank tests. The mesh convergence study is performed on the hull without the rudder and without the stator fins as seen in Table 3.22.

The results of the three simulations series show that mesh convergence is obtained at the medium and the highest speeds, but not at the lowest speed. The lack of mesh convergence at the lowest speed is investigated by inspecting the free surface height. It is concluded that the lack of mesh convergence at the lowest speed is caused by insufficient mesh resolution of the Kelvin wave zone in the longitudinal and transverse directions. The Kelvin waves are briefly described in Section 2.1. Lower ship speeds generate divergent waves with shorter wave lengths. Therefore, the mesh of the Kelvin waves should be finer in order to properly resolve the waves at all ship speeds.

The settings of the free surface refinement zones are modified with finer mesh in the longitudinal and transverse directions. The results of the mesh convergence study with the modified settings can be seen in Figure 4.12.

The resistance coefficients of the mesh convergence study are slightly lower than those of the towing tank results because the rudder and stator fins are not included in the simulations. The conclusions of the study are still valid as the effect of the rudder and stator fins on the convergence is assumed to be negligible. Furthermore, it is important to remember that the discrepancies are similar to the uncertainties of the measurements from the towing tank [37].

Table 4.13: Cell sizes of refinement zones in the model scale CFD resistance setup. Cell sizes are made non-dimensional using eq. (4.1).

Name of RZ	**Cell Size l^* [-]**
Far Free Surface RZ	96
Middle Free Surface RZ	192
Near Free Surface RZ	384
Bulbous Bow RZ	77
Transom RZ	128
Vertical Free Surface RZ	1281

From Figure 4.12 it is seen that the results are converged at 2M cells, but with lower discrepancy at 3.7M cells. It is decided not to optimize the volume mesh further because most of the results are within the uncertainty of the towing tank measurements data [37]. The cell size Δl is non-dimensionalized using the ship length:

$$l^* = \frac{L_{pp}}{\Delta l} \tag{4.1}$$

where l^* is the non-dimensional cell size. The non-dimensional cell size can be interpreted as the number of cells needed to obtain one ship length. Larger values of l^* indicate smaller cell sizes.

The mesh with 3.7M cells is used for all subsequent resistance simulations in model scale, and the settings of the refinement zones can be seen in Table 4.13.

Temporal Discretization The CFD setup is simulated using an implicit unsteady solver as described in Section 3.4.2. The size of the time step is determined by conducting a time step study. The time step is non-dimensionalized using the ship speed and ship length:

$$t^* = \Delta t \frac{V_{design}}{L_{PP}} \tag{4.2}$$

where t^* is the non-dimensional time step. A physical interpretation of this non-dimensional time step is the number of ship lengths the ship translates per time step.

The time step study is conducted by running a series of simulations with different time step sizes while all other settings are kept constant. The simulation series are conducted using the 3.7M cell mesh at a Froude number equal to 0.1736. The study is performed on the hull, without the rudder and without the stator fins as seen in Table 3.22. The total resistance coefficient of the CFD simulations are compared to the resistance test data from the towing tank. The results of the time step study can be seen in Figure 4.14.

The resistance coefficients of the time step study are slightly lower than those of the towing tank results as the rudder and stator fins are not present in the simulation series. The conclusions of the study are still valid as the effect of the rudder on the convergence is assumed to be negligible.

Figure 4.14 shows that a smaller time step gives a smaller discrepancy between the resistances of the CFD and the towing tank. As in the mesh convergence study in Section 4.3.1, it important to keep in mind that the discrepancies are in the same order of magnitude as the uncertainty of the

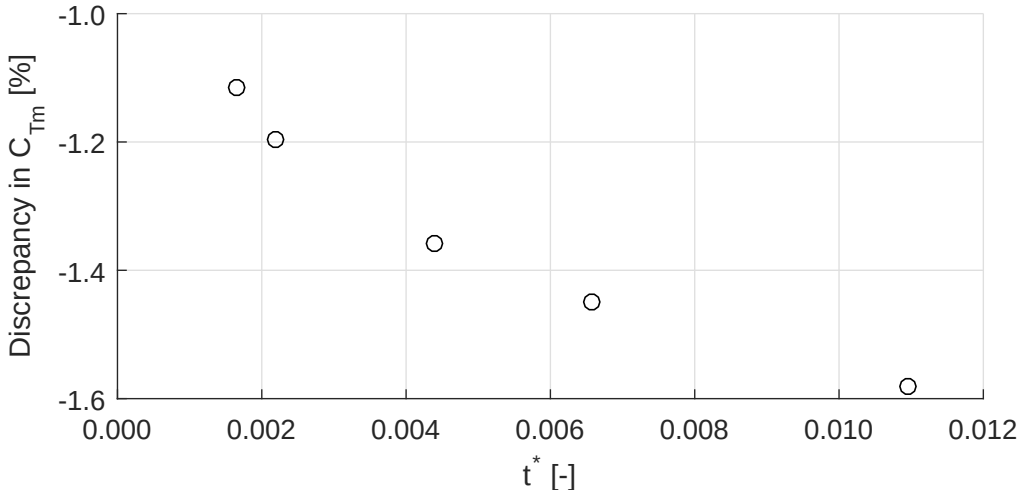

Figure 4.14: Results of the time step study of the model scale CFD resistance setup. Total resistance coefficient C_{Tm} of the CFD simulations relative to the results of the towing tank resistance test as a function of time step size t^*. The simulations are conducted at a Froude number Fn equal to 0.1736 and with 3.7M cells.

towing tank test [37]. It can be seen in Figure 4.14 that a reduction in time step from the largest to the smallest time step size only reduces the discrepancy by approximately half a percent point while requiring over six times the computational time. In this case, it is a high computing cost compared to the reduction of the discretization error. A time step size of 6.6×10^{-3} is determined to be the right balance between reduced discretization error and computational cost.

Other time step study simulations have also been conducted. The results, which are not included in the thesis, show that when the number of cells is increased, the impact on the discrepancy of changing the time step size is reduced. This means that increasing the number of cells reduces the requirement of the time step size in order to obtain similar discrepancies.

For the full scale resistance CFD simulations, the increased cost of a small time step can be reduced by varying the time step size during the simulation. This method is described in detail in Section 4.3.1.

Comparison A series of simulations are conducted using the final model scale resistance setup. The series of simulations are conducted at the same speeds as the resistance test of the towing tank. The setup parameters of the series of simulations can be seen in Tables 4.11 and 4.13. The series of simulations are performed on the hull with the rudder, but without the stator fins as seen in Table 3.22.

The discrepancy in the total resistance coefficient between CFD simulation and towing tank test data at each speed can be seen in Figure 4.15.

The total resistance coefficient estimated using CFD is very similar to the towing tank results. For the speed range of Fn 0.16 to 0.19, which is in the range of the sea trial data, the discrepancies are within 1%. The discrepancy is within the uncertainty of the towing tank test. Furthermore, it is important to state that the towing tank tests are conducted with fins and the CFD calculations

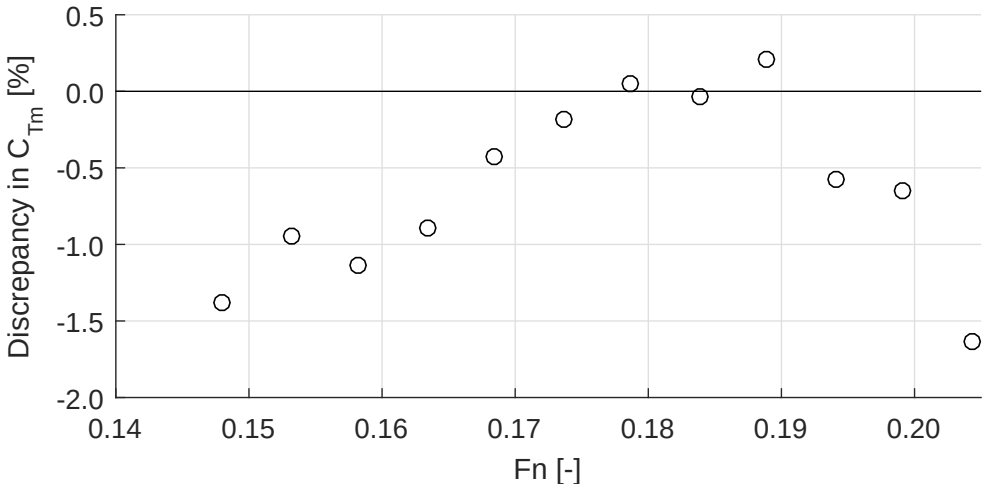

Figure 4.15: Results of the model scale resistance setup. Total resistance coefficient C_{Tm} of the CFD simulations relative to the results of the towing tank resistance test as a function of Froude number Fn. The simulation series are conducted using a 3.7M cell mesh with a time step size t^* equal to 6.6×10^{-3}.

are conducted without. Including the fins in the CFD calculations would increase the resistance slightly.

As additional validation of the resistance setup, the setup has been blind tested on an additional ship. The data were provided by the DNV GL office in Hamburg. The only data provided for the simulations were the ship geometry, displacement and draft. After a short spatial and temporal convergence study, the final simulations were performed and the results were sent to Hamburg. The results are not included in this thesis. After the results were received, the Hamburg office provided the towing tank test results. The results showed a relative difference in total resistance below 1% between CFD and towing tank test. This is the same discrepancy as in the case studied in this thesis.

With the satisfying convergence studies of both the temporal and spacial discretization and the very small discrepancies from model tank test in the studied case and in the blind testing, the model scale resistance setup is considered trustworthy.

Full Scale Resistance

The setup validated in the previous sections is modified from model to full scale. The following sections present validation and convergence studies of the spatial and temporal discretization, followed by a comparison with the extrapolated resistance results from the towing tank.

Boundary Layer Mesh A wall y^+ study in model scale has been carried out in Section 4.3.1. It has been decided not to study the influence of the y^+ value on the frictional resistance in full scale, but to use the results of the model scale study. It was concluded that wall y^+ values in the range of 35 to 50 gives a reasonable estimation of the frictional resistance. Due to the increases flow velocity in full scale, the number and thickness of the boundary layers have to be changed, in

Table 4.16: Boundary layer settings of the full scale CFD resistance setup, used to achieve wall y^+ values in the range of 35 to 50.

Number of boundary layers	15
Total boundary layer thickness	$7.9 \times 10^{-4} L_{PP}$
boundary layer stretching	1.4

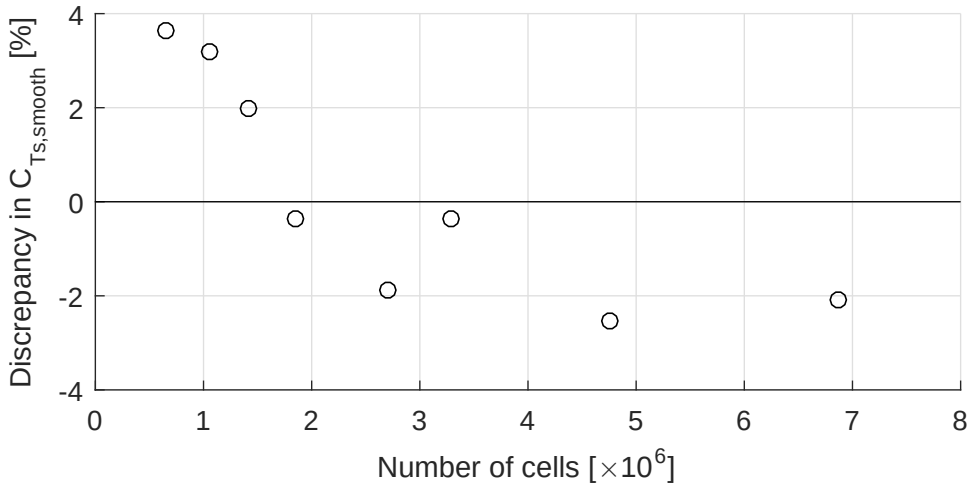

Figure 4.17: Results of the volume mesh convergence study for the full scale resistance setup. Total resistance coefficient with smooth hull and without bilge keels $C_{Ts,smooth}$ of the CFD simulations relative to the extrapolated resistance results of the towing tank as a function of the number of cells. The simulations are conducted at a Froude number Fn equal to 0.1736.

order to maintain the average wall y^+ value. Model scale and full scale boundary layer settings can be seen in Table 4.11 and Table 4.16 respectively.

Spatial Discretization The volume mesh and refinement zones of the full scale CFD setup are similar to those of the model scale setup, as seen in Section 4.3.1. A mesh convergence study of the full scale setup is conducted by running a series of simulation with different mesh settings while all other settings are kept constant. The simulation series is conducted on the hull without the rudder and without the stator fins (see Table 3.23) and at a Froude number equal to 0.1726. The results of the mesh convergence study can be seen in Figure 4.17.

The resistance of the rudder and stator fins are included in the extrapolated resistance data, but not in the CFD setup. This could be one reason for the discrepancies. It is assumed that the exclusion of the rudder does not influence the convergence of the study, and therefore the conclusions are still valid.

It is found that the settings of the vertical free surface, bulbous bow and transom refinement zones directly scaled from the model scale simulations are sufficient for properly resolving the full scale free surface. It is found that the model scale settings of the far, middle and near refinement zones are too coarse and therefore smaller cell sizes in these three zones are used. It has been decided to use the 4.7M cell mesh for the final full scale simulations. The final cell sizes of the

Table 4.18: Cell sizes of refinement zones in the full scale CFD resistance setup. Cell sizes are made non-dimensional using eq. (4.1).

Name of RZ	**Cell size l^* [-]**
Far Free Surface RZ	137
Middle Free Surface RZ	275
Near Free Surface RZ	549
Bulbous Bow RZ	69
Transom RZ	92
Vertical Free Surface RZ	915

Figure 4.19: The three stages of the time step study of the full scale resistance setup.

refinement zones in model and full scale can be seen in Table 4.13 and Table 4.18 respectively. The cell size is made non-dimensional using eq. (4.1).

Temporal Discretization Similarly to the model scale setup, the full scale setup is simulated using an implicit unsteady solver. A time step study has been conducted to determine the time step size.

The full scale simulations have shown to be quite sensitive to the time step size during the first couple of time steps. If the time step size is too large, the simulation experiences numerical instability, which causes the simulation to break down. The time step size needed to successfully simulate the first few time steps is very small. Using this time step size throughout the simulation would require inconveniently large computational effort. Therefore, it has been decided to run the simulation in three stages, each using a different time step size: Firstly a small time step for initializing the flow (first stage), then a large time step for fast convergence (second stage), and lastly a medium time step for minimizing the discretization error (third stage). This approach balances the required computational cost, the numerical instability, and the discretization error. The three stages are illustrated in Figure 4.19.

The time step size of the first stage is chosen purely to avoid numerical instabilities. The time step sizes of the second and third stages are studied in the time step study. The study is conducted on the hull without the rudder and without the stator fins (see Table 3.23). The results of the study are compared to the results of the extrapolated towing tank test. The results of the study can be seen in Figure 4.20. The time step size is made non-dimensional using eq. (4.2).

The resistance of the rudder and the stator fins are included in the extrapolated towing tank results, but not in the CFD setup. This gives an offset to the discrepancies. It is assumed that the exclusion of the rudder and stator fins does not influence the convergence behaviour of the study, and therefore the conclusions are still valid.

Simulations with a non-dimensional time step size larger than 0.011 have a very fluctuating signal which makes it difficult to compute a reliable time average. The same is true for time step sizes smaller than 0.0022. This gives a range of stable time step sizes between 0.0022 and 0.011.

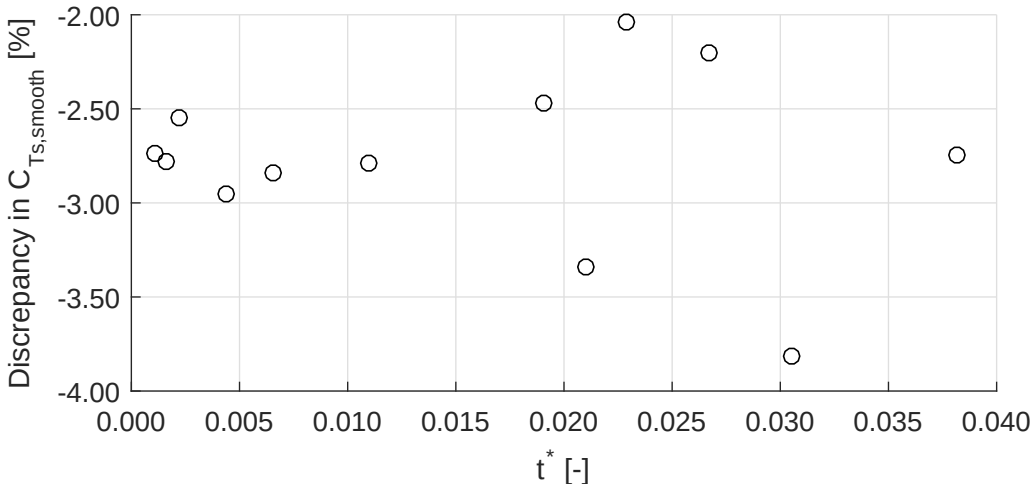

Figure 4.20: Results of the time step study of the full scale CFD resistance setup. Total resistance coefficient with smooth hull and without bilge keels $C_{Ts,smooth}$ of the CFD simulations relative to the extrapolated resistance results of the towing tank as a function of time step size t^*. The simulations are conducted at Froude number Fn equal to 0.1712 and with 4.7M cells.

Table 4.21: Time step sizes of the three stages used in the full scale CFD resistance setup.

Stage	**Time step size t* [-]**
First	7.6×10^{-5}
Second	1.1×10^{-2}
Third	2.2×10^{-3}

The largest time step size in the stable range is chosen for the second stage, and the smallest time step size in the range is chosen for the third stage. The time step size of the three stages in the final setup can be seen in Table 4.21.

Comparison The full scale CFD setup is simulated at all speeds tested in the towing tank and compared to the extrapolated resistance results of the towing tank. The simulations are performed using the hull and the rudder, but not the stator fins (see Table 3.23). The setting of the final setup can be seen in Tables 4.16, 4.18 and 4.21. The discrepancy in the total resistance coefficient between the CFD simulations and the extrapolated resistance results of the towing tank can be seen in Figure 4.22.

From Figure 4.22 it is seen that the total resistance coefficients of the CFD setup is very similar to the extrapolated towing tank results. For the speeds in the range of the sea trial from a Froude number of 0.16 to 0.19, the discrepancies are below 1.5 %, which is satisfying since it is about the same as the uncertainty of towing tank measurements. The discrepancies are also similar to those of the model scale setup, as seen in Figure 4.15. Again, the underestimation could be caused by the fact that the fins are not included in the CFD simulations.

The setup has shown independence of spatial and temporal discretization and small discrepancies compared to the extrapolated resistance from the towing tank.

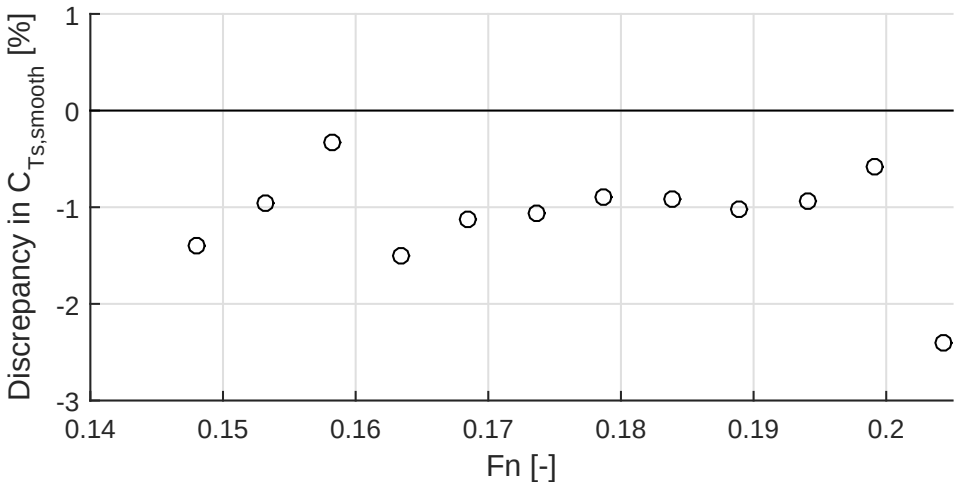

Figure 4.22: Results of the full scale resistance setup. Total resistance coefficient with smooth hull and without bilge keels $C_{Ts,smooth}$ of the CFD simulations relative to the extrapolated results of the towing tank as a function of Froude number Fn. The simulation series are conducted using a 4.7M cell mesh, with the time step sizes shown in table 4.21.

Table 4.24: Boundary layer mesh settings of the CFD open water setup, used to achieve wall y^+ values below 1.

Propeller and Hub	
Number of boundary layers	11
Total boundary layer thickness	$2.7 \times 10^{-3} D$
Near wall boundary layer thickness	$3.7 \times 10^{-5} D$

4.3.2 CFD Open Water Test

As described in Section 3.4.1, a validation procedure is required in order to trust the results of the CFD simulations. This section presents the results of the validation for the open water simulations in model scale.

Boundary Layer Mesh

A number of boundary layers (see Section 2.3.5) are used on the surface of the propeller hub and blades as well as at the boundary between the rotating and stationary domains.

It is decided to fully resolve the boundary layer of the propeller hub and blades. To fully resolve the boundary layer, the simulations are performed with wall +y values of the propeller blade and hub below 1. A single boundary layer is used on each side of the interface between the static and rotating domain in order to make a good alignment of the two domains. The obtained y^+ values on the propeller in open water can be seen in Figure 4.23, and the boundary layer settings can be seen in Table 4.24.

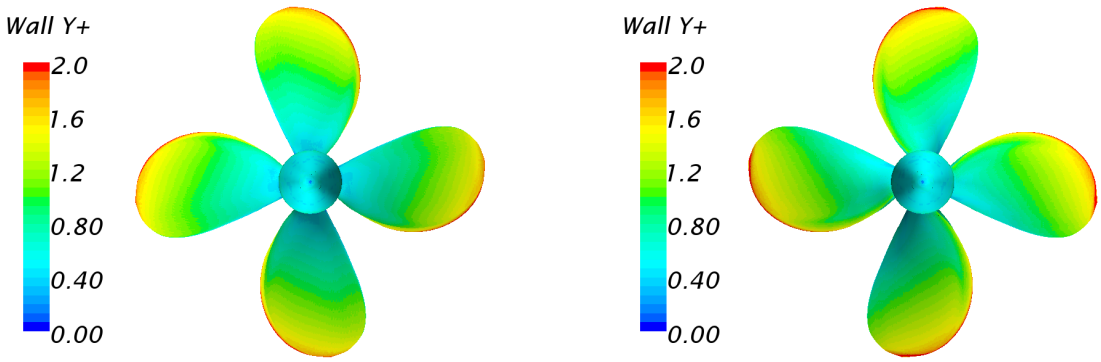

Figure 4.23: Wall $y+$ value on the pressure side (left) and suction side (right) of the propeller in the open water setup. Advance ratio is equal to 0.6.

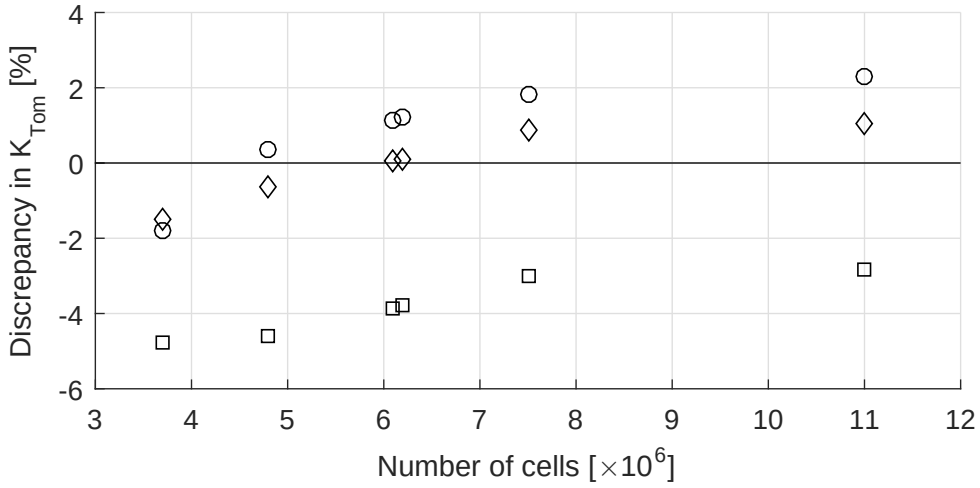

Figure 4.25: Results of the volume mesh convergence study for the open water setup. Thrust coefficient K_{Tom} of the CFD simulations relative to the results of the towing tank open water test as a function of the number of cells. Advance ratio J equal to 0.30 (circle), advance ratio J equal to 0.45 (diamond) and advance ratio J equal to 0.60 (square).

Spacial Discretization

A mesh convergence study has been conducted in order to determine the volume mesh settings and the settings of the refinement zones. The mesh convergence study is conducted by running a series of simulations with different volume mesh settings while all other settings are kept constant. Three simulation series are conducted at J equal to 0.30, 0.45 and 0.60 respectively. The propeller characteristics of the CFD simulations are compared with the open water test data from the towing tank. The discrepancies of the propeller characteristics are shown in Figures 4.25 to 4.27.

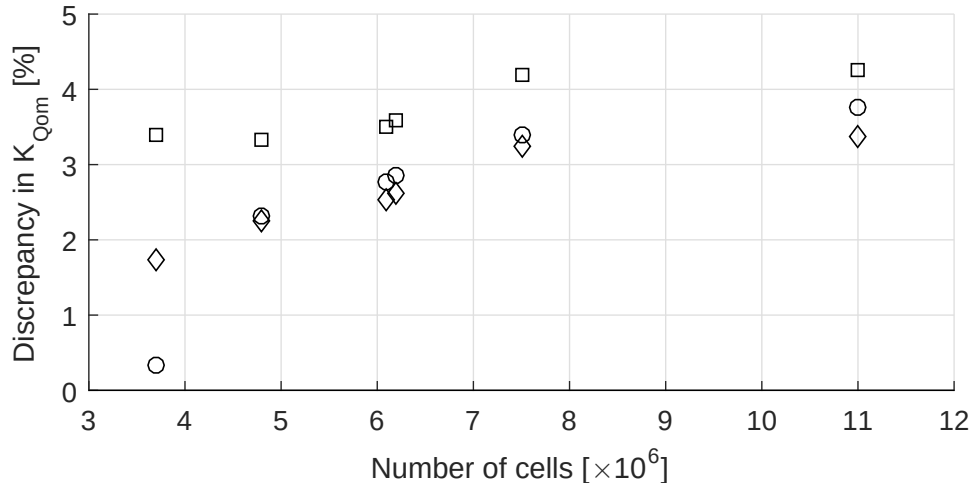

Figure 4.26: Results of the volume mesh convergence study for the open water setup. Torque coefficient K_{Qom} of the CFD simulations relative to the results of the towing tank open water test as a function of the number of cells. Advance ratio J equal to 0.30 (circle), advance ratio J equal to 0.45 (diamond) and advance ratio J equal to 0.60 (square).

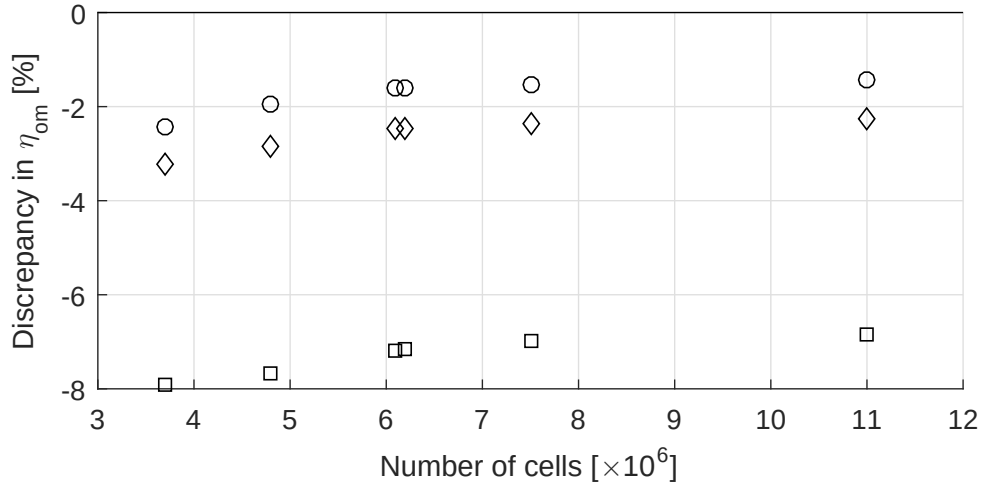

Figure 4.27: Results of the volume mesh convergence study for the open water setup. Open water efficiency $\eta_{om}$of the CFD simulations relative to the results of the towing tank open water test as a function of the number of cells. Advance ratio J equal to 0.30 (circle), advance ratio J equal to 0.45 (diamond) and advance ratio J equal to 0.60 (square).

Table 4.28: Cell sizes of the refinement zones in the CFD open water setup.

Name of RZ	Cell size
Far Propeller RZ	4.26×10^{-2} D
Near Propeller RZ	2.13×10^{-2} D

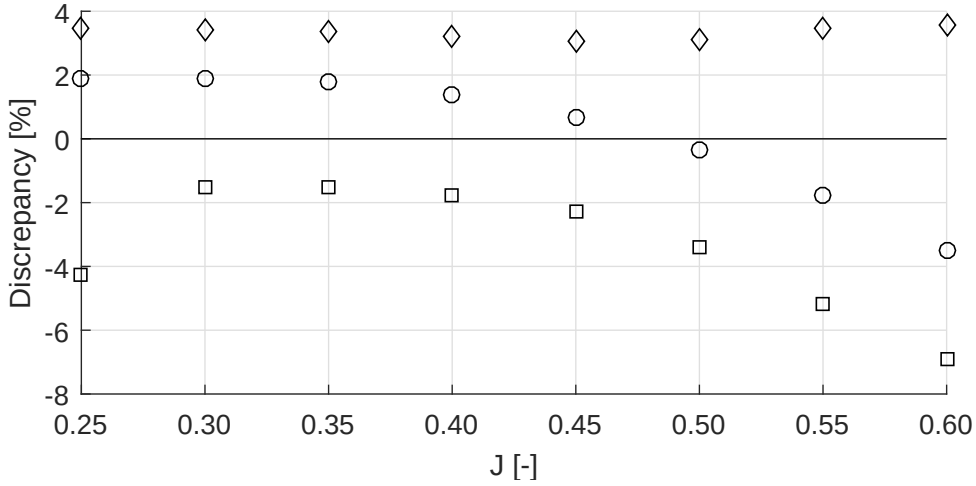

Figure 4.29: Results of the CFD open water test. Thrust coefficient K_{Tom} (circle), torque coefficient K_{Qom} (diamond) and efficiency η_{om} (square) of the stock propeller in open water relative to the results of the towing tank open water test as a function of advance ratio J.

It can be seen in Figures 4.25 to 4.27 that the solution converges for all advance ratios. It can therefore be concluded that the propeller characteristics are independent of the mesh size for sizes larger than approximately 7.5M cells. In all subsequent open water simulations, the mesh with 7.5M cells will be used.

Furthermore, it can be seen in the Figures 4.25 to 4.27 that the thrust coefficient is overestimated by $1-2\%$ for J equal to 0.3 and 0.45, and underestimated by 3% for J equal to 0.6, compared to the towing tank test. The torque is overestimated by $3-5\%$ for all advance ratios. The open water efficiency is a combination of the thrust and torque coefficients and is therefore underestimated by under 3% for J equal to 0.3 and 0.45 and 7% for J equal to 0.6.

The final mesh setting of the open water setup can be seen in Table 4.28.

Comparison

The propeller performance of the stock propeller is calculated with the mesh settings with approximately 7.5M cells. The CFD results compared with the towing tank results can be seen in Figure 4.29.

It can be seen in Figure 4.29 that the discrepancies are reasonable. Generally the torque is overestimated by $3-4\%$. The thrust is overestimated by approximately 2% at the lower advance ratios and underestimated by approximately $2-4\%$ at the higher advance ratios. This results in an underestimation of the efficiency of up to 7%. There are several possible explanations for the

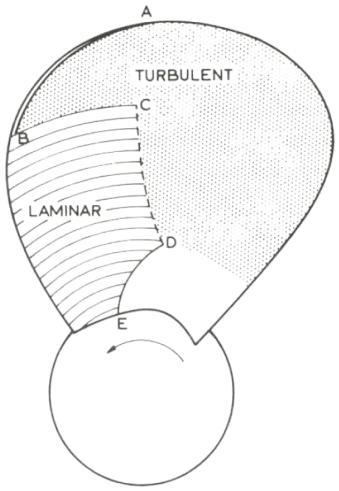

Figure 4.30: Flow regimes on the suction side of a propeller blade in model scale, from [38, 39].

discrepancy between the CFD results and the towing tank results seen in Figure 4.29. The propeller geometry used in the CFD setup is slightly different from the stock propeller geometry used in the towing tank (see Section 3.1.2). This difference could cause discrepancies in the propeller characteristics. Another explanation for the discrepancy is the turbulence modelling used in the CFD setup. The near wall flow regime on the propeller in model scale is laminar at first and changes to turbulent somewhere on the blade as illustrated in Figure 4.30.

The CFD simulation in this report enforces turbulent flow in the domain both for model scale and full scale since the $k - \epsilon$ model assumes that the flow is fully turbulent. Therefore, the CFD setup is not able to model the laminar flow on the propeller. The full scale flow on the propeller is fully turbulent so this possible discrepancy will only occur in model scale. The use of a transition model in the model scale CFD setup has been discussed, but ultimately it has been decided not use such a model. The use of ordinary turbulence models [40] and transition-sensitive turbulence model in analysis of marine propeller performance [41] have been studied in the literature and a sensitive in the choice of turbulence model is found. Not implementing a transitional model saves a significant amount of time and it only causes modelling errors in model scale.

4.3.3 CFD Self-Propulsion Test

This section presents the results of the self-propulsion simulations in model scale and full scale. The two setups are presented in Section 3.4.4.

Model Scale Self-Propulsion

The self-propulsion setup is the combination of the full scale resistance setup and the open water setup, as described in Section 3.4.4. Before the results from the self-propulsion simulations can be trusted, convergence studies of the temporal and spacial discretization must performed. After the convergence studies, the results of the self-propulsion simulation are compared to the results of

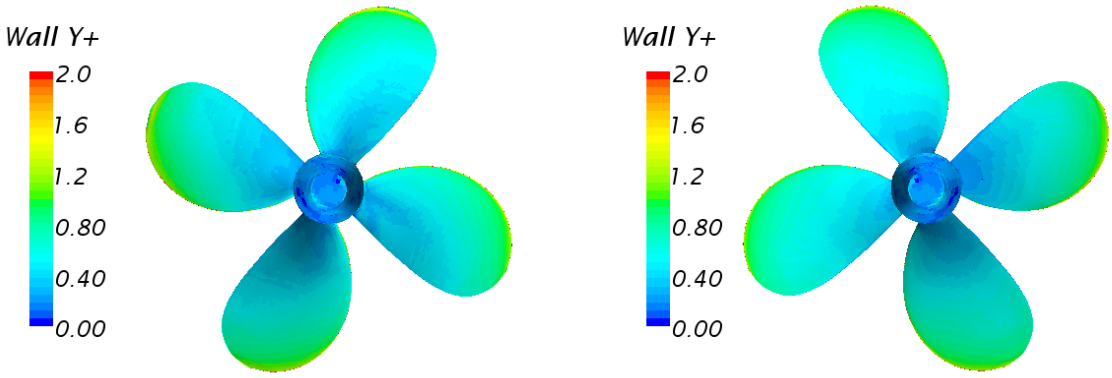

Figure 4.31: Wall y^+ value on the pressure side (left) and suction side (right) of the propeller in self-propulsion simulation at Froude number Fn equal to 0.1736.

the self-propulsion test from the towing tank in order to validate the self-propulsion setup. This section presents the results of the convergence studies and the comparison between the CFD and the towing tank results.

Only the mean value of the signal has been investigated in the convergence studies. The amplitude and the nature of the signal have not been studied. The time-dependent details of the thrust and torque signal are relevant in e.g. cavitation studies, noise and vibration studies and fatigue fracture studies, but is out of the scope of this thesis. For this thesis, only the time averaged thrust and torque signals are important because only the time-averaged delivered power is needed for the comparison with the towing tank results.

Boundary Layer Mesh The self-propulsion setup uses the same boundary layer mesh setting as the model scale resistance setup on the hull. The settings can be seen in Table 4.11.

The boundary layer on the propeller in the self-propulsions setup is fully resolved, exactly as it is for the open water setup. Therefore, the simulations are performed with wall y^+ values below 1, using the same settings as the open water setup. The setting of the boundary layer mesh on the propeller can be seen in Table 4.24. The wall y^+ on the propeller in a self-propulsion test in model scale can be seen in Figure 4.31.

It is seen from Figure 4.31 that the wall y^+ values are lower than they are in the open water simulations, as shown in Figure 4.23. This is expected since the velocities are smaller due to the wake of the ship hull. Furthermore, it is seen that most of the cells have a wall y^+ below 1 as required for fully resolving the boundary layer.

Temporal Discretization A time step convergence study has been conducted in order to determine the time step size of the transient solver. The study has been conducted by running a series of simulations with different time step sizes while all other settings of the setup are kept constant. The time step sizes are shown in non-dimensional values using eq. (3.42). The simulation series are conducted using a mesh with 10.7M cells in the rotating region and 1.2M cells in the static region at a Froude number equal to 0.1736.

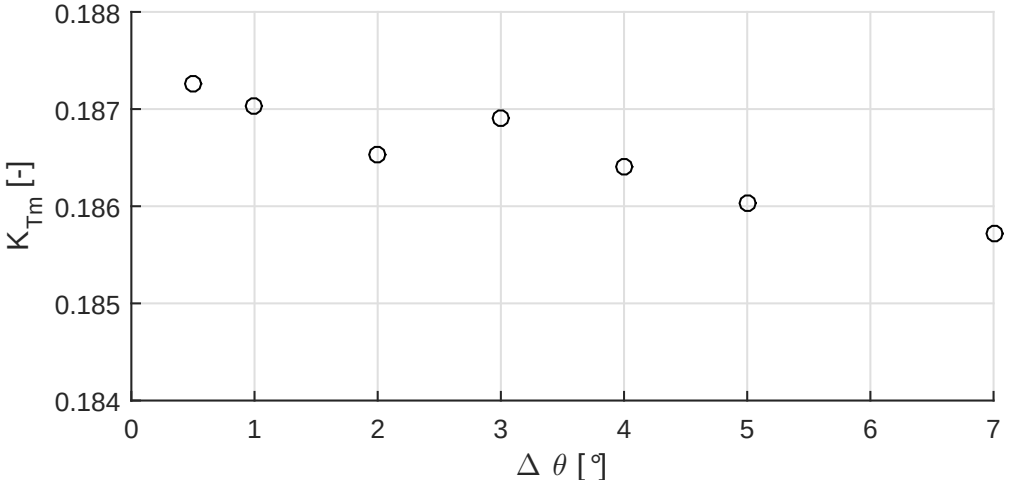

Figure 4.32: Results of the time step study for the self-propulsion setup. Thrust coefficient K_{Tm} of the CFD simulations relative to the results of the towing tank self-propulsion test as a function of time step size $\Delta theta$. The simulations are conducted at a Froude number Fn equal to 0.1736.

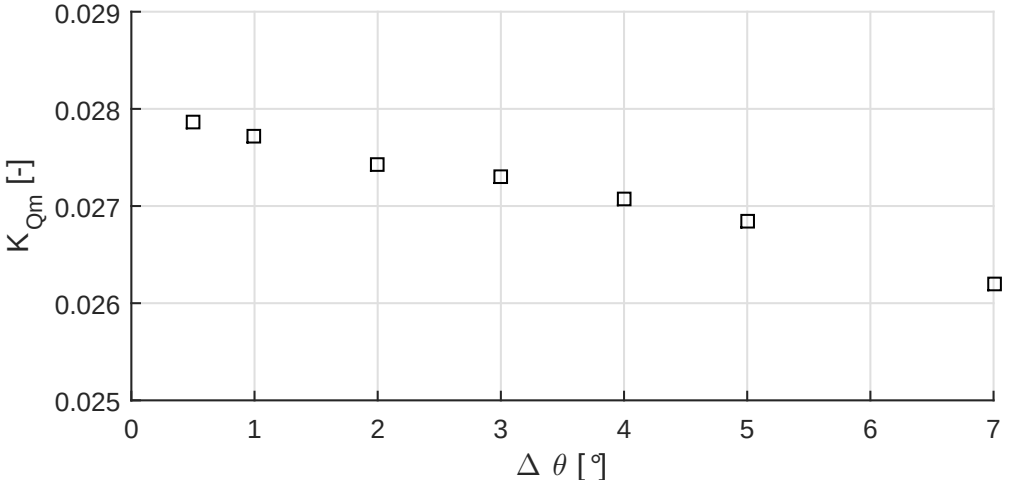

Figure 4.33: Results of the time step study for the self-propulsion setup. Torque coefficient K_{Qm} of the CFD simulations relative to the results of the towing tank self-propulsion test as a function of time step size $\Delta theta$. The simulations are conducted at a Froude number Fn equal to 0.1736.

The study has been conducted on the hull with the rudder, but without the stator fins, as shown in Table 3.37. The simulations has been conducted with the same propeller rotation rate. From the simulation series, the propeller thrust and torque coefficients are obtained. The results of the time step study can be seen in Figures 4.32 and 4.33.

In can be seen in Figures 4.32 and 4.33 that the solution in not completely converging in the temporal discretization. A possible explanation for the lack of convergence could be that the vessel has a large wake fraction resulting in separation and/or that transient flow structures are present.

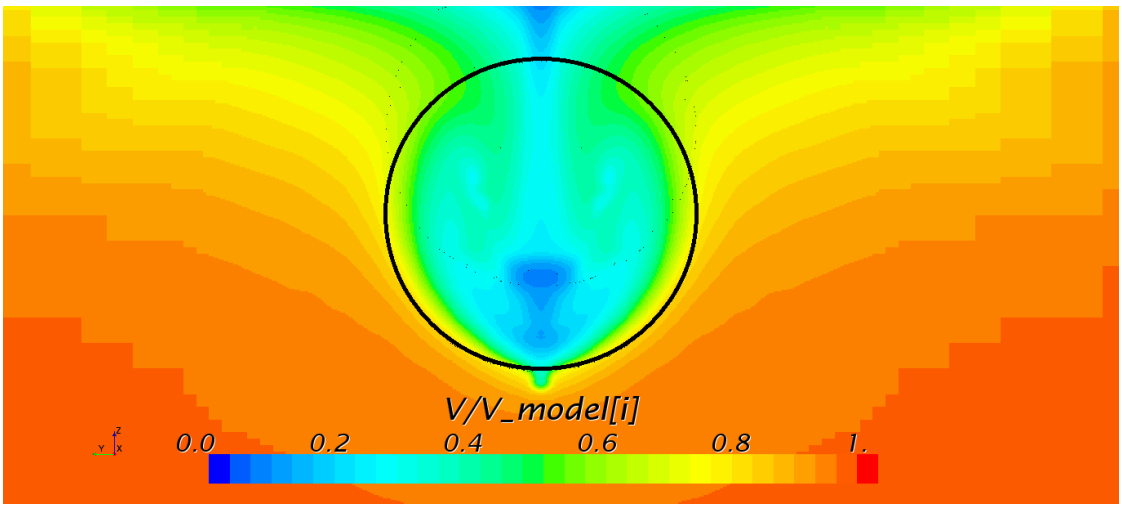

Figure 4.34: Nominal wake field, normalized with the free stream velocity. Result of the model scale resistance setup including stator fins. Black ring is the propeller diameter. The simulation is conducted at a Froude number Fn equal to 0.1736.

Separation and transient flow structures could be dependent on the temporal discretization and thereby influence the convergence. The nominal wake field can be seen in Figure 4.34.

The time step study simulations are computationally heavy especially at $\Delta\theta$ equal to 0.5 and 1.0. Therefore, is was not possible, with the available computational power, to use time steps smaller than $0.5\Delta\theta$. Even through the solution has not completely converged, the solution is not considered to be diverging. It has been decided to perform all further self-propulsion simulations in model scale with $\Delta\theta$ equal to 2. This decision is a trade-off between temporal discretization error and usage of computational resources.

Spatial Discretization To ensure that the solution is independent of the mesh discretization, a mesh convergence study has been performed. The mesh around the ship has been studied in Section 4.3.1 and the mesh around the propeller in Section 4.3.2. Only settings of the near propeller refinement zone (see fig. 3.35) are changed in this mesh convergence study as it is assumed that the mesh of the static region is sufficiently discretized because it has been validated in Section 4.3.1.

The meshes of the study can be seen in Table 4.35. The simulations have been conducted with the same propeller rotation rate as the towing tank self-propulsion test, and at the same Froude number equal to 0.1736. The simulations have been conducted on the hull with the rudder, but without the stator fins, as shown in Table 3.37.

The results of the mesh convergence study show that the difference in thrust and torque between all five meshes in Table 4.35 are smaller than the uncertainty of the signals. This is a strong indication that the solution is independent of the mesh discretization. Based on the results of the mesh convergence study, it has been decided to use Mesh 1, which is the coarsest mesh, for all further simulations. The mesh settings of Mesh 1 can be seen in Table 4.36.

Table 4.35: Studied meshes of the mesh convergence study, for the model scale CFD self-propulsion setup.

Mesh #	**Number of cells**
Mesh 1	6.2M
Mesh 2	6.6M
Mesh 3	7.6M
Mesh 4	9.1M
Mesh 5	21.2M

Table 4.36: Cell sizes of refinement zones in the model scale CFD self-propulsion setup. Cell sizes are made non-dimensional using eq. (4.1).

Name of RZ	**Cell size l^* [-]**
Bulbous Bow RZ	69
Transom RZ	92
Name of RZ	**Cell size [-]**
Far Propeller RZ	$4.26 \times 10^{-2} D$
Near Propeller RZ	$2.13 \times 10^{-2} D$

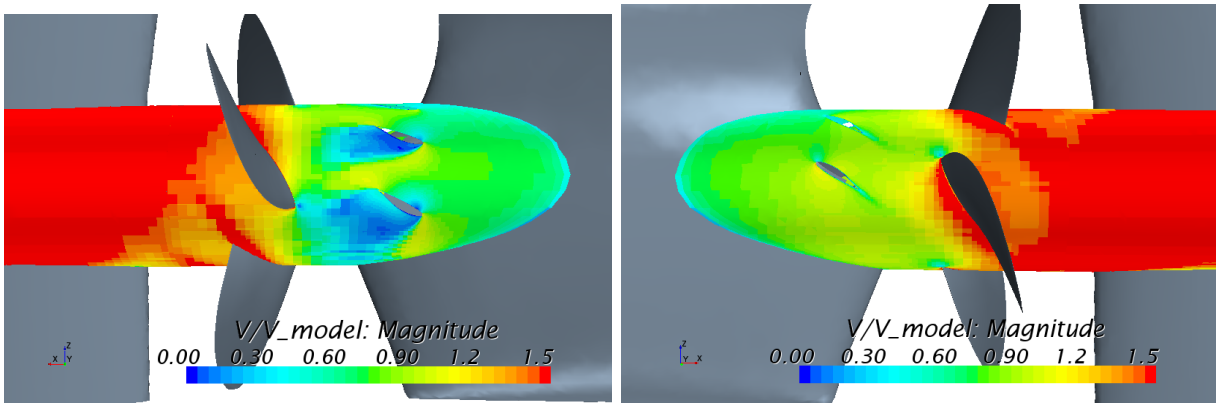

Figure 4.37: Separation downstream of the stator fins. From model scale self-propulsion simulation at a Froude number equal to 0.1736. The colour indicates the velocity magnitude at r/R equal to 0.5. Seen from starboard side (left), and from port side (right).

Stator Fins A set of self-propulsion simulations have been conducted both with and without the stator fins in order to investigate the performance of the fins and their influence on the flow. The results of the study show that the stator fins significantly improve the performance of the propeller even though there is significant flow separation on the two fins on starboard side. The flow around the stator fins can be seen in Figure 4.37.

The study has also shown that the results of the simulations with the stator fins has resulted in smaller discrepancies relative to the towing tank self-propulsion tests, compared to the simulation without the stator fins. This is reasonable since the stator fins have also been included in the towing tank test. It was therefore decided to include the stator fins in all subsequent self-propulsion

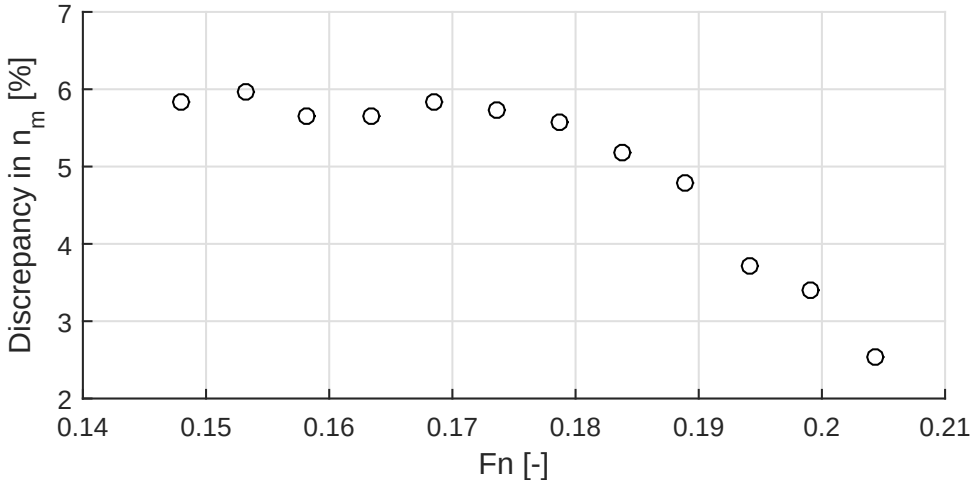

Figure 4.38: Results of the model scale self-propulsion setup. Propeller rotation rate n_m of the CFD simulations relative to the results of the towing tank self-propulsion test as a function of Froude number Fn.

simulations. It would have been better to conduct all previous simulations, both resistance and self-propulsion, with the stator fins, but unfortunately that has not been possible due to time limitations of the project. It is important to remember that the resistance simulations conducted prior to the self-propulsion test are mainly meant as validation steps to ensure trustworthy results in the self-propulsion stimulations. When the stator fins are included in the self-propulsion simulations, the influence of not having included the stator fins before is very limited.

Comparison This section presents the results from the self-propulsion simulations compared to the results from the towing tank self-propulsion test. The self-propulsion simulations are conducted at the same Froude numbers as the self-propulsion test from towing towing tank. The series of simulations are conducted both with and without the stator fins, as discussed previously.

As described in Section 3.4.4, a solver has been used in order to obtain the correct tow force by changing the rate of rotation of the propeller. As described in Section 3.4.4, the simulations have been performed with a variable propeller rotation rate in order to balance the forces and obtain the same towing force as used in the towing tank tests. The obtained towing forces of the simulations are within 0.4% of the towing force of the towing tank test (calculated using eq. (3.9)). The propeller rotation rate for the balanced solution can be seen in Figure 4.38.

It is seen from Figure 4.38 that the rate of rotation is overestimated in the simulations. Simulations have also been conducted without balancing the forces, but using a fixed propeller rotation rate instead. The results are not shown in this thesis. These simulations show an underestimation of the thrust and an overestimation of the resistance compared to the towing tank results. The over- and underestimation both contribute to an increase in the propeller rotation rate when balancing the forces because the balancing of the forces has been done according to eq. (3.41). That explains why the propeller rotation rate in Figure 4.38 is consistently overestimated.

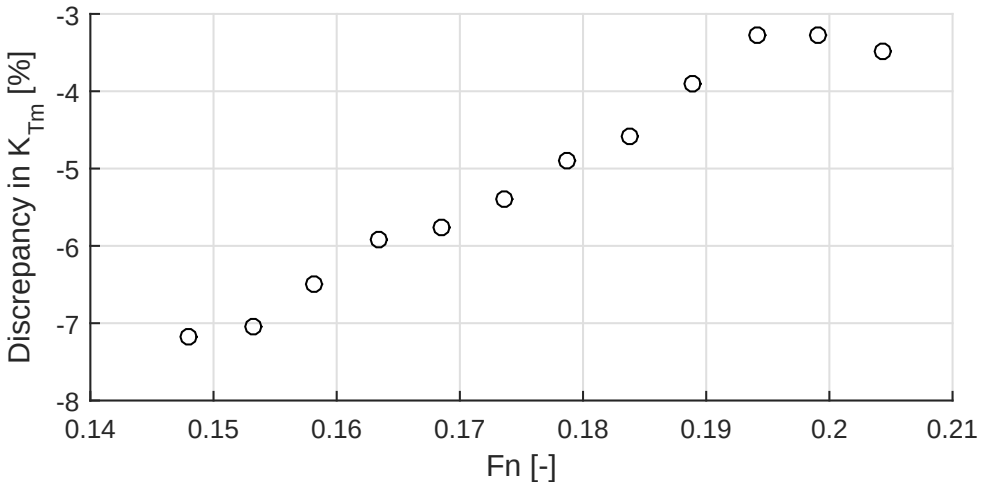

Figure 4.39: Results of the model scale self-propulsion setup. Thrust coefficient K_{Tm} of the CFD simulations relative to the results of the towing tank self-propulsion test as a function of Froude number Fn.

The thrust coefficient eq. (3.13) of the simulations can be seen in Figure 4.39. The thrust is overestimated, but the thrust coefficient is underestimated. This is the case because the propeller rotation rate is overestimated, as explained. It can be seen that the magnitude of the thrust discrepancy in Figure 4.39 is related to the discrepancy of the propeller rotation rate in Figure 4.38. For the low Froude numbers, the discrepancies are approximately $6-7\%$ and for the high Froude numbers the discrepancies are approximately $2-4\%$.

The obtained torque coefficients can be seen in Figure 4.40. It is seen that the torque coefficient is overestimated by approximately $6-7\%$ compared to the towing tank results. An overestimation of the torque coefficient is also seen in the open water simulations in Figure 4.29. In the open water simulations, the overestimation of the torque coefficient is $3-4\%$.

Based on the convergence studies and comparisons to the towing tank tests, the results of the model scale self-propulsion setup are reasonable.

Full Scale Self-Propulsion

The full scale setup is based on the model scale setup validated in the previous section. The modification from the model scale setup to the full scale setup is described in Section 3.4.4.

In this section, first the changes to the boundary layer are discussed followed by a brief convergence study in temporal and spatial descretization. Then the wake field and flows around the stator fins are presented and discussed. Finally, the results from self-propulsion results are presented.

For the full scale simulations, only calculations in the Froude number range of 0.175 to 0.195 will be performed. This is the range where the speed trial are conducted and where the model scale setup shows the smallest discrepancies.

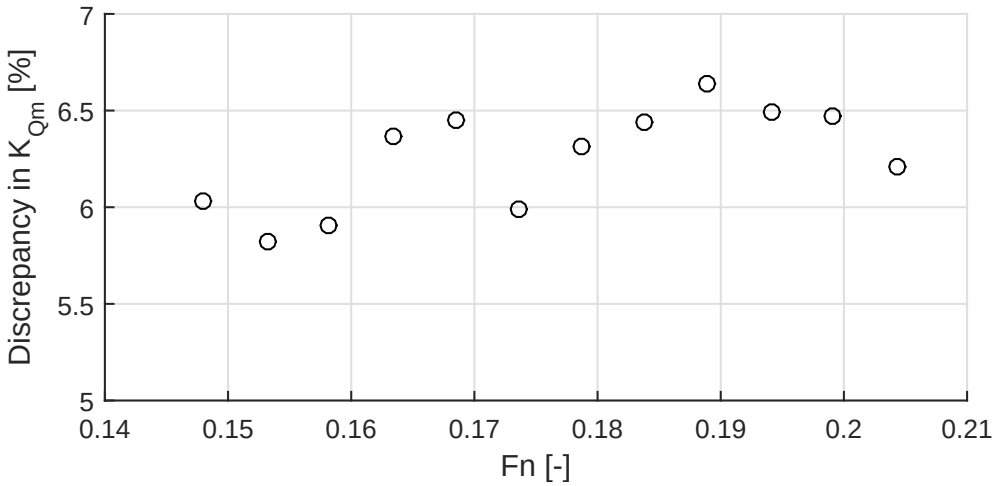

Figure 4.40: Results of the model scale self-propulsion setup. Torque coefficient K_{Qm} of the CFD simulations relative to the results of the towing tank self-propulsion test as a function of Froude number Fn.

Boundary Layer Mesh The wall y^+ value on the propeller in the model scale self-propulsion setup is below 1 as required in order to fully resolve the boundary layer. In the full scale self-propulsion simulations, the Reynolds number is much larger and the boundary layer is much thinner. It has not been possible to obtain numerically stable full scale simulations using a boundary layer mesh with wall y^+ values below 1 in full scale. Therefore, it has been decided to use wall y^+ values above 30 instead. This way the boundary layer is not resolved, but instead wall functions are used to calculate the effects in the boundary layer.

To study the differences of using wall y^+ values below 1 and using wall y^+ values above 30, three model scale self-propulsion simulations have been conducted using wall y^+ value above 30. The results of these simulations are not included in this thesis, but they are compared to the earlier model scale self-propulsion simulations conducted with wall y^+ values below 1. The relative difference in thrust and torque between the three simulations with wall y^+ values above 30, and the one with wall y^+ value below 1 is no larger than 0.5%. This shows that the use of either values below 1 or above 30 has little influence on the thrust and torque results in model scale. It is assumed that the same is true for the full scale simulations.

Temporal and Spatial Discretization The following convergence studies are performed to ensure convergence in the temporal and spatial discretization as described is Section 3.4.1. The studies will not be as comprehensive is the case of the resistance, open water and model scale self-propulsion simulations.

The reason for this is that it is expected that modelling errors contribute more to the uncertainty than to the discretization errors. The two most significant contributions to the modelling errors are the use of the stock propeller instead of the actual propeller and that the roughness and air resistance are based on the ITTC procedure and not modelled in the CFD simulations. Therefore, it does not make sense to intensively study the convergence and ensure very small discretization

Table 4.41: Studied time step sizes of the time step convergence study for the full scale self-propulsion setup.

Time Step #	Time Step Size
Time Step 1	$1\Delta\theta$
Time Step 2	$2\Delta\theta$
Time Step 3	$3\Delta\theta$
Time Step 4	$4\Delta\theta$

Table 4.42: Studied meshes of the mesh convergence study, for the full scale self-propulsion setup.

Mesh #	Number of Cells
Mesh 1	9.6M
Mesh 2	9.7M
Mesh 3	9.8M
Mesh 4	12.0M

errors when the modelling errors is much larger. However, it is still important to ensure that the setup does not have a high dependence on the spatial and temporal discretization.

For the full scale self-propulsion setup, a time step study has been conducted. The time step study is a slightly smaller version of the study conducted in model scale. The study consists of four time step sizes which can be seen in Table 4.41. The time step sizes are shown in non-dimensional values using eq. (3.42). The studies have been conducted at a Froude number equal to 0.1736, using a mesh of 9.8M cells. The studies have been conducted on the hull with both the rudder and stator fins attached, as seen in Table 3.38.

The simulations have been conducted with a constant rate of rotation equal to the rate of rotation from the extrapolated towing tank tests from eq. (3.31). The relative difference in thrust and torque from these four simulations is smaller than 0.5%. This indicates that the solution is almost independent of the temporal discretization and that the discretization error is small. It has been decided to use a time step size of $2\Delta\theta$, which is the same as in the model scale self-propulsion simulations.

As described in Section 3.4.4, the mesh is scaled from the model scale to full scale using the scaling factor. A mesh convergence study has been conducted for the full scale self-propulsion setup. The study is conducted using four different meshes. The meshes of the study can be seen in Table 4.42. The study has been conducted at a Froude number equal to 0.1736. The study has been conducted on the hull with both the rudder and stator fins attached, as seen in Table 3.38. The relative difference in thrust and torque of the simulations in the study are smaller than 1.5%. It is concluded that the meshes give consistent results and that the spacial discretization error is smaller than the expected modelling error due to the use of the stock propeller instead of the actual propeller. It is decided to use Mesh 3 with 9.8M cells for subsequent simulations. The mesh settings of Mesh 3 are the same as for the model scale self-propulsion simulation, which can be seen in Table 4.43.

Wake field and Stator Fins In the model scale self-propulsion simulations, it was found that the stator fins caused separation due to the high angle of attack combined with the significant

Table 4.43: Cell sizes of refinement zones in the full scale CFD self-propulsion setup. Cell sizes are made non-dimensional using eq. (4.1).

Name of RZ	**Cell size l^* [-]**
Bulbous Bow RZ	69
Transom RZ	92
Name of RZ	**Cell size [-]**
Far Propeller RZ	$4.26 \times 10^{-2} D$
Near Propeller RZ	$2.13 \times 10^{-2} D$

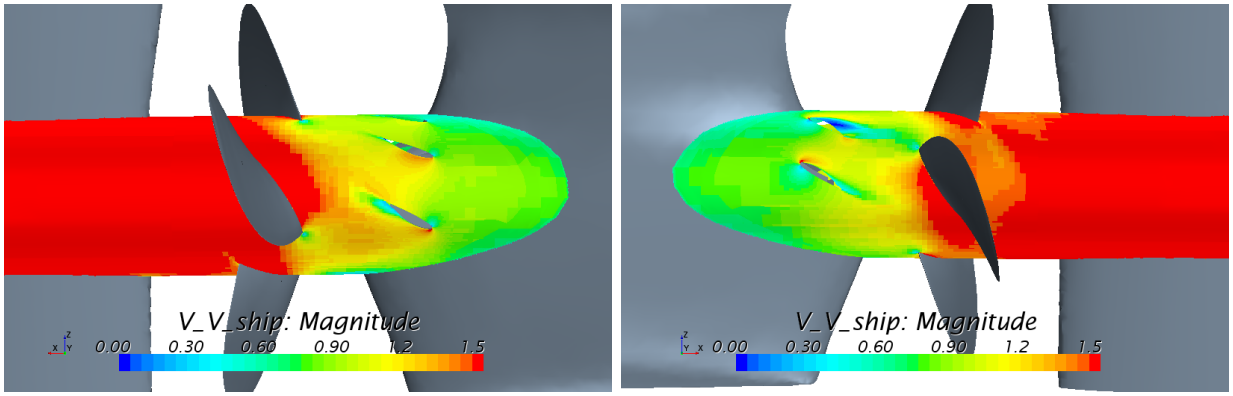

Figure 4.44: Separation downstream of the stator fins. From full scale self-propulsion simulation at a Froude number equal to 0.1736. The color indicates the velocity magnitude at r/R equal to 0.5. Seen from starboard side (left), and from port side (right)

wake field. The flow around the stator fins in full scale can be seen in Figure 4.44. It can be seen that there is almost no separation compared to the flow in model scale seen in Figure 4.37. As seen in Figure 4.45, the nominal wake field in full scale is much smaller than in model scale. The increased water flow to the propeller prevents the stator fins from stalling.

Final Results With the convergence studies performed, the full scale self-propulsion setup is ready for the simulations. In these simulations, three stages are used as shown in Figure 3.36. The results of the simulations can be seen in Figure 4.46 where MCR is the maximum continuous rating. The study has been conducted on the hull with both the rudder and stator fins attached, as seen in Table 3.38.

The CFD results will be compared with sea trial data in the next chapter.

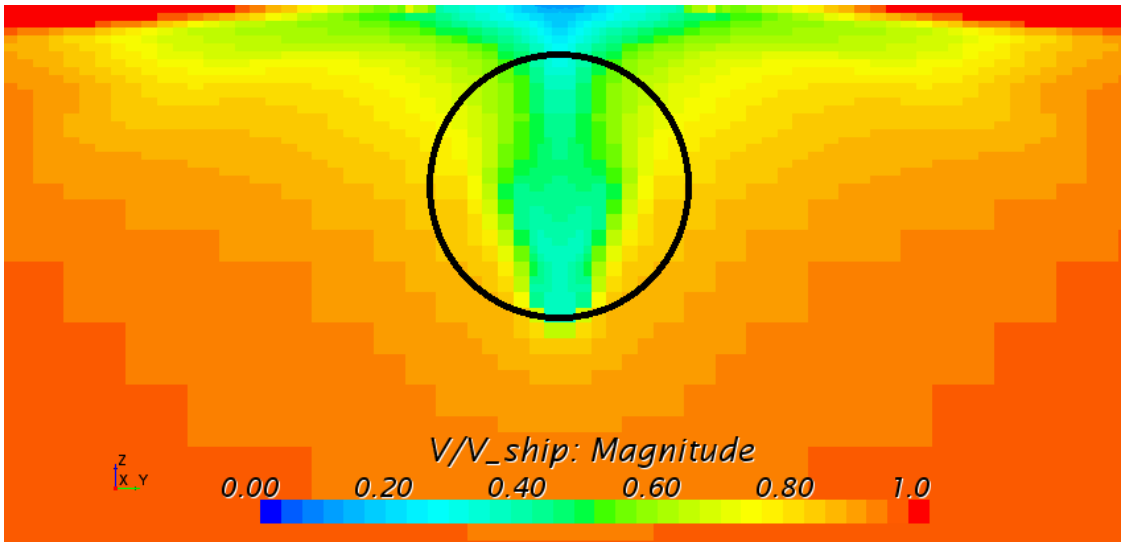

Figure 4.45: Velocity field, normalized with the free stream velocity. Result of the full scale resistance setup without stator fins. Black ring is the propeller diameter. The simulation is conducted at a Froude number Fn equal to 0.1736.

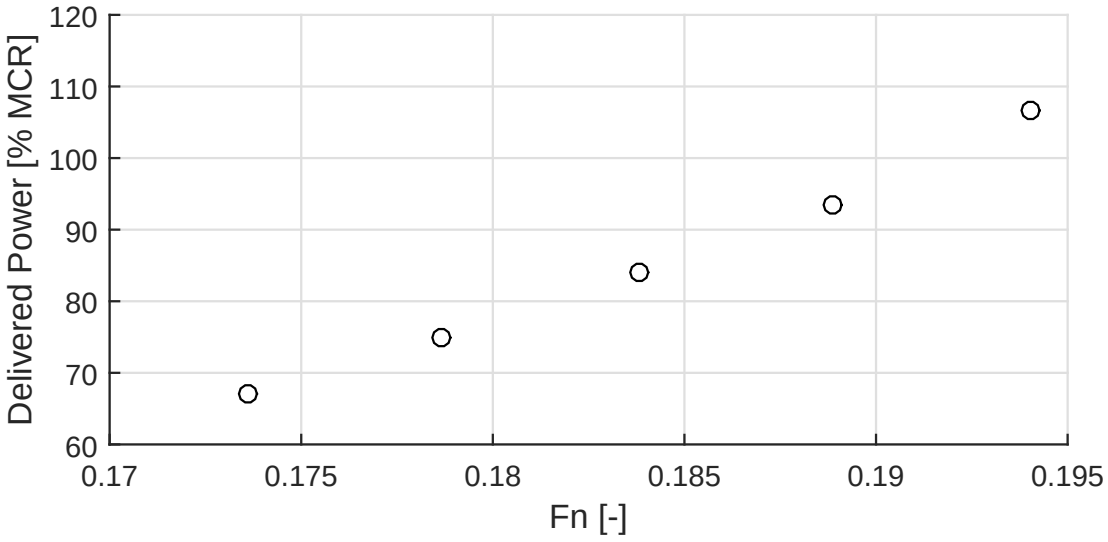

Figure 4.46: Results of the full scale self-propulsion CFD setup.

CHAPTER 5

Discussion

This chapter will discuss the results presented in the previous chapter. Firstly Section 5.1 of this chapter assesses the accuracy of the sea trial results, and the following Section 5.2 compare and discuss the results of the extrapolated towing tank results. Finally Section 5.3 is devoted the full scale CFD simulations.

5.1 Comparison of Sea Trial and In-Service Performance Data

The results from the sea trials presented in Section 4.2 show high correlation between speed and power, and low scatter of the data points. This indicates that the accuracy of the speed trial data is high. However, there might be systematic errors in the speed trial data. The correction for wind, waves and current is a possible source for systematic errors. As mentioned, the new ISO 15016:2015 procedure defines strict standards for conducting sea trials and ensures accurate measurements and corrections. The power measurements are another possible source for systematic errors. The constants of the engine manufacturer formula in eq. (3.34) are approximations. Systematic errors can not be determined solely from the data provided for this thesis. A way to validate the results from the sea trial is by comparing the results with performance measurements on the ship after the delivery while it is in service.

The ship owner has provided in-service performance data corrected for wind and waves. The data is the mean performance of all four sister ships in the first 3-9 months of operation. The power is based on torque measurements directly on the shaft and not the engine manufacturer formula as in case of the sea trial measurements. The ship owner has estimated the uncertainty to be approximately $\pm 3.5\%$ MCR. Uncertainties in the performance data include uncertainties in the raw torque measurement, the correction for wind and waves and the averaging of the data from the four sister ships.

The results of the sea trial are compared to the in-service performance data in Figure 5.1. It can be seen that the ships use more power during operation than during sea trial. On average, the sea trial data shows 8% less power than the in-service performance data. This is expected since the ships are in excellent condition at the sea trial with minimal fouling on the ship hull. Even though both the sea trial data and the in-service performance data have uncertainties, the relatively low offset in power shows that the sea trial data and the in-service performance data measures delivered power in the same range. As mentioned earlier, there is only a small scatter of the sea trial data, which indicates reasonable consistency in the measurements. The combination of reasonable offset to the in-service data and consistency indicates that the sea trial results have reasonable accuracy. Because the sea trial results are assumed to be accurate, the sea trial results can be used as reference for the extrapolated towing tank results and the full scale CFD results.

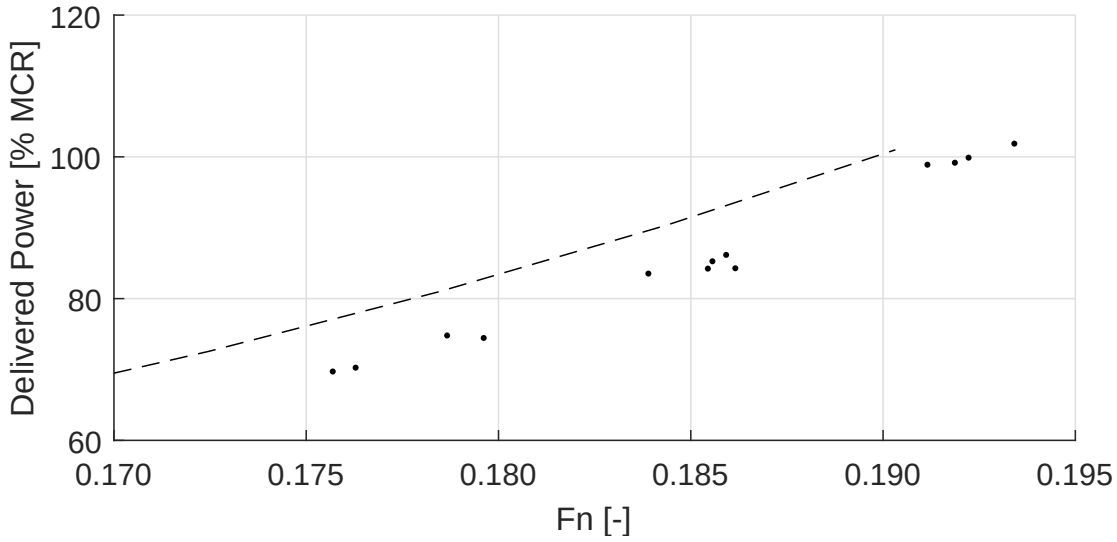

Figure 5.1: Comparison of the corrected speed trial results (dot) and the in-service performance data (dash line). Delivered power P_{Ds} as a function of Froude number Fn.

5.2 Comparison of Sea Trial and Towing Tank Test

The sea trial results presented in Section 4.2 are compared to the extrapolated self-propulsion results from the towing tank test presented in Section 4.1.6. The comparison can be seen in Figure 5.2. By comparing the sea trial and towing tank results directly, it is assumed that there is no loss in the shaft. Machinery experts at DNV-GL assess that this is a fair assumption since there is no gear.

As it can be seen in Figure 5.2, the extrapolated towing tank results give a reasonable good estimation of the delivered power. The extrapolated towing tank results are overestimating the power by approximately 3% to 9% with an average of 6% compared to the sea trial results. Considering that towing tank tests are conducted at a much lower Reynolds number and extrapolated, the observed discrepancies are satisfactory. The power overestimation from the towing tank could indicate that the ITTC procedure gives a conservative estimate of the ship performance.

The towing tank tests are based on measurements which have uncertainties, and the ITTC extrapolation procedure also adds uncertainties to the estimation of the full scale ship performance. The accuracy of the ITTC procedure is under constant debate. As an example, recent research has questioned the assumption of Reynolds independence of the form factor, as described in Section 2.2.4. The discrepancies seen in Figure 5.2 show that the ITTC procedure works well in this case and that the procedure is a good method for estimating the performance of this ship design. The ITTC procedure has been regularly improved and updated, and is based on over 100 years of knowledge and experience from towing tanks around the world.

Is it important to remember that the extrapolation of the towing tank results are performed by the authors using the standard ITTC procedure described in Section 3.2.4. Based on the authors experiences, many towing tanks use slightly different coefficients and corrections than the standard ITTC procedure recommends. These changes to the standard procedure are based on experience,

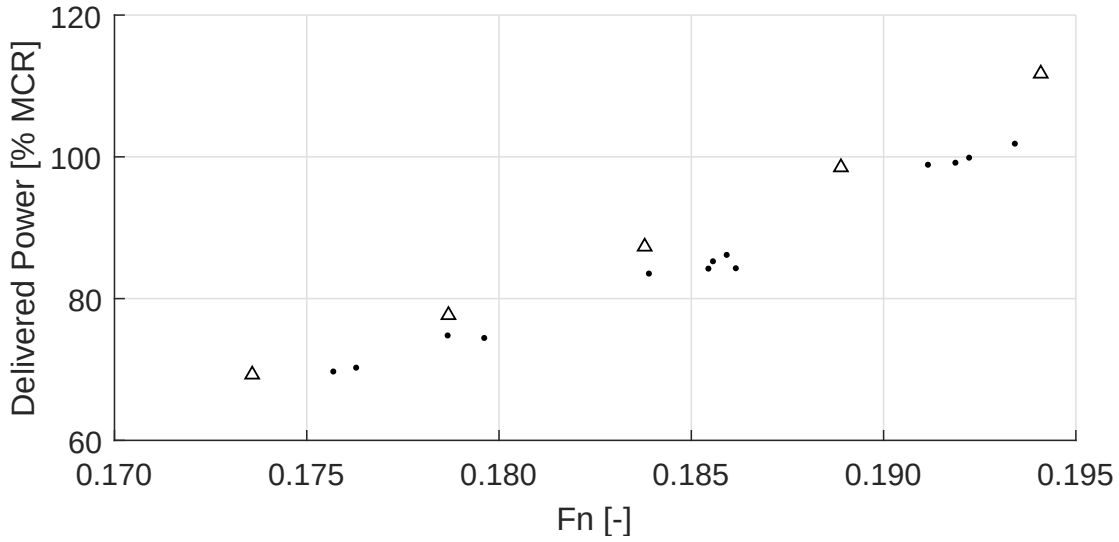

Figure 5.2: Comparison of the corrected speed trial results (dot) and the extrapolated self-propulsion results from the towing tank (triangle). Delivered power P_{Ds} as a function of Froude number Fn.

tradition, studies of systematic errors and validation studies of each tank. It has not been possible to have the exact extrapolation procedure that the towing tank uses at our disposal. Therefore, the extrapolation procedure used in this thesis is the standard ITTC procedure.

5.3 Comparison of Sea Trial and Full Scale CFD

The final results of the full scale self-propulsion CFD simulations can be seen in Figure 5.3 together with the extrapolated towing tank results and the sea trial results.

It can be seen in Figure 5.3 that the CFD results are close to the sea trial results. Compared to the sea trial results, the CFD results overestimates the delivered power by approximately 0% to 5% with an average of 2%. It is important to remember that the CFD simulations are performed using the stock propeller and not the actual propeller. In Section 4.1.6 it is shown that the delivered power from the extrapolated towing tank tests using the stock propeller characteristics instead of the actual propeller characteristics is 4% to 5% lower. This could indicate that the stock propeller performs slightly better in full scale than the actual propeller. This indication is based on several assumptions. One assumption is that the ITTC extrapolation procedure of the open water characteristics is accurate. Research as [34, 42] has questioned the accuracy of the procedure. The comparison is based on open water and self-propulsion tests which both have measurement uncertainties. The origin of the actual propeller characteristics and the method with which it is calculated is not known to the authors.

It would be interesting to perform CFD simulations with the actual propeller, but it has not been possible to get the actual propeller geometry due to confidentiality. Therefore, it is important to remember that the difference of 4 to 5% is not an accurate value but more an indication that

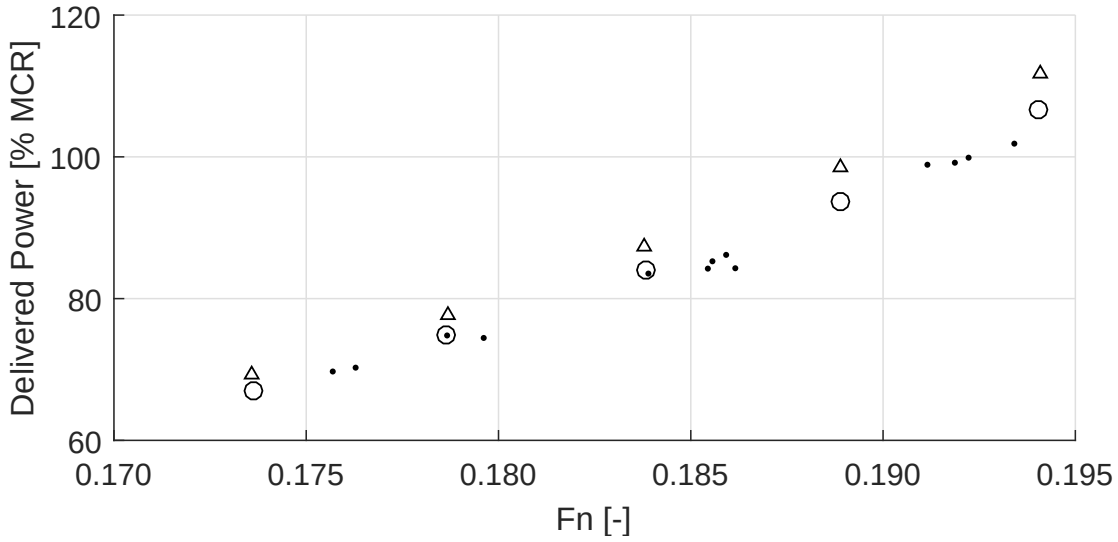

Figure 5.3: Comparison of the corrected speed trial results (dot), the extrapolated self-propulsion results (triangle) from the towing tank and the full scale CFD self-propulsion results (circle). Delivered power P_{Ds} as a function of Froude number Fn.

the performance of the stock propeller is similar to or possibly slightly better than the actual propeller.

Another source of uncertainty is the fact that the roughness resistance on the hull, the air resistance on the super structure and the added bilge keel resistance are all estimated using the ITTC procedure (see Section 3.2.4) and not modelled in the CFD simulations. The ITTC procedure for estimating these resistance contributions has been developed as a part of extrapolating towing tank tests to full scale and is therefore not meant to be used separately for full scale CFD results. By using the procedure on the CFD results, it is expected that uncertainties are introduced. The ITTC procedure estimates that out of the total resistance, the hull roughness is approximately 4% to 5%, the air resistance is approximately 3% to 4% and the bilge keels is approximately 1% to 2%. It could have been interesting to model or simulate the hull roughness, air resistance and bilge keels in the CFD simulations. However, due to time constraints, it has been decided not to implement these elements in the CFD setups.

Prior to this thesis, experts from DNV GL have had discussions with a world leading paint manufacturer. The paint manufacturer has expressed that a roughness of 150 μm is high. A hull roughness of 90 μm to 120 μm is a more reasonable estimate. It is noted that the paint manufacturer is not neutral because they have an interest in estimating a low roughness for their paint. Furthermore, it is not known if the roughness given by the paint manufacturer takes welding seems and anodes into account. However, this could indicate that the roughness resistance which has been added to both the towing tank results and the CFD results is too high. As seen in Figure 5.3, both the CFD and towing tank results are overestimating the power. That could possibly be explained by an overestimation of hull roughness resistance.

As mentioned in Section 3.4, the CFD method simplifies the physics by modelling the turbulence behaviour instead of resolving the flow. The choice of turbulence model is crucial to the accuracy

of the results. However, by modelling the turbulence, uncertainties are expected. An example of a study with different turbulence models in ship hydrodynamics is [3]. Furthermore the free surface is removed from the self-propulsion simulation and the wave making resistance is estimated separately. This modelling error caused by removing the free surface is small based on experience from CFD experts at DNV GL.

Based on the discussion above, the results seen in Figure 5.3 show that the full scale CFD simulations provides results similar to the sea trials which indicates a great potential for CFD simulation in predicting the performance of ships. Previously it has not been possible to validate towing tank results in the fully loaded condition because speed trial data in fully loaded condition is very rare. The reason for the limited speed trial data is the practicalities related to fully load the ship at the speed trial. If full scale CFD is shown trustworthy, CFD simulations can easily be performed in the fully loaded condition, which is much more interesting than the ballast condition. In order to gain more trust in CFD simulations of self-propelled ships in full scale, more test cases are required. If other cases show results similar to this thesis, it could change the way the maritime world predicts the performance of ships in the future.

CHAPTER 6

Conclusions

The overall goal of the project has been to develop and validate a CFD model of a full scale self-propelled ship. This goal has been fulfilled.

The sea trial results of the four sister ships have shown similar performance. A comparison of the sea trial results and monitored in-service performance data has shows that the delivered power in-service is on average approximately 8% higher than the sea trial results. This is expected since fouling on the hull is present in service but not at the sea trial. The combination of the similar measured performance for the sister ships and the reasonable offset to the monitored in-service performance indicates that the sea trial results are a trustworthy reference for the extrapolated towing tank data and full scale CFD.

The development of the CFD model has gone through several stages. First a resistance setup has been validated. The resistance setup has been developed prior to this project. In parallel, an open water setup has been created and validated. The results of the resistance and open water CFD calculations have been compared with towing tank results and the results showed small discrepancies of similar magnitude to the measurement uncertainties.

The resistance setup and the open water setup have been combined into a CFD setup that simulates a self-propulsion test. First, the self-propulsion test has been simulated in model scale. The results from the model scale self-propulsion simulations have shown reasonable similarity to the towing tank results.

Based on the model scale setup, self-propulsion test have been simulated in full scale and compared to sea trial data and the extrapolated self-propulsion test from the towing tank. The comparison has shown that the full scale self-propulsion CFD simulations overestimate the delivered power by approximately 2% on average compared to the sea trial results. This discrepancy is reasonable since the simulations have been performed with the stock propeller instead of the actual propeller and the fact that air resistance, bilge keel resistance and hull roughness resistance are calculated using the ITTC procedure instead of being modelled in CFD.

The provided towing tank test results have been extrapolated to full scale using the ITTC procedure. It was found that this prediction overestimated the delivered power with 6% in average compared to the sea trial results.

The strengths, weaknesses and uncertainties related to the sea trial, CFD and towing tank predictions have been discussed. This thesis has shown that both the traditional towing tank approach and full scale CFD can make reasonable estimations of the full scale performance of a ship. In the case studied in this thesis, the CFD approach gave an estimation closer to the sea trial results. To conclude whether the full scale CFD or the towing tank approach is superior in prediction of the performance of a ship, more similar studies are required. However, this thesis has indicated that CFD has great potential to be the method for estimating full scale performance in the future.

CHAPTER 7

Future Work

As mentioned in the conclusion more studies like this are required in order to determine the accuracy of full scale CFD and extrapolated towing tank tests.

It is recommended for future studies of similar kind, that the availability of and access to key data (e.g. the ship and propeller geometry, sea trial results, towing tank results) are checked before the project start. A full list of required and optional data can be found in Appendix A. The difference in delivered power from sea trial, extrapolated towing tank test and full scale CFD is relatively small so low uncertainties are required for all data in order to be be able to make strong conclusions.

A disadvantage of the CFD approach is that the turbulence is modelled using a turbulence model. Therefore it could be interesting to study the influence of using a different turbulence model(e.g. $k-\omega$ SST) in the self-propulsion simulations.

Furthermore, it would also be very interesting to include roughness, bilge keel and air resistance in the CFD simulation. Thereby, the CFD approach will be completely independent of the ITTC procedure.

Bibliography

[1] Satu K. Hänninen, Tommi Mikkola, and Jerzy Matusiak. Computational and experimental study on local ship loads in short and steep waves. *Journal of Marine Science and Technology (Japan)*, 19(1):103–115, 2014.

[2] J. Wackers, B. Koren, H. C. Raven, A. van der Ploeg, A. R. Starke, G. B. Deng, P. Queutey, M. Visonneau, T. Hino, and K. Ohashi. Free-Surface Viscous Flow Solution Methods for Ship Hydrodynamics. *Archives of Computational Methods in Engineering*, 18(1):1–41, 2011.

[3] Lars Larson. Gothenburg 2010, a workshop on numerical ship hydrodynamics.

[4] IMO. ISO 15016:2015. *MEPC 68/INF.14*, page 1, 2015.

[5] A. Molland, S. Turnock, and D. Hudson. *Ship Resistance and Propulsion*. Cambridge University Press, 2011.

[6] John Newman. *Marine Hydrodynamics*. MIT Press, 1977.

[7] Milton Van Dyke. *An Album of Fluid Motion*. 1982.

[8] W. Froude. *The Papers of William Froude*. 1955.

[9] G. Hughes. Friction and form factor resistance in turbulent flow and a proposed formulation for use in model and ship correlation. *Transactions of the Royal Institution of Naval Architects*, 96:314–376, 1954.

[10] ITTC. Recommended Procedures and Guidelines, 1978 ITTC Performance Prediction Method, 2005.

[11] J. Carlton. *Marine Propellers and Propulsion, 3. edition*. Butterworth-Heinemann, 2012.

[12] 26th ITTC Resistance Committee. The Resistance Committee, Final Report and Recommendations to the 26th ITTC. *26th International Towing Tank Conference*, I:17–71, 2011.

[13] L. Eça. On the accuracy of the numerical prediction of scale effects on ship viscous resistance. *International Conference on Computational Methods in Marine Engineering*, pages 1–10, 2005.

[14] Karl E. Schoenherr. Resistance of flat surfaces. *Trans SNAME*, pages 40:279–313, 1932.

[15] C. W. B. Grigson. A planar friction algorithm and its use in analysing hull resistance. *RINA*, 1999.

[16] Tahara Y. Katsui T., Asai H., Himeno Y. The Proposal of a New Friction Line. *Fifth Osaka Colloquium on Advanced CFD Applications to Ship Flow and Hull Form Design*, 2005.

[17] ITTC. ITTC – Recommended Procedures, Testing and Extrapolation Methods, Resistance Resistance, Test, 7.5-02 -02-01. *ReVision*, pages 266 – 273, 2002.

[18] A. Garcia-Gomez. On the form factor scale effect. *Ocean Engineering*, 26(1):97–109, 2000.

[19] D. Park. A study on the effect of flat plate friction resistance on speed performance prediction of full scale. 2015.

[20] Keh S. Min and Seon Hyung Kang. Study on the form factor and full-scale ship resistance prediction method. *Journal of Marine Science and Technology*, 15(2):108–118, 2010.

[21] H. C. Raven, A. Van Der Ploeg, A. R. Starke, and L. Eça. Towards a CFD-based prediction of ship performance - progress in predicting full-scale resistance and scale effects. *Transactions of the Royal Institution of Naval Architects Part A: International Journal of Maritime Engineering*, 150(4):31–42, 2008.

[22] K. Minsaas. Grunnlag for fartsprognoser. *Technical report, Marintek (former: Norges Hydrodynamiske Laboratorier) , Trondheim, Norway.*, 1982.

[23] D. Wilcox. *Turbulence Modelling for CFD, 2nd edition.* DCW. Industries, 1998.

[24] Cuong Nguyen. Turbulence Modeling. *MIT*, 1(8):1–6, 2005.

[25] D. C. Wilcox. Turbulence Modeling for CFD, 3rd edition, 2006.

[26] D. C Wilcox. Formulation of the k-omega Turbulence Model Revisited. *AIAA Journal*, 46(11):2923–3838, 2008.

[27] F. R. Menter. Two-Equation Eddy-Viscosity Turbulence Models for Engineering Applications. *American Institute of Aeronautics and Astronautics*, 32(8):1989–1605, 1994.

[28] CD-Adapco. STAR-CCM+ Documentation, Version 10.04, 2015.

[29] A.E.P. Veldman. BOUNDARY LAYERS IN FLUID DYNAMICS. *Lecture Notes in Applied Mathematics, University of Groningen.*, 2011.

[30] Salim M. Salim. Wall y+ strategy for dealing with wall-bounded turbulent flows. *Proceedings of the International MultiConference of Engineers and Computer Scientists*, II, 2009.

[31] R. Azcueta. Computation of Turbulent Free-Surface Flows Around Ships and Floating Bodies. *PhD Thesis*, 2001.

[32] ITTC. Recommended Procedures and Guidelines, Testing and Extrapolation Methods Propulsion, Propulsor Open Water Test, 7.5-02 -03-02.1, 2011.

[33] ITTC. Recommended Procedures and Guidelines, Propulsion/Bollard Pull Test, 7.5-02-03-01.1. – *Recommended Procedures and Guidelines*, page 16, 2011.

[34] Stephan Helma. An Extrapolation Method Suitable for Scaling of Propellers of any Design. *Fourth International Symposium on Marine Propulsors*, 2015.

[35] Eirik Eisinger. A Method for Describing Ocean Environments for Ship Design. *Masters Thesis, University of Oslo*, 2016.

[36] Paul Berrisford, D Dee, K Fielding, M Fuentes, P Kallberg, S Kobayashi, and S Uppala. The ERA-Interim Archive. *ERA report series*, 1(1):1–16, 2009.

[37] M Kume, K. I.; Hirata, N.; Hasegawa, J.; Tsukada, Y.; Hinatsu. Uncertainty Analysis Method for Ship Performance Test. *Senpaku Gijutsu Kenkyusho Hokoku/papers of Ship Research Institute*, 37(5):163–189, 2000.

[38] G. Kuiper. Cavitation inception on ship propeller models. *Ph.D. thesis, Delft University of Technology*, 1981.

[39] Douwe R. Rijpkema, J. Baltazar, and J.A.C. Falcão de Campos. Viscous flow simulations of propellers in different Reynolds number regimes. *Proceedings of the 4th International Symposium on Marine Propulsors*, I, 2015.

[40] Ridha Abid. Evaluation of two-equation turbulence models for predicting transitional flows. *International Journal of Engineering Science*, 31(6):831–840, 1993.

[41] Xiao Wang. Computational Analysis of Marine-Propeller Performance Using Tranition-Sensitive Turbulence Modeling. *Journal of Fluid Engineering*, 134(1), 2012.

[42] G. Kuiper. The Wageningen Propeller Series, 1992.

APPENDIX A

Required Data

The following is a list of data required to perform a study similar to the study of this thesis.

Required data:

- Principal dimensions
- Speed with main engine characteristics
- General arrangement (G/A)
- High quality 3D geometry of hull, rudder, propellers (the one used in model test and actual on ship) and other appendages.
- Exact location of propeller and appendages.
- Full towing tank report with model scale results in sea trial condition. Including results from resistance test, open water test and self-propulsion. Water temperature at each test. Information on used corrections to the results (e.g. corrections to the open water characteristics).
- Sea trial report with results corrected for current, wind and waves.

Optional data:

- Sea trial report with raw measurements of speed, rpm, engine power, current, wind and waves.
- Extrapolated results from a towing tank test.
- 3D geometry of superstructure.
- In-service performance data.
- Added resistance test from towing tank.
- Wind tunnel test report.

DTU Mechanical Engineering
Section of Fluid Mechanics, Coastal and Maritime Engineering
Technical University of Denmark

Nils Koppels Allé, Bld. 403
DK-2800 Kgs. Lyngby
Denmark
Phone (+45) 4525 1360
Fax (+45) 4588 4325

www.mek.dtu.dk